THE IMPACT OF [1,2,5]CHALCOGENAZOLO[3,4,F]-BENZO[1,2,3]TRIAZOLE STRUCTURE ON THE OPTOELECTRONIC PROPERTIES OF CONJUGATED POLYMERS

A THESIS SUBMITTED TO
THE GRADUATE SCHOOL OF NATURAL AND APPLIED SCIENCES
OF
MIDDLE EAST TECHNICAL UNIVERSITY

BY

ECEM AYDAN ALKAN

IN PARTIAL FULFILLMENT OF THE REQUIREMENTS
FOR
THE DEGREE OF MASTER OF SCIENCE
IN
CHEMISTRY

JANUARY 2020

Approval of the thesis:

THE IMPACT OF [1,2,5]CHALCOGENAZOLO[3,4,F]-BENZO[1,2,3]TRIAZOLE STRUCTURE ON THE OPTOELECTRONIC PROPERTIES OF CONJUGATED POLYMERS

submitted by **ECEM AYDAN ALKAN** in partial fulfillment of the requirements for the degree of **Master of Science** i**n Chemistry Department, Middle East Technical University** by,

Prof. Dr. Halil Kalıpçılar
Dean, Graduate School of **Natural and Applied Sciences** _____

Prof. Dr. Cihangir Tanyeli
Head of the Department, **Chemistry** _____

Prof. Dr. Levent Toppare
Supervisor, **Chemistry, METU** _____

Examining Committee Members:

Prof. Dr. Ali Çırpan
Chemistry, METU _____

Prof. Dr. Levent Toppare
Chemistry, METU _____

Prof. Dr. Yasemin Arslan Udum
Advanced Technologies Dept., Gazi University _____

Assoc. Prof. Dr. Görkem Günbaş
Chemistry, METU _____

Assist. Prof. Dr. Erol Yıldırım
Chemistry, METU _____

Date: 10.01.2020

I hereby declare that all information in this document has been obtained and presented in accordance with academic rules and ethical conduct. I also declare that, as required by these rules and conduct, I have fully cited and referenced all material and results that are not original to this work.

Name, Last name: Ecem Aydan Alkan

Signature:

ABSTRACT

THE IMPACT OF [1,2,5]CHALCOGENAZOLO[3,4,F]-BENZO[1,2,3]TRIAZOLE STRUCTURE ON THE OPTOELECTRONIC PROPERTIES OF CONJUGATED POLYMERS

Aydan Alkan, Ecem
Master of Science, Chemistry
Supervisor: Prof. Dr. Levent Toppare

January 2020, 98 pages

[1,2,5]Chalcogenazolo[3,4-f]benzo[1,2,3]triazole units are strong electron-acceptor moieties that narrow the band gap of resulting conjugated polymers due to the electron deficiency on both sides of their structure. In this study, the effect of acceptor strength on optoelectronic properties were aimed and investigated by incorporating these moieties into donor-acceptor type conjugated polymers. Central chalcogen atom of the chalcogenazole linkage differentiated as sulfur and selenium to compare their effects on the optoelectronic properties of the polymers. Therefore, two novel conjugated near-IR (NIR) absorbing donor–acceptor type copolymers comprising [1,2,5]chalcogenazolo[3,4-f]-benzo[1,2,3]triazole derivatives as the acceptors and benzodithiophene as the donor, spaced with thiophene as the π-bridge, were designed and synthesized via Stille polycondensation reaction. Branched alkyl chains (the extended 2-octyl-1-dodecyl alkyl chain; $-C_8C_{12}$) were substituted to 5H-[1,2,3]triazolo[4',5':4,5]benzo[1,2-c][1,2,5]thiadiazole and 5H-[1,2,3]triazolo[4',5':4,5]benzo[1,2-c][1,2,5]selenadiazole for enhanced solubility of polymers which ease the processability hence device constructions. The strong

electron-withdrawing units lead to a substantial change on the absorption properties via promoting the intramolecular charge transfer (ICT) band alongside the π–π* transition with a wide range of absorption extended to the NIR region. The resultant soluble polymers were characterized via cyclic voltammetry to determine HOMO and LUMO energy levels as -5.00 eV and -3.92 for PSBT and -4.86 eV and -4.04 eV for PSeBT, respectively. Electronic band gaps of the copolymers were calculated as 1.08 eV for PSBT and 0.82 eV for PSeBT, respectively. Finally, an electrochromic device (ECD) was constructed and characterized using the polymer PSeBT, due to its lower band gap and better switching colors displayed in all RGB than its sulfur analogue.

Keywords: NIR Absorbing Polymers, Narrow Band Gap, Strong Electron-Acceptor Units, Chalcogenazole, Electrochromic Device (ECD)

ÖZ

[1,2,5]KALKOJENAZOLO[3,4-F]BENZO[1,2,3]TRIAZOL YAPISININ KONJUGE POLİMERLERİN OPTOELEKTRONİK ÖZELLİKLERİ ÜZERİNDEKİ ETKİSİ

Aydan Alkan, Ecem
Yüksek Lisans, Kimya
Tez Yöneticisi: Prof. Dr. Levent Toppare

Ocak 2020, 98 sayfa

[1,2,5]Kalkojenazolo[3,4-f]benzo[1,2,3]triazol üniteleri yapılarının iki tarafındaki elektron eksikliği sayesinde bulundukları konjuge polimerlerin bant aralıklarını daraltan güçlü elektron akseptör parçalardır. Bu çalışmada, bahsedilen parçaların donör-akseptör tipi konjuge polimerlere dahil edilmesiyle akseptör gücünün optoelektronik özellikler üzerindeki etkileri amaçlanmış ve araştırılmıştır. Kalkojenazol yapılarının merkezindeki kalkojen atomunun polimerlerin optoelektronik özellikleri üzerindeki etkileri karşılaştırılması için sülfür ve selenyum olarak farklılaştırılmıştır. Bu nedenle, yakın kızılötesi (NIR) bölgesinde soğuran özgün konjuge donör-akseptör tipi iki kopolimer, akseptör olarak [1,2,5]kalkojenazolo[3,4-f]-benzo[1,2,3]triazol türevlerini ve donör olarak benzoditiyofen içeren ve tiyofen π-köprüsü ile ayrılmış yapısı ile dizayn edilmiş ve Stille polikondenzasyon reksiyonu ile sentezlenmiştir. Dallanmış alkil grubu (genişletilmiş 2-oktil-1-dodesil alkil grubu; -C8C12) 5H-[1,2,3]triazolo[4',5':4,5]benzo[1,2-c][1,2,5]tiyadiazol ve 5H-[1,2,3]triazolo[4',5':4,5]benzo[1,2-c][1,2,5]selenadiazol yapılarına polimerlerin

çözünürlüğünün geliştirilmesi ve işlenebilirliğinin kolaylaştırılması için takılmıştır ve bu sayede cihaz yapılarının iyileştirilmesi amaçlanmıştır. Güçlü elektron-çeken üniteler absorpsiyon özelliklerinde azımsanmayacak değişikliklere, NIR bölgesine kadar uzanan geniş absorpsiyon aralığında π–π* geçişi yanı sıra molekül içi yük transferi (ICT) bantını teşvik ederek sebep olmuştur. Elde edilen çözünür polimerler HOMO ve LUMO enerji seviyelerini belirlemek amacıyla dönüşümlü voltometri ile karakterize edilmiştir ve sırası ile PSBT için -5.00 eV ve -3.92 eV olarak ve PSeBT için -4.86 eV and -4.04 eV olarak bulunmuştur. Kopolimerlerin elektronik bant aralıkları sırası ile PSBT için 1.08 eV ve PseBT için 0.82 eV olarak hesaplanmıştır. Son olarak, kükürt türevinden daha düşük bant aralığı ve tüm RGB arasında daha iyi renk geçişi yapabilme özelliklerinden dolayı SeBT polimeri kullanılarak bir elektrokromik cihaz kurulmuştur ve karakterizasyonları yapılmıştır.

Anahtar Kelimeler: Yakın Kızılötesi Absorplayan Polimerler, Dar Bant Aralığı, Güçlü Elektron akseptör Üniteler, Kalkojenazol, Elektrokromik Cihaz (ECD)

To my precious family…

ACKNOWLEDGMENTS

I would like to thank Prof. Dr. Levent Toppare for his guidance and endless support. He was very encouraging and his discussions and advices during my studies were very helpful. I am very grateful that I had chance to work with him.

I would like to thank Assoc. Prof. Dr. Görkem Günbaş for his valuable advices and suggestions during organic synthesis.

I would like to thank Prof. Dr. Yasemin Arslan Udum and Hatice Sarıgül for their contributions in electrochemical characterizations of the polymers. Especially, I would like to thank Prof. Dr. Yasemin Arslan Udum for answering all of my questions about electrochemistry patiently.

I would like to thank Dr. Gönül Hızalan Özsoy and Mert Can Erer for the trails of photovoltaic applications.

I would like to thank Prof. Dr. Ali Çırpan for his guidance, support and helpful advices.

I would like to thank Assist. Prof. Dr. Erol Yıldırım for his guidance and helpful advices during understanding the spectroelectrochemical properties of the polymers and his contributions in computational studies.

I would like to thank Dr. Seza Göker for being my mentor during organic synthesis and her precious advices and Mustafa Yaşa for his helps with the synthesis procedures.

I would like to express my special thanks to one of my best friends Osman Karaman for his valuable friendship and emotional supports that keep me motivated. He was always helping me whenever I needed both in laboratory and my life. He is a true gentleman that he always waited for me when I was working in laboratory at late hours.

I would like to express my gratitude to Figen Varlıoğlu Yaylalı for her helps during my polymerization reactions and Gizem Atakan for her helps during stannylation reactions.

I am very grateful to Hande Özel, Ece Büber, Eda Bolayır, Cevahir Ceren Akgül, Dilay Kepil, Çağlayan Kızıleniş and Sena Tarım for their support, precious friendships and lovely conversations during coffee breaks.

I cannot describe my gratitude to my parents Ayten and Kemal Aydan for their endless love and sacrifice through my life. Without their support, encourage and belief I could not be the one who I am today. I would like to thank specially my sister Selen Aydan for encouraging and her support. I am the luckiest person for having her in my life.

My final and most special thank is to my husband Kıvanç Alkan, who was always very supportive to me. His love is the most important thing that gives me courage and power. Here, I would like to thank him for doing his best to help me making my dreams come true. He always knows how to cheer me up when I lose my motivation.

TABLE OF CONTENTS

LIST OF TABLES

TABLES

LIST OF FIGURES

FIGURES

LIST OF ABBREVIATIONS

ABBREVIATIONS

ACN	Acetonitrile
Ag	Silver
CB	Conduction Band
CIE	La Commission Internationale de l'Eclairage
CP	Conjugated Polymers
CV	Cyclic Voltammetry
D-A	Donor-Acceptor
DCM	Dichloromethane
DMF	Dimethylformamide
DMSO	Dimethyl sulfoxide
E_g^{el}	Electronic Band Gap
E_g^{op}	Optical Band Gap
ECD	Electrochromic Device
FTIR	Fourier-Transform Infrared
GPC	Gel Permeation Chromatography
HOMO	Highest Occupied Molecular Orbital
HRMS	High Resolution Mass Spectroscopy
ICP	Intrinsically Conductive Polymers
ICT	Intramolecular Charge Transfer
ITO	Indium Tin Oxide

L, a, b	Luminance, Hue, Saturation
LUMO	Lowest Unoccupied Molecular Orbital
NHE	Normal Hydrogen Electrode
NIR	Near Infrared
NMR	Nuclear Magnetic Resonance Spectrometer
OFET	Organic Field Effect Transistor
OLED	Organic Light Emitting Diode
OPV	Organic Photovoltaic
PA	Polyacetylene
PAn	Polyaniline
PEDOT	Polyethylenedioxythiophene
PPP	Polyparaphenylene
PPV	Polyphenylene vinylene
PPy	Polypyrrole
Pt	Platinum
PTh	Polythiophene
PTMA	Poly(2,2,6,6- tetramethylpiperidinyloxy-4-yl methacrylate
Bu_4NPF_6	Tetrabutylammonium hexafluorophosphate
THF	Tetrahydrofuran
TLC	Thin Layer Chromatography
TMS	Trimethylsilane
VB	Valence Band

LIST OF SYMBOLS

SYMBOLS

λ_{max}	Maximum Absorption Wavelength
λ_{onset}	Onset Absorption Wavelength

CHAPTER 1

INTRODUCTION

1.1 Conjugated Polymers

Conjugated polymers are macromolecules possessing backbone chain of alternating double and single bonds. The overlap of p-orbitals on the polymer chain enables the delocalization of electrons throughout the whole system. The delocalized electrons become mobile on the conjugated system when a doping process is applied on the polymer to transform it into conducting form.[1] The first discovered conjugated polymer was polythiazyl which was found to be a superconductor at 0.26 K. It is an air stable and insoluble solid which can be found as single crystals, powder and film with a metallic appearance.[2] However, the main interest in conjugated polymers was started after the discovery of conductivity of polyacetylene (PA). Alan J. Heeger, Alan MacDiarmid and Hideki Shirakawa obtained conjugated PA when acetylene monomer was doped with bromine and iodine vapor; increasing the resulting electrical conductivity of the starting monomer by 10 orders of magnitude.[3] In 2000, this discovery was awarded by Nobel Prize in Chemistry and many studies were conducted in the research field of PA aiming to develop easily processable and lightweight doped polymers.[4] However, this polymer was inconvenient in commercial applications due to its poor properties such as air instability and processing difficulty. Therefore, many researches were conducted in order to discover new air stable, low weight, and easily processable conjugated polymers with promising electronic features.

The undeniable advantages of conjugated polymers over their inorganic analogues such as flexibility, low cost, ease of processability and tunable band gap by structural modifications attracted an increasing attention.[5] As a result of these favorable properties of conjugated polymers, a wide range of applications have been proposed

for them. Some of these applications are organic photovoltaics (OPV)[6], organic field effect transistors (OFETs)[7], biosensors[8] and electrochromic devices (ECDs)[9].

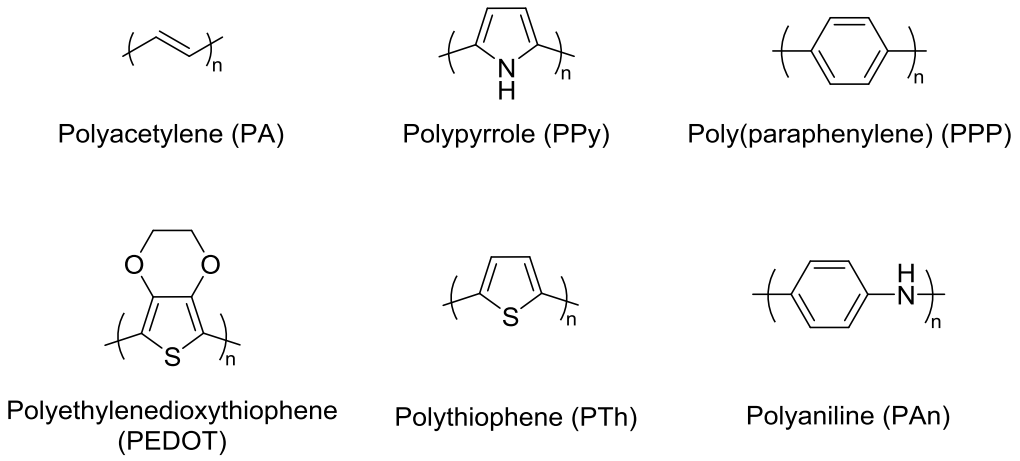

Figure 1.1. Examples of conjugated polymers

1.1.1 Conductivity in Conjugated Polymers

Conjugated polymers can be classified as semiconductors and their conductivity lies between insulators and metallic conductors. They have the electrical and optical properties of metals and semiconductors while possessing the properties of conventional polymers, such as easy and inexpensive synthesis and flexibility.[10] (Figure 1.2)

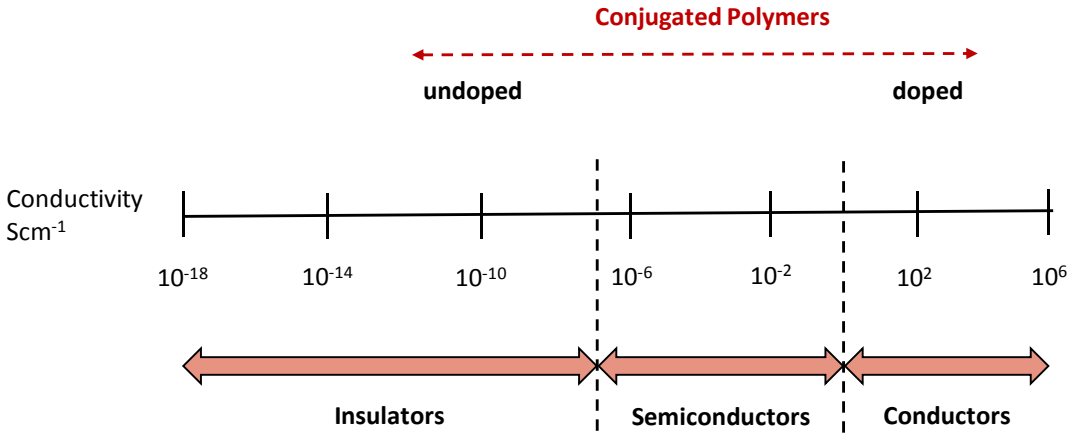

Figure 1.2. Conductivity range of conjugated polymers

1.1.1.1 Doping Process

Electronic properties of conjugated polymers can be modified easily by surface functionalization and doping.[11] In traditional polymers the valence electrons are bound in sp^3 hybridized covalent bonds. The electrons that are bounded by the sigma bonds do not contribute to the electrical conductivity of the polymers due to their low mobility. However, the backbones of conjugated polymers consist of adjacent sp^2 hybridized carbon centers. One of the electrons on each center stands in the p_z orbital, which is orthogonal to the other three sigma-bonds. All of these p_z orbitals on the molecule combine with each other generating a wide set of delocalized orbitals. The electrons on these delocalized orbitals gain high mobility when the molecule doped by oxidation or reduction. In the case of doping by oxidation, some of the delocalized electrons are removed and the conjugated p-orbitals form a one-dimensional electronic band.[12] Therefore, electrons on the band become mobile when a partial emptiness obtained. Distinctively, electrons are added to an unfilled band stimulating the mobility of electrons along the electronic band in the case of doping by reduction. Doping process can be accomplished either chemically or electrochemically, but the most common method among them is the electrochemical

process.[13] Electrochemical doping could be achieved easily by applying a suitable potential to the conjugated polymers in order to make them conductors.[14]

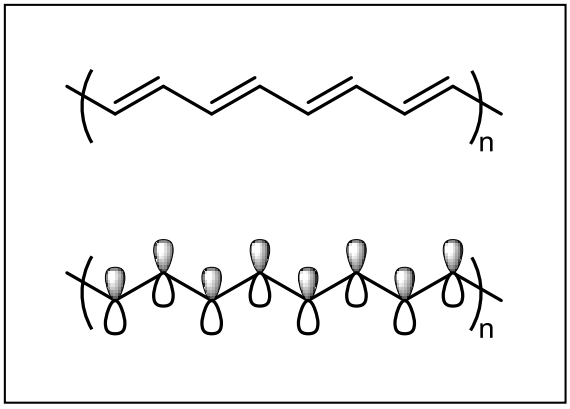

Figure 1.3. The π-system model of Polyacetylene (PA)

Polyacetylene (PA) has a degenerate ground state energy hence, it forms a neutral soliton when it is doped. Unlike PA, most of the conjugated polymers do not have degenerate ground states showing no proof for the formation of solitons. When the oxidation is applied to such polymers, an electron is removed from the valence band and a radical cation is formed named as positive polaron. The further oxidation removes another electron yielding the formation of a dication named as positive bipolaron. In the case of doping by reduction, an electron is added to the valence band forming a radical anion named as negative polaron. The further reduction adds another electron yielding the formation of a dianion named as negative bipolaron. Solitons, polarons and bipolarons are known as the charge carriers on the conjugated system.[15]

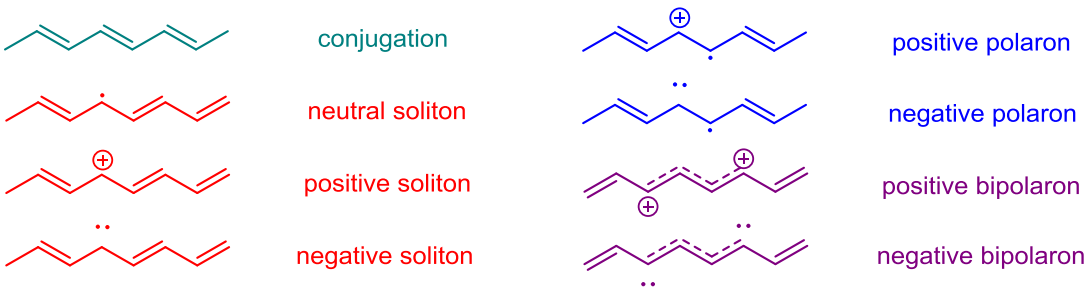

Figure 1.4. Charge carriers

1.1.1.2 Band Gap

One of the key parameters that can control the conductivity of semiconductors is band gap. The last band filled with π electrons known as the Highest Occupied Molecular Orbital (HOMO) and the first empty π orbital band known as the Lowest Unoccupied Molecular Orbital (LUMO). The energy difference between these two energy levels is the band gap. If it is portrayed in a different way, it is the energy gap between the valence band and the conduction band. In metallic conductors there is an overlap between these bands and electrons are free to move to participate in conduction. In electrical insulators there is a large gap between valence band and the conduction band where electrons cannot pass to the conduction band resulting in no conduction. However, there is a small energy gap between the valence band and the conduction band of semiconductors such as conjugated polymers.[16] HOMO and LUMO levels and the band gap of a conjugated polymer are the most important parameters that identify its optoelectronic properties.[17] HOMO and LUMO energy levels and band gap of conjugated polymers can be arranged by some modifications on the polymer structure. Donor-acceptor approach is one of the methods that helps to obtain optimum band gap of a conjugated polymer. Length of the polymer chain is also another parameter that affects the band gap where increasing the conjugation length decreases the band gap.[18]

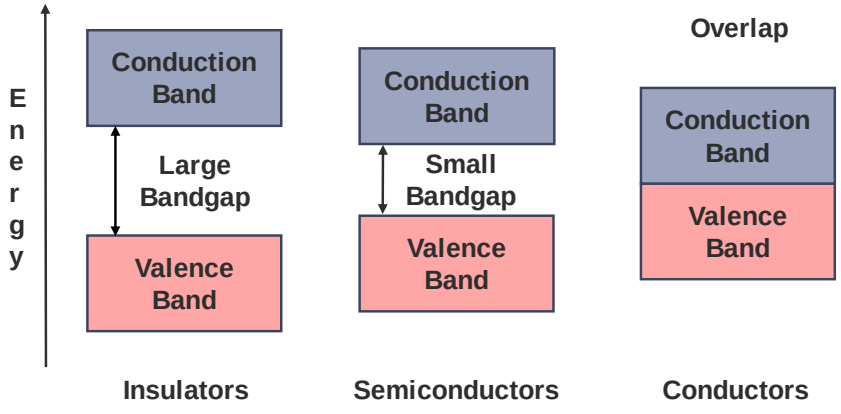

Figure 1.5. Molecular orbital diagram representing the differences in the band gaps of the materials

1.2 Syntheses of Conjugated Polymers

Conjugated polymers can be synthesized via both electrochemical and chemical methods.[17] Most popular chemical methods that can be used for the synthesis of conjugated polymers are oxidative chemical polymerization[19], Stille polycondensation reaction[20], Suzuki-Miyaura polycondensation reaction[21] and Sonogashira polycondensation reaction.[22]

1.2.1 Electropolymerization

Synthesis of conjugated polymers could be achieved electrochemically by introducing an electroactive functional monomer in an inert organic solvent system that contains a supporting electrolyte. Two approaches for the electrochemical synthesis of conjugated polymers are anodic polymerization and cathodic polymerization. The most extensively preferred approach is anodic polymerization which takes place by irreversible oxidation where cathodic polymerization is much less often and occurs by irreversible reduction. Anodic polymerization is used in order to synthesize homopolymers of electron rich monomers such as pyrrole or thiophene due to their tendency for oxidation. Electrochemical polymerization is an advantageous method for the synthesis of conjugated polymers, since it is simple, cost-effective and reproducible. Also, ease of the production of electrochemically active conductive polymer film in a single section glass cell, necessity for no further purification and control of film thickness and morphology are some of the other advantages of this technique.[23] Electrochemical polymerization is performed by inserting three electrodes which are reference electrode, counter electrode and working electrode into the solution containing an electrolyte and a monomer. Acetonitrile (ACN) and propylene carbonate are generally preferred solvents for electropolymerization due to their high relative permittivity and large potential range. Redox reaction is promoted by applying voltage to electrodes to synthesize the polymers. Electropolymerization could be done using cyclic voltammetry method or potentiostatic method by applying cyclic voltage or constant voltage,

respectively. In order to perform electropolymerization, monomer is dissolved in an inert organic solvent that includes supporting electrolyte and anodic potential is applied for the oxidation of the monomer. This initial oxidation leads to the formation of radical cation of the monomer followed by the formation of a natural dimer via reaction of radical cation with other monomers present in solution. Oxidized radical cations are formed by further oxidation and they react with the monomers to form oligomers and then, the polymer.[24,25] The oxidation potential decreases during the polymerization due to the extension of conjugation. The selected solvents and electrolytes, concentration of monomer, scan rate and electrodes are important parameters that affect the properties of resulting polymers.

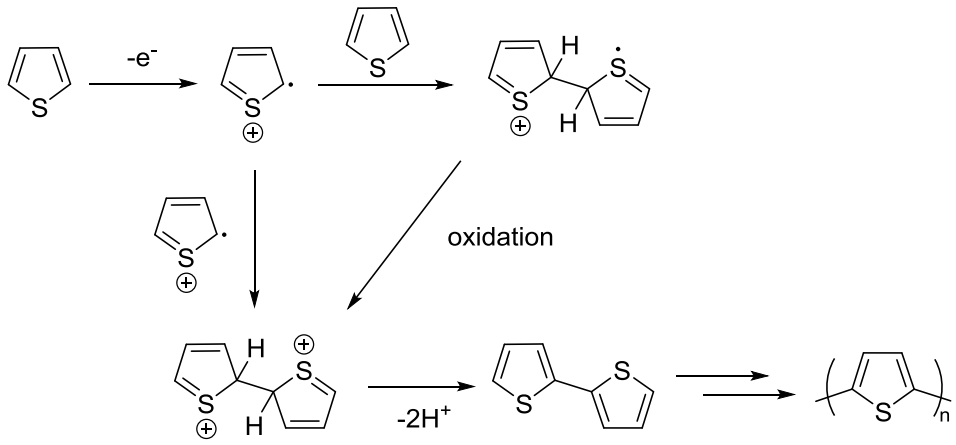

Figure 1.6. Mechanism of electrochemical polymerization of thiophene

1.2.2 Oxidative Chemical Polymerization

Conjugated polymers could be synthesized by oxidative chemical polymerization method using anhydrous Lewis acids such as $FeCl_3$ and $AlCl_3$ as catalysts.[26] The electron rich aromatic compounds like pyrrole, aniline, furan and thiophene are preferred as the monomers. The process is carried out in a solution and resulting polymers precipitates as insoluble crystals. Polymers with higher molecular weight and relatively higher conductivity could be obtained by this method.[27]

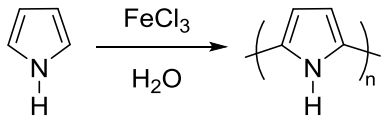

Figure 1.7. Chemical oxidative polymerization of pyrrole

1.2.3 Stille Polycondensation Reaction

Stille polycondensation reaction is a widely used method for the synthesis of conjugated polymers due to its undeniable advantages. Some of these advantages are mild reaction conditions and toleration to different functional groups. Also, the reaction is regioselective and stereospecific with high yields of product.[28] This method involves the coupling of aromatic compounds with bifunctional units as organostannanes and organohalides via palladium-catalyzed coupling reaction. Mechanism of Stille coupling reaction composed of three main steps namely oxidative addition, transmetallation and reductive elimination.[29] The active catalyst for the reaction is Pd(0) which can be generated in variety of ways. When Pd(II) is used as the catalyst in the reaction, it needs to be activated by a reduction to Pd (0) using organostannyl groups forming a biaryl compound. The first step of the reaction mechanism is oxidative addition of organohalide unit to the active catalyst takes place generating the Pd(II) intermediate. It is followed by transmetallation step where ligand substitution on Pd(II) intermediate occurs by the cleavage of Sn-C bond. This step is thought as the rate determining step of Stille coupling reaction. Finally, the cycle is completed by the reductive elimination step where the product is formed and the Pd (0) catalyst were regenerated to proceed in the reaction cycle. The total mechanism is shown in Figure 1.4. Two important parameters that affect the Stille coupling reaction are the catalyst and the solvent. $Pd(PPh_3)_4$ is one of the most preferred catalysts for this reaction in spite of its drawbacks such as being unstable to air. However, this drawback leads the ligand PPh_3 to be oxidized easily to Ph_3PO by even very little amount of oxygen that exists in the reaction medium. Also, the excess PPh_3 acts as an inhibitor in the reaction. $PdCl_2(PPh_3)_2$ could also be

used as catalyst for Stille coupling reaction but its air stability is much less than $Pd(PPh_3)_4$. Another catalyst that could also be used for Stille coupling reaction is $Pd_2(dba)_3$ and it is a more air stable alternative. Solvent of the reaction is another significant parameter since it establishes the stabilization of catalyst. It also sustains the resulting polymer in the medium during the reaction to obtain high molecular weight. THF and toluene are widely used solvents for the Stille coupling reaction since they offer good solubility for the polymer and the starting materials.[30]

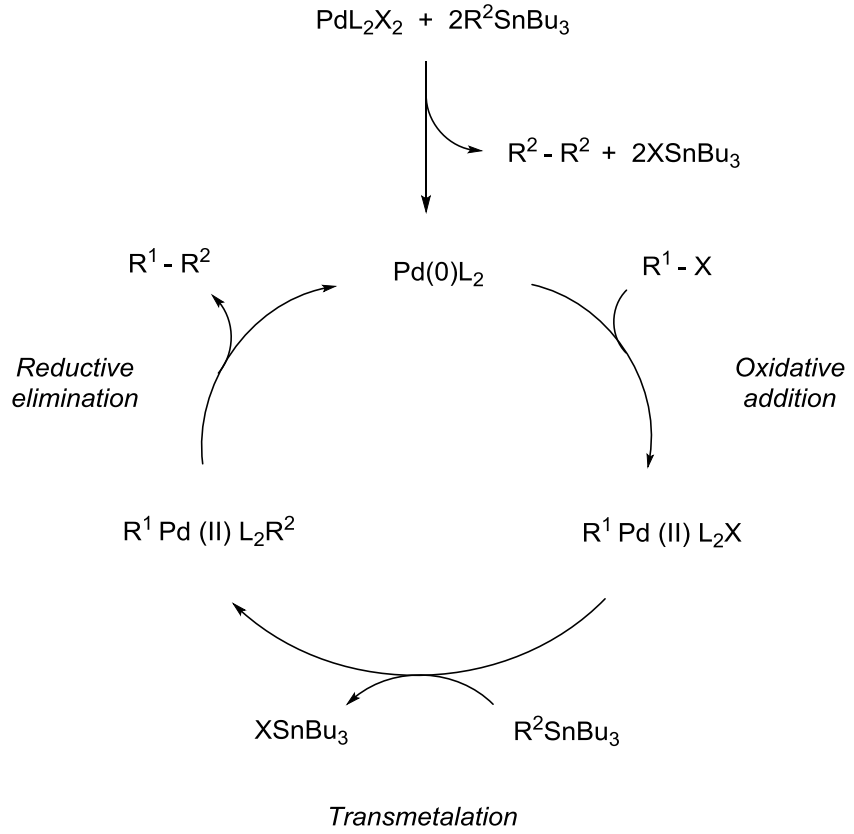

Figure 1.8. Mechanism of Stille coupling reaction

1.2.4 Suzuki Miyaura Polycondensation Reaction

Suzuki reaction is a widespread method that is used for carbon-carbon bond formation. It offers mild reaction conditions and has tolerance for the wide range of functional groups. Suzuki coupling reaction can be classified as a cross-coupling

reaction that involves the coupling of organohalides and organoboron compounds which are boronic acids or esters catalyzed by a Pd(0) complex.[31] As in the case with Stille coupling reaction, catalytic reaction cycle of Suzuki coupling reaction also consist of three main steps namely oxidative addition, trans metalation and reductive elimination. Distinctively, a base is involved in the reaction mechanism and the catalytic cycle. Base is considered to be replaced with the halide on Pd(II) intermediate before the intramolecular transmetalation.[32] The most common catalyst used in Suzuki coupling reaction is $Pd(PPh_3)_4$ since its ligand PPh_3 could be oxidized easily. Reaction is performed in two phase solvent mixture of organic and aqueous solvent mediums. Toluene, THF and dioxane are most widely used organic solvents and K_3PO_4, K_2CO_3 and Na_2CO_3 are the frequently used bases. Generally, a phase transfer catalyst is used to transfer the base which is dissolved in aqueous medium such as an aliquat 336. The complete reaction mechanism is demonstrated in Figure 1.5. This method is not suitable for the compounds which are sensitive and unstable in basic medium due to the basic reaction conditions. However, the non-toxic nature of organoboronic compounds is an important feature for the preference of Suzuki coupling reaction.

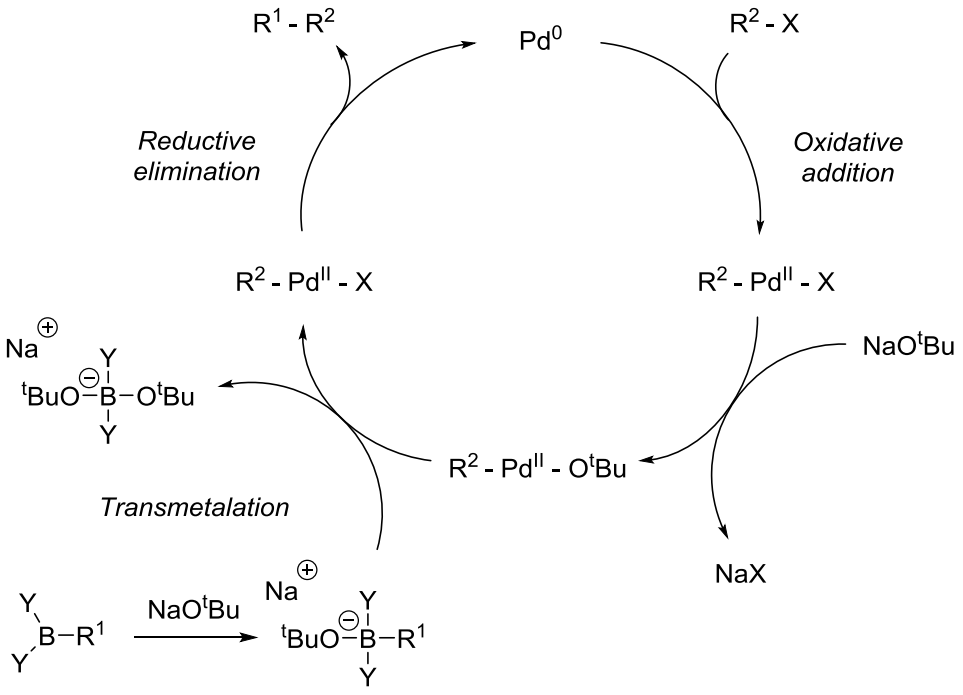

Figure 1.9. Mechanism of Suzuki coupling polymerization

1.2.5 Sonogashira Polycondensation Reaction

The Sonogashira reaction is a cross coupling reaction that used for carbon-carbon bond formation in organic synthesis. The reaction involves the coupling of a terminal alkyne and an aryl or vinyl halide by the catalization of palladium catalyst as well as copper co-catalyst. The Sonogashira coupling reaction is used extensively since it can be performed under mild conditions. The reaction can be carried out in aqueous medium at room temperature by using mild base, which allows the usage of Sonogashira coupling reaction for the synthesis of complex molecules and conjugated polymers.[33] Similar with Stille and Suzuki coupling mechanisms, palladium precatalyst species need to be activated to form a Pd(0) complex. Then, the active Pd(0) catalyst mediate into the aryl or vinyl halide to produce Pd(II) species by oxidative addition. This step is believed to be rate determining step. The obtained complex reacts with copper acetylide in the transmetallation step forming another complex and regenerating the copper catalyst. It is followed by the reductive elimination step where the final product is formed and palladium catalyst is

regenerated.[34] The complete mechanism of the Sonogoshira coupling reaction is shown in Figure 1.6. The base used in the reaction is typically an amine such as diethylamine which also acts as the solvent. The reaction medium should be basic in order to neutralize the halogen halide that produced as byproduct of the reaction, so the alkylamine compounds could be used as solvent. DMF, ACN and THF are the other solvents that could be used in the reaction.[35]

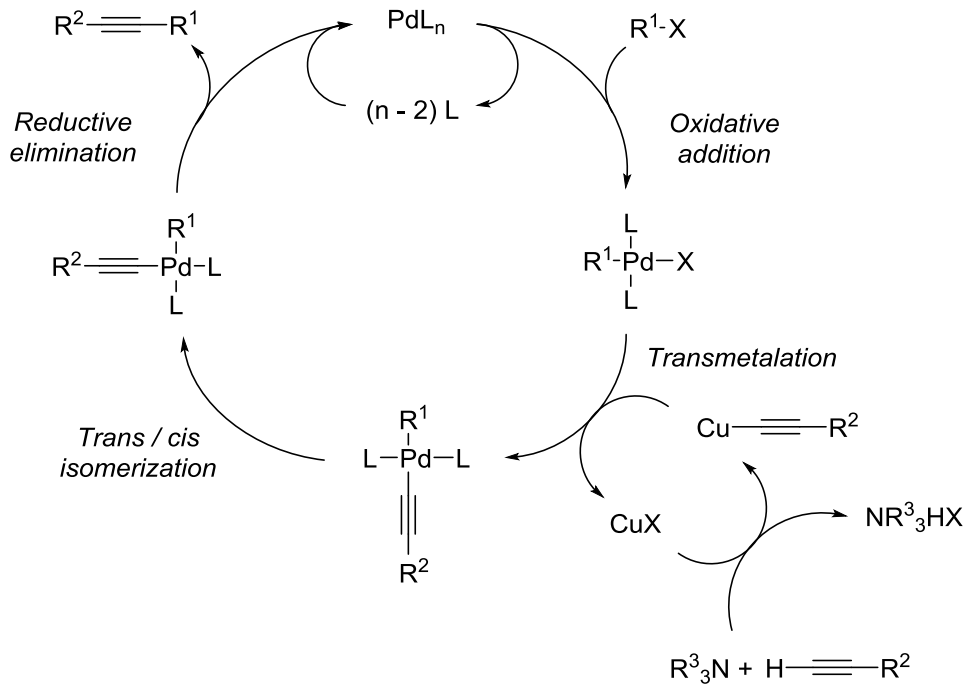

Figure 1.8. Mechanism of Sonogashira coupling polymerization

1.3 Band Gap Engineering

Band gap of a conjugated polymer is a very important parameter since it determines the conductivity and color of the material hence the optoelectronic properties such as absorption wavelength. The electronic and optical properties of a material are crucial in terms of application areas. Therefore, fine tuning of the band gap is necessary to control the final properties of the polymer. There are some synthetic strategies for arranging the band gap of conjugated polymers to achieve desired applications. These strategies are based on five main factors that affect the band gap

of conjugated polymers which are planarity, bond length alternation, resonance effects, donor acceptor approach and intramolecular interactions.[36]

Aromatic systems have high stability and structural flexibility due to the resonance effect. Therefore, aromatic systems have the most proper basic structures in order to synthesize low band gap conjugated polymers. However, increasing the aromaticity on the polymer structure increases the band gap due to high rigidity of the system. Inserting double bonds into polymer chain alongside the aromatic rings is an effective approach to reduce the band gap of a conjugated polymer. Ethylene linkages also help to reduce the torsion angle that caused by steric interactions between adjacent aromatic rings and to provide a planar geometry for the conjugated system. Moreover, smaller bond length alternation value is obtained by introducing double bonds between the adjacent rings. The reason for that is the equalization of the carbon-carbon bond length on the polymer chain. Intramolecular interactions between the polymer chains can be obtained by inserting functional structures on the polymer backbone. Donor-acceptor approach is one of the most efficient strategies to alter the band gap of conjugated polymers. Inserting electron donating groups into the polymer backbone raises the HOMO level and inserting electron withdrawing groups lowers the LUMO level of the material, resulting in a reduced band gap. Havinga et al. proposed the usage of alternating electron donating and accepting units in the polymer chain.[37] Since then, low band gap conjugated polymers are obtained by synthesizing donor-acceptor type alternating copolymers.

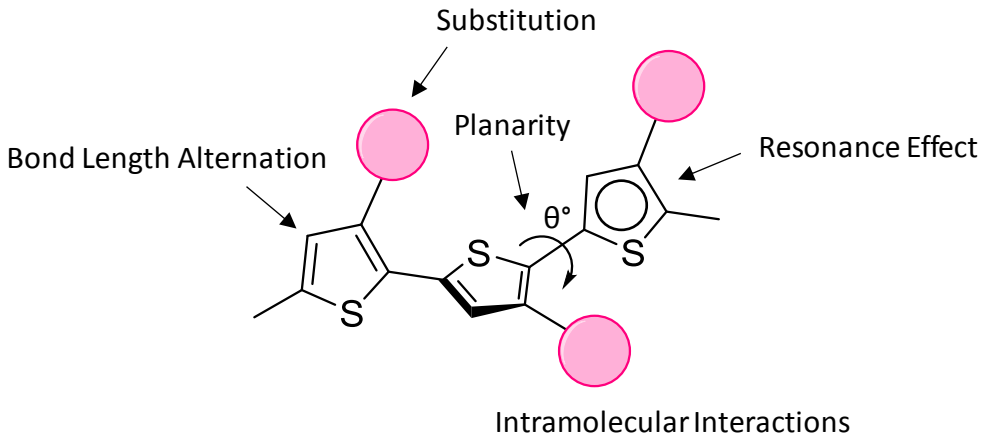

Figure 1.9. Structural factors determining the band gap of conjugated polymers

1.3.1 Donor-Acceptor Approach

Donor-acceptor (D-A) approach was initially proposed by Havinga et al. to reduce the band gap of conjugated polymers.[37] Narrow band gap and high chain mobility are required for intrinsic conduction of the polymers and obtained via wide bandwidths. As it was mentioned above, donor-acceptor concept is an effective way to adjust the band gap. In this approach, electron rich donor and electron deficient acceptor units are introduced alternatively in close conjugation along the polymer chain. Alternating donor and acceptor units result in the broadening of the valence and conduction bands causing the reduction of band gap. In this approach, HOMO energy level of the donor unit and LUMO energy level of the acceptor unit act as the HOMO level and the LUMO level of the polymer. Reducing the band gap by this approach enhances the electronic and optical properties of the polymer by increasing the intrinsic conductivity and changing the color of the polymer.[38]

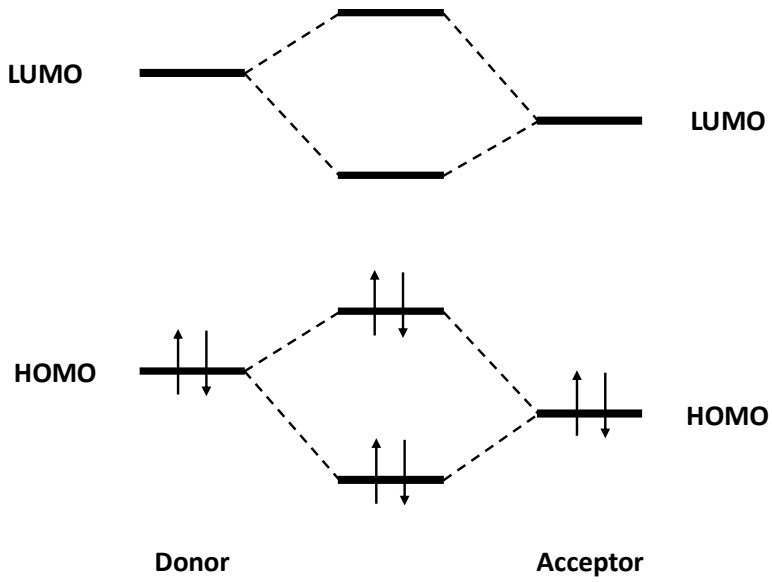

Figure 1.10. Orbital interactions between donor and acceptor units of D-A type conjugated polymers

1.4 Electrochromism

Chromism is defined as the reversible color change of materials by external stimulation. There are several types of chromism in terms of the external factors that cause it. These are thermochromism, photochromism, solvatochromism, halochromism and electrochromism.[39] Thermochromism is induced by change of temperature, when photochromism is induced by the light irradiation based on the isomerization between two different molecular structures. Solvatochromism caused by the polarity of the solvent and halochromism is initiated by the pH change. Finally, electrochromism is provided by gain and loss of electrons on the material. Electrochromism is the reversible change in the optical properties of a material such as color and opacity by applied voltage. It is the result of absorption of the material at different wavelengths during redox processes. Different absorption bands of the materials cause color change which can be detected by human eye. Electrochromism was initially discovered by thin films of WO_3 and MO_3.[40] After many researches conducted in this area, electrochromic materials gained popularity due to their

potential of usage in optical devices. This situation led new electrochromic materials to be discovered.[41]

1.4.1 Electrochromic Materials

1.4.1.1 Metal Oxides

Oxides of transition metals such as cerium, chromium, cobalt, iridium, iron, manganese, molybdenum, nickel, palladium, ruthenium, tungsten and vanadium possess electrochromism either as anodically or cathodically coloring materials. Especially the oxides of iridium, molybdenum, nickel and tungsten display the most intense color change upon applied potential among all these materials. The history of electrochromic materials began with the discovery of tungsten trioxide, WO_3.[40] Berzelius showed the color change of WO_3 by the reduction with hydrogen gas.[42] Following that, Wöhler performed an experiment by reducing WO_3 using sodium metal yielding a color change.[43] WO_3 displays a very pale yellow color in its oxidized state of W^{+6} where it shows a deep blue color upon electrochemical reduction to the state of W^{+5}. Oxides of molybdenum, tungsten and vanadium are cathodically coloring materials. On the contrary, some of the metal oxides which are cobalt, iridium and nickel are anodically coloring materials.[44]

1.4.1.2 Viologens

Viologens or 1, 1'-disubstituted 4,4'-bipyridinium ions by another name, are the salts that are synthesized from 4,4'-bipyridine molecules. In 1933, Michaelis et al. reported the electrochromic properties of these salts and named them as "viologens".[45] Due to their unique electrochromic properties, viologens have been used as herbicides, indicator and electron-transfer mediators. In recent years, viologens or viologen/polymer blends are gained interest for the construction of electrochromic display devices such as liquid crystal displays (LCDs) or light

emitting diodes (LEDs). Viologens have three redox states, which are V^{+2}, V^{+} and V^{0}. The most extensively used viologen is methyl viologen. When it is reduced to the radical cation form it displays color due to intramolecular electronic transition of a delocalized positive charge. The most stable state is dication form which is colorless due to the higher aromaticity.[46]

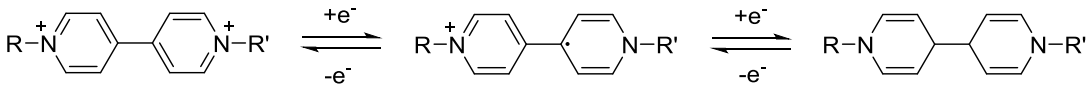

Figure 1.11. Redox states of viologen

1.4.1.3 Prussian Blue

Prussian blue was the earliest synthetic pigment due to its intense blue color discovered accidentally in 1706.[47] It has the chemical formula of $Fe_4^{III}[Fe^{II}(CN)_6]_3$ and it is produced by oxidation of ferrous ferrocyanide salts. After the discovery of electrochemical properties of Prussian blue, it has withdrawn great attention in electrochromic device applications. Prussian blue is an example for polynuclear transition-metal hexacyano metallates which are insoluble compounds. There is intervalence charge transfer (IVCT) between the different mixed-valence iron states cause to the intense blue color. Prussian blue is produced by the oxidation of ferrous ferrocyanide salts which are white solids having the formula of $M_2Fe[Fe(CN)_6]$ where M^+ is Na^+ or K^+. This material has no deep color due to the mixed valency since the iron in this material is all ferrous. Oxidation of this salt with hydrogen peroxide or sodium chlorate helps to the production of ferricyanide affording to Prussian blue. Although, Prussian blue is prepared from cyanide salts, it is not toxic since the cyanide groups are tightly bound to iron.[48]

1.4.1.4 Conjugated Conducting Polymers

Conjugated conducting polymers are advantageous materials for electrochromic device applications since they combine the electronic and optical properties of semiconductors with the mechanical properties of polymers.[41] Polymers of aniline, thiophene, pyrrole and carbazole molecules are some examples for electrochemically active conducting polymers. They are insulators in their neutral states but they become electroactive upon doping process. Positive charge carriers are formed on delocalized π-electron system of the polymer upon p-doping which is cation addition via oxidation process. Negative charge carriers are formed upon n-doping which is anion addition. Conjugated polymers can switch colors between a colored and a transparent state or they can show multicolored states upon applied potentials.[49] Band gap is the most significant parameter that determines the electrochemical properties of conjugated polymers. The optical band gap of the conjugated polymers is related with the maximum absorption wavelengths hence the color displayed by the polymer.

1.5 Electrochromic Devices

Electrochromic devices (ECDs) attracted increasing attention due to their unique optical properties such as continuous and reversible absorption, optical transmission, emittance and/or reflectance by applied voltage.[50] These properties enable ECDs to be used in the applications of electrochromic mirrors, smart glasses[51] and electrochromic display devices[52]. ECDs are a kind of electrochromic cells. The device structure of ECD consists of two electrodes separated by two electrochromic layers with an ion-conducting electrolyte between them. The device works by applying external voltage to the conducting electrodes which are standing at the either side of both electrochromic layers. ECDs can be separated into two main categories which are reflective devices and absorptive/transmissive devices. They contain at least two electrodes which are separated by an ionically conductor and

electronically insulator ion-containing electrolyte. One of the electrodes is an optically transparent electrode which is generally a glass slide coated with a transparent conductive oxide such as indium tin oxide (ITO) or fluorinated tin oxide (FTO). If the ECD is operating in absorptive/ transmissive mode, second electrode is also optically transparent electrode coated with transparent conductive oxide. Distinctively, if the device is operating in reflective mode, the second electrode is a polished metal which has good electronic conductivity and reflective. ECD can also be categorized in two types according to the electrolyte used in the device construction, such as laminated ECD where electrolyte is a liquid gel and solid-state ECD where electrolyte is a solid inorganic or organic material. In the basic construction of an absorptive/ transmissive type ECD, one of the electrochromic materials is cathodically coloring and the other one is anodically coloring. The working principle of the device is based on switching between a colored state and a transparent state or between multicolored states. Electrochromic layers are coated onto transparent conductive oxide coated electrodes and they are placed face to face with the electrolyte in between them. ECDs are used in rear-view mirrors, displays, smart windows, sunroofs and shutters.

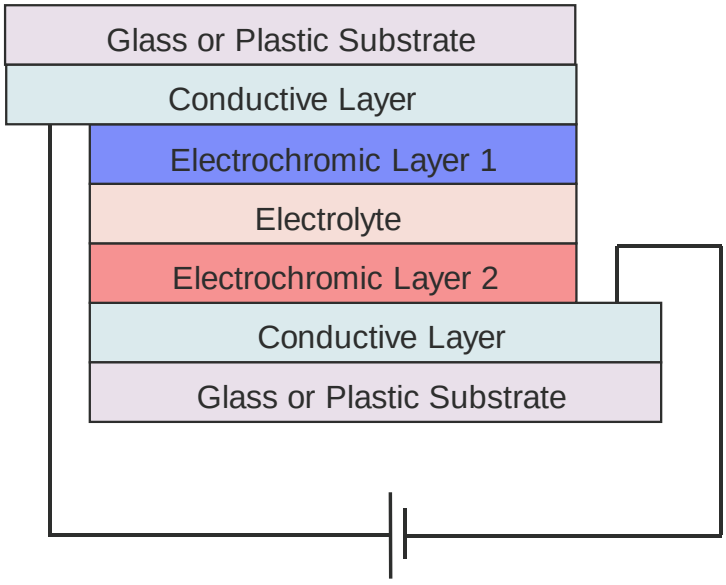

Figure 1.12. General diagram of electrochromic devices

1.5.1 Examples of Electrochromic Devices

1.5.1.1 Rear-view Mirrors

Rear-view mirrors are in the category of reflective electrochromic devices. They are self-darkening mirrors having electrochromic gel between two glass sheets that regulate reflections of flash light by the help of a sensor. Sensor attached on the mirror detects the intensity of flash light coming from the following vehicles in night and sends voltage to the electrochromic gel causing it to darkening of gel hence the mirror. Darkening of the gel is proportional with the intensity of detected light, allowing the driver to see through the mirror without discomfort.[53]

1.5.1.2 Smart Windows

Smart windows are electrochromic devices that can automatically control the amount of light and solar energy that passes through the windows improving the indoor comfort. They are very popular since controlling the transmittance and reflectance of light is important by the means of energy efficiency of buildings, aircrafts, and etc. When the direct sun does not pass through, the windows are fully bleached at their neutral states, and after the direct sun hits to the window they switch to a darker transparent state.[51]

1.5.1.3 Electrochromic Displays

Electrochromic displays have a wide range of research area since they have promising commercialization potentials in flat-panel display devices and novel paper-like display devices, the so-called e-paper.[9] It is necessary to use electrochromic materials that exhibit clear color changes from transparent to RGB colors (red, blue, green) for these applications. The flat-panel display and novel paper-like display application technology could be used in a wide range of

electronic devices such as advertising boards, calculators, watches, and tablet screens.[52]

1.6 Near-IR Absorbing Conjugated Polymers

Popularity of conjugated polymers that absorb in near-IR (NIR) region increased considerably in recent years owing to their unique properties.[54] They are promising materials for many applications such as electrochromic windows, photothermal conversion agents[54], camouflage materials, thermal emission detectors[55] and organic photovoltaics.[56] Low-band gap conjugated polymers possess some unique properties such as stability in spectrochemical p- and n- doping processes and absoption in NIR region during doping process. As it was mentioned above, these materials have a great potential for electrochromic device applications.[57] Most of the commercial electrochromic systems have a limited design that functions only in visible region of solar spectrum. However, solar energy consists of 7.9% ultraviolet (UV), 45.5% visible radiation and 46.7 % near-IR (NIR) radiation meaning over the half of total solar energy is not in the visible region of the spectrum. The extended absorption band reaching to NIR region promoted by low band gap leads the polymer to harvest more light from the solar spectrum which is a rare and useful property in many application areas.[58] Regarding these facts, NIR absobing conjugated polymers are great candidates to enhance the optical and electronic properties of resulting devices such as electrochromic windows providing substantial energy savings for international air-conditioning and heating.

1.7 Aim of the Study

Improvements of the applications of conjugated polymers strongly depends on the band gap and optoelectronic properties. Preparation of low band gap conjugated polymers is possible by using donor-acceptor approach and stabilization of quinoid resonance structure. The motivation of this study is investigating the effect of strong

electron withdrawing units on the band gap and optoelectronic properties of conjugated polymers. Research studies showed that benzo[1,2-*c*;4,5-c']bis[1,2,5]thiadiazole (BBT) derivatives are strong electron acceptors revealing high mobilities and low band gaps with low LUMO levels.[59,60] However, the disadvantage of those units is poor solubility due to the rigid structure of molecule, strong quinonoid contributions and hypervalent sulfurs. Selenium analogues of BBT are even less soluble since short interatomic contacts are attributed to secondary bonding interactions. Inserting long and branched alkyl chains on the polymer backbone is an effective solution to overcome the solubility problem resulting in high molecular weight and processable polymers. Therefore, branched alkyl chains are substituted to 5H-[1,2,3]triazolo[4',5':4,5]benzo[1,2-c][1,2,5]thiadiazole and 5H-[1,2,3]triazolo[4',5':4,5]benzo[1,2-c][1,2,5]selenadiazole units for enhanced solubility of polymers which ease the processability hence device constructions. [1,2,5]Chalcogenazolo[3,4-f]-benzo[1,2,3]triazole derivatives are pointed as strong electron acceptor units due to the hypervalent sulfur and selenium in the chalcogenazole linkage narrowing the band gap of the polymers due to their ability of adopting a quinoidal structure on the π-electron system through D-A interactions.[61] However, chalcogenazole linkages are better described as three-center-four-electron bond which the central chalcogen (sulfur/selenium) atom is expected to bear a +1 charge.[62] Therefore, decrease in the LUMO energy levels and the band gaps of the polymers is observed due to the electron deficiency on these systems. Strong interactions between the donor and acceptor units in the polymer backbone cause to electron polarization and electron transfer on the π-bridge which stands in between the electron donor and electron acceptor on the polymer backbone due to the resonance contribution. These strong interactions and the charge transfer through the π-bridge cause to intramolecular charge transfer (ICT) alongside the π–π* transition within the polymer backbone.[63,64] Additionally, the interaction between donor and acceptor units are remarkably affected by conjugated linkers and hence the optical, electrochemical, charge transport and photovoltaic properties of D-π-A conjugated copolymers are enhanced. Furthermore, thiophene enables strong and

broad absorption, suitable molecular energy levels to ensure good charge separation properties resulting in good stability, high contrast and fast switching times. Polymers comprising thiophene could be good candidates for electrochromic device applications.

In this study, two novel near-IR absorbing conjugated polymers are aimed to be synthesized considering the importance of these materials in many application areas. The donor-acceptor type conjugated copolymers are designed and synthesized comprising [1,2,5]chalcogenazolo[3,4-f]-benzo[1,2,3]triazole derivatives as the acceptor units and benzodithiophene as the donor unit with thiophene π-bridge. The polymers were synthesized via Stille polycondensation reaction obtaining the described design and were characterized to determine the optoelectronic properties revealing the multichromic oxidation and reduction states of both polymers. Finally, an electrochromic device was constructed and characterized using the polymer PSeBT, due to its lower band gap and better switching colors displayed in all RGB than its sulfur analogue.

CHAPTER 2

EXPERIMENTAL

2.1 Materials and Methods

All chemicals were commercially available and used without further purification in the syntheses and characterizations of the polymers unless otherwise mentioned. All dry solvents used in reactions were directly obtained from the MBraun MBSPS5 solvent drying system. Column chromatography was performed using thick-walled glass columns and Silica Gel 60 (Merck 230-400 mesh) for the purification processes. Thin-layer chromatography (TLC Merck Silica Gel 60 F254) was performed by commercially available 0.25 mm silica gel plates for monitoring the reactions and assisting the purification processes. The relative proportions of solvents in chromatography solvent mixtures refer to the volume: volume ratio. Structural characterizations of compounds were performed with ^{1}H and ^{13}C NMR spectra which were recorded on Bruker Avance III Ultrashield (400 MHz) spectrometer using $CDCl_3$ and *d6*-DMSO as the solvents. The chemical shifts were reported in parts per million (ppm) downfield from an internal TMS (trimethylsilane) reference. Coupling constants (J) were reported in hertz (Hz), and the spin multiplicities were specified by the symbols of s (singlet), d (doublet), t (triplet) and m (multiplet). High-resolution mass spectroscopy measurements were performed by Waters Synapt G1 High Definition Mass Spectrometer. Gel Permeation Chromatography (GPC) was carried out to determine the average molecular weights and polydispersity index of polymers with Shimadzu GPC, with the standards of polystyrene where the eluent was chloroform. FTIR spectra of the polymers were obtained by Bruker IFS 66/S Hyperion 1000. Electrochemical studies were utilized by GAMRY Reference 600 Potentiostat by using a three-electrode cell system using indium tin oxide (ITO) coated glass slide as the working electrode, Pt wire as the

counter electrode, and Ag wire as the reference electrode in 0.1 M solution of tetrabutylammonium hexafluorophosphate/acetonitrile (ACN). HOMO and LUMO energy levels of polymers were calculated considering the value of NHE as -4.75 eV with respect to the vacuum level. Spectroelectrochemical characterizations and kinetic studies of the polymers were carried out with Jasco V770.

2.2 General Synthetic Route of Monomers and Polymers

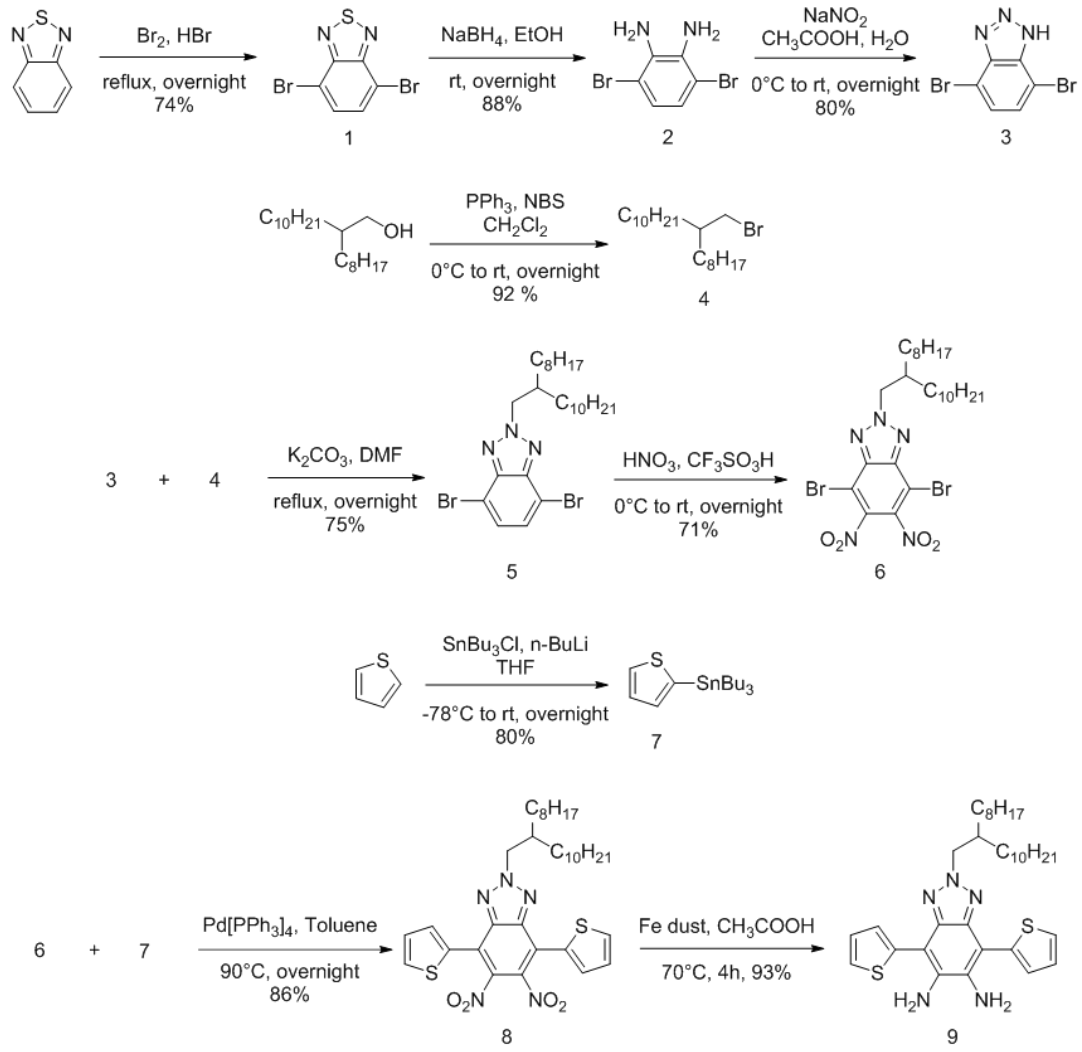

Figure 2.1. Synthetic pathway of monomers part 1

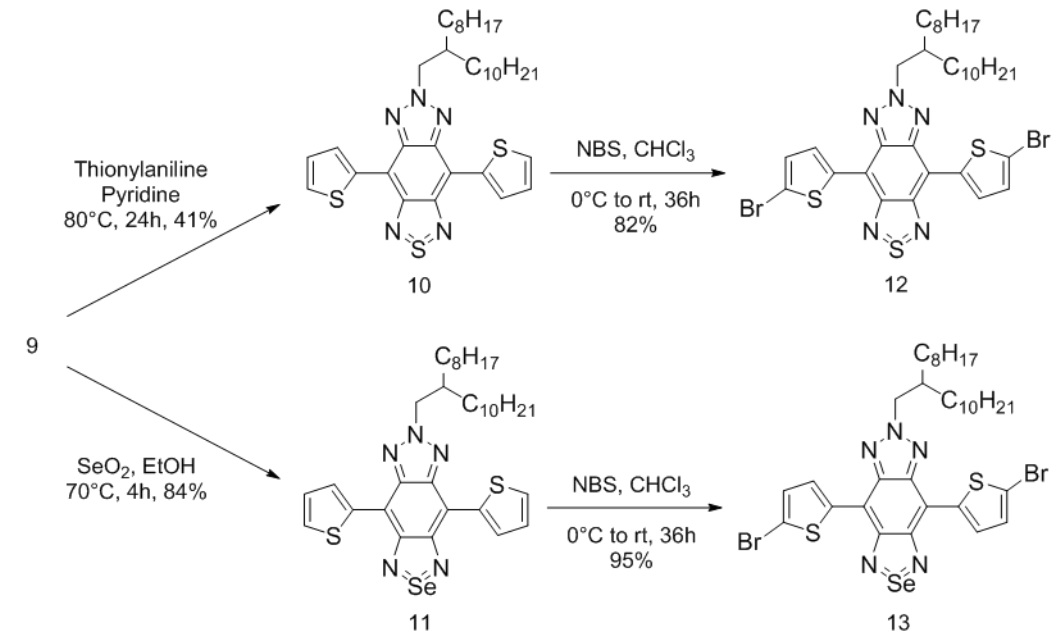

Figure 2.2. Synthetic pathway of monomers part 2

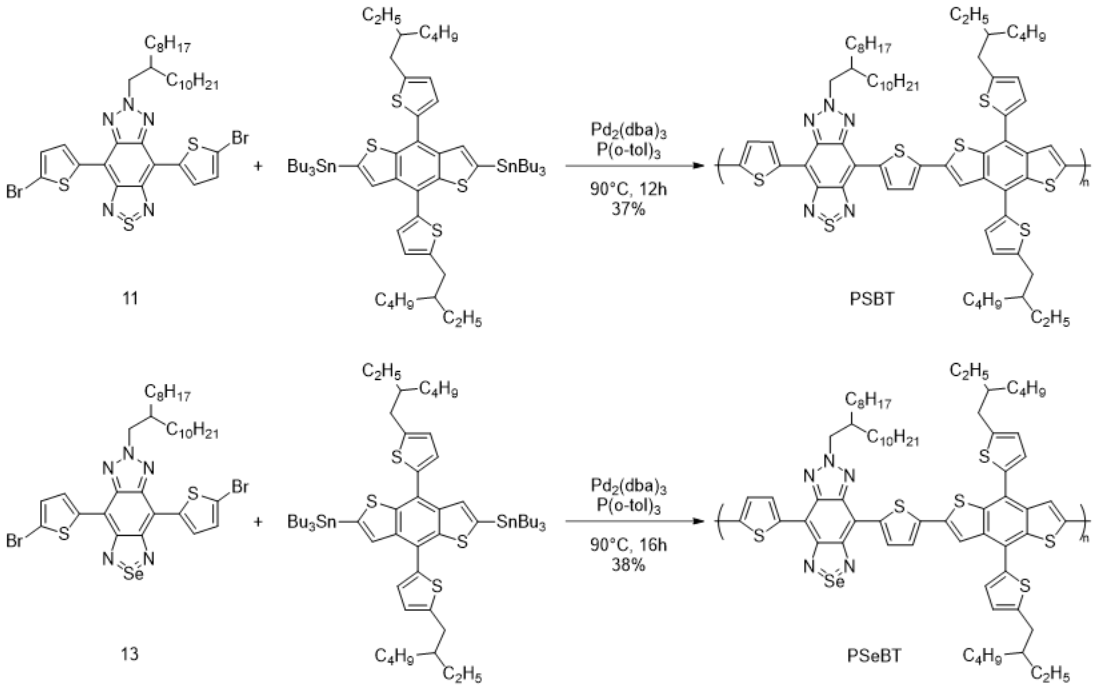

Figure 2.3. Synthetic pathway of polymers

2.3 Synthesis of Monomers

2.3.1 Synthesis of 4,7-dibromobenzothiadiazole (1)

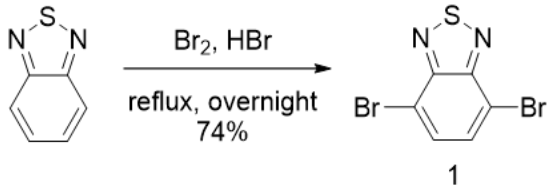

Figure 2.4. Synthetic route of 4,7-dibromobenzothiadiazole (1)

Benzothiadiazole (4.00 g, 29.4 mmol) was dissolved in HBr (72 mL, 47%) and a solution of bromine (3.2 mL, 62.3 mmol) in HBr (32 mL, 47%) was added drop wise at 100 °C. Temperature of reaction was raised to 135 °C and reaction mixture was stirred overnight. The mixture was cooled to room temperature and excess bromine was washed with $NaHSO_3$ solution through the filter paper. Residue was dissolved in DCM and extracted with brine and distilled water. Organic layers were combined and dried over anhydrous $MgSO_4$ and solvent was removed under reduced pressure. Pure product was obtained as yellow solid by washing with cold diethyl ether (6.14 g, 74%). ^{1}H NMR (400 MHz, $CDCl_3$) δ: 7.71 (s, 2H); ^{13}C NMR (100 MHz, $CDCl_3$) δ: 152.9, 132.4, 113.9.

2.3.2 Synthesis of 3,6-dibromobenzene-1,2-diamine (2)

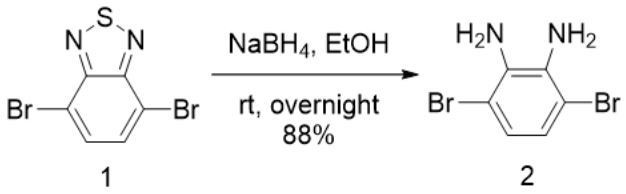

Figure 2.5 Synthetic route of 3,6-dibromobenzene-1,2-diamine (2)

4,7-Dibromobenzothiadiazole (5.80 g, 19.7 mmol) was dissolved in ethanol (110 mL) and $NaBH_4$ (29.0 g, 0.77 mol) was added portion wise into the mixture at 0 °C. Reaction mixture was stirred overnight at room temperature. Ethanol was removed

under reduced pressure and the remnant was dissolved in diethyl ether. The product was extracted using distilled water, organic phases were combined and dried over anhydrous $MgSO_4$. Solvent was removed under reduced pressure and product was obtained without further purification as an ivory solid (4.62 g, 88%). ^{1}H NMR (400 MHz, DMSO-*d6*) δ: 6.59 (s, 2H), 4.98 (s, 4H); ^{13}C NMR (100 MHz, DMSO-*d6*) δ: 133.1, 120.6, 106.6.

2.3.3 Synthesis of 4,7-dibromo-1H-benzo[d][1,2,3]triazole (3)

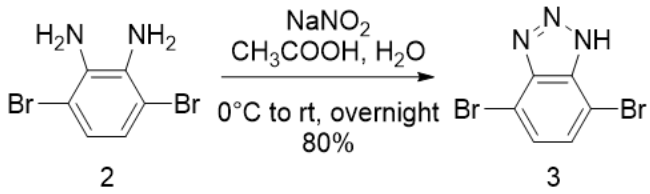

Figure 2.6. Synthetic route of 4,7-dibromo-1H-benzo[d][1,2,3]triazole (3)

3,6-Dibromobenzene-1,2-diamine (4.15 g, 15.6 mmol) was dissolved in acetic acid (40 mL) and a solution of $NaNO_2$ (1.21 g, 17.5 mmol) in water (48 mL) was added at 0 °C. Reaction mixture was stirred at 0 °C for 2 h, then it was allowed to reach room temperature and stirred overnight. Reaction mixture was filtered to obtain the crude product and washed with distilled water. Pure product was obtained as brown solid by recrystallization with methanol (3.46 g, 80%). ^{1}H NMR (400 MHz, DMSO-*d6*) δ: 7.61 (s, 2H); ^{13}C NMR (100 MHz, DMSO-*d6*) δ: 152.2, 132.7, 113.1.

2.3.4 Synthesis of 9-(bromomethyl)nonadecane (4)

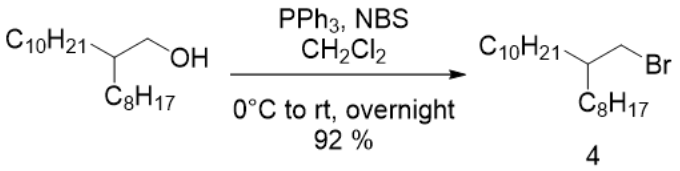

Figure 2.7. Synthetic route of 9-(bromomethyl)nonadecane (4)

2-Octyl-1-dodecanol (7.66 mL, 21.5 mmol) was mixed with DCM (20 mL) under argon atmosphere. Triphenylphospine (8.11 g, 30.9 mmol) was added into the mixture at 0 °C and mixture was stirred for 30 minutes. N-Bromosuccinimide was added into the reaction mixture portion wise at 0 °C, then reaction mixture was stirred at room temperature overnight. DCM was removed under reduced pressure and crude product was obtained by washing the residue with cold hexane. The pure product was obtained as a colorless oil by column chromatography on silica gel using hexane (7.17 g, 92 %). ^{1}H NMR (400 MHz, $CDCl_3$) δ: 3.44 (d, 2H, J=4.7 Hz), 1.61 - 1.56 (m, 1H), 1.32 - 1.22 (m, 32H), 0.88 (t, 6H, J=6.7 Hz); ^{13}C NMR (100 MHz, $CDCl_3$) δ: 39.62, 39.50, 32.57, 31.93, 29.82, 29.67, 26.58, 22.72, 14.13.

2.3.5 Synthesis of 4,7-dibromo-2-(2-octyldodecyl)-2H-benzo[d][1,2,3]triazole (5)

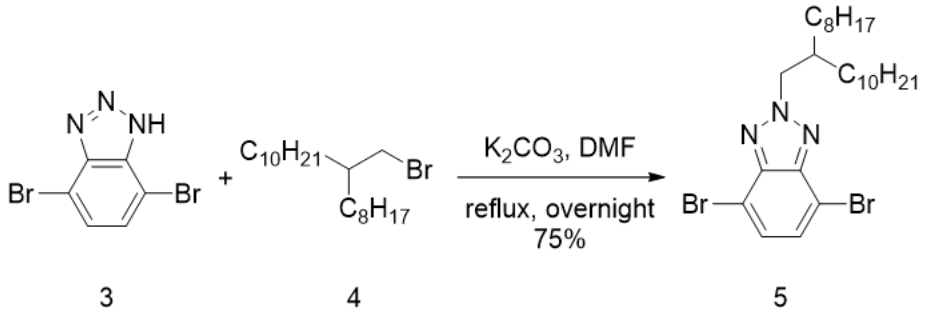

Figure 2.8. Synthetic route of 4,7-dibromo-2-(2-octyldodecyl)-2H-benzo[d][1,2,3]triazole (5)

4,7-Dibromo-1H-benzo[d][1,2,3]triazole (3.16 g, 11.4 mmol) and potassium carbonate (2.21 g, 16.0 mmol) were dissolved in anhydrous DMF (45 mL) and reaction temperature was raised to 100 °C. 9-(Bromomethyl)nonadecane (4.94 g, 13.7 mmol) was added into the mixture at 100 °C and mixture was stirred overnight. DCM was used to extract the product and the organic layer was washed with water and brine, respectively. Organic layers were combined and dried over Na_2SO_4. Then, the solvent was removed under reduced pressure. Product was purified by column chromatography on silica gel using 1:1 hexane: dichloromethane and recovered as a yellowish oil (4.78 g, 75 %). ^{1}H NMR (400 MHz, $CDCl_3$) δ: 7.42 (d, 2H, J=2.4 Hz), 4.66 (d, 2H, J=7.3 Hz), 2.38 – 2.28 (m, 1H), 1.38 – 1.15 (m, 32H), 0.90 – 0.82 (m, 6H); ^{13}C NMR (100 MHz, $CDCl_3$) δ: 143.6, 129.4, 110.0, 61.13, 39.02, 31.86, 31.18, 29.77, 29.58, 29.41, 29.33, 29.23, 26.03, 22.65, 14.10.

2.3.6 Synthesis of 4,7-dibromo-5,6-dinitro-2-(2-octyldodecyl)-2H-benzo[d][1,2,3]triazole (6)

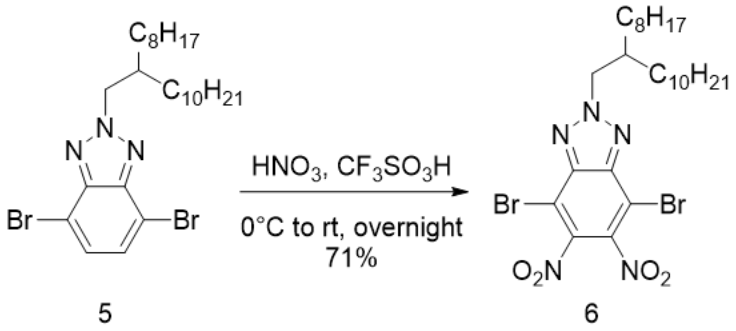

5 6

Figure 2.9. Synthetic route of 4,7-dibromo-5,6-dinitro-2-(2-octyldodecyl)-2H-benzo[d][1,2,3]triazole (6)

Trifluoromethane sulfonic acid (5.10 mL, 57.4 mmol) was added into dry DCM (110 mL) under argon atm at 0 °C. Fuming nitric acid 100% (1.2 mL, 28.7 mmol) was also added into the mixture drop wise at 0 °C and reaction mixture was stirred for 1h in order to obtain a white crystalline solid. Solution of 4,7-dibromo-2-(2-octyldodecyl)-2H-benzo[d][1,2,3]triazole (4.00 g, 7.18 mmol) in DCM (36 mL) was added drop wise into the reaction mixture at room temperature and reaction was stirred overnight. Reaction mixture was poured into ice-water, after the mixture allowed to reach the room temperature, the product was extracted with DCM and washed with distilled water and $NaHCO_3$ solution. Pure product was obtained as pale yellow solid by column chromatography on silica gel using 1:1 hexane: dichloromethane[65] (3.32 g, 71 %). ^{1}H NMR (400 MHz, $CDCl_3$) δ: 4.70 (d, 2H, J=7.0 Hz), 2.30 - 2.21 (m, 1H), 1.30 – 1.15 (m, 32H), 0.80 (t, 6H, J=6.7 Hz); ^{13}C NMR (100 MHz, $CDCl_3$) δ: 143.1, 141.9, 107.2, 62.16, 39.30, 31.91, 31.14, 29.71, 29.60, 29.42, 29.33, 29.24, 26.02, 22.69, 14.11.

2.3.7 Synthesis of tributyl(thiophen-2-yl)stannane (7)

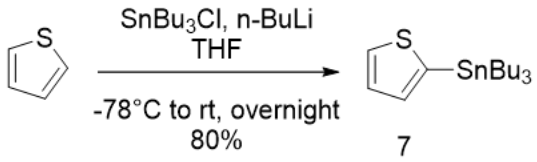

Figure 2.10. Synthetic route of tributyl(thiophen-2-yl)stannane (7)

Thiophene (2 g, 23.8 mmol) was dissolved in dry THF (22 mL) under argon atmosphere. At -78 °C, n-butyl lithium (10.5 mL 2.5 M in hexane, 26.1 mmol) was added drop wise and the solution was stirred for 1.5 h while maintaining the temperature. Then, tributyltin chloride (7.7 mL, 28.5 mmol) was added drop wise and the mixture allowed to reach the room temperature. Reaction mixture was stirred for 24 h at room temperature, then solvent was removed under reduced atmosphere. Crude product was extracted using dichloromethane and washed with distilled water and brine. Organic layers were combined and dried over anhydrous $MgSO_4$. Product was obtained as yellow oil after the removal of solvent under reduced pressure (8.89 g, 80 %). ^{1}H NMR (400 MHz, $CDCl_3$) δ: 7.68 (d, 1H, J=4.6 Hz), 7.30 (dd, 1H, J_1=4.6 Hz, J_2=3.2 Hz), 7.23 (d, 1H, J=2.6 Hz), 1.65 – 1.54 (m, 6H), 1.39 – 1.33 (m, 6H), 1.18 – 1. 10 (m, 6H), 0.95 – 0.90 (m, 9H); ^{13}C NMR (100 MHz, $CDCl_3$) δ: 136.2, 135.2, 130,6, 127.8, 29.00, 27.31, 13.71, 10.83.

2.3.8 Synthesis of 5,6-dinitro-2-(2-octyldodecyl)-4,7-di(thiophen-2-yl)-2H-benzo[d][1,2,3]triazole (8)

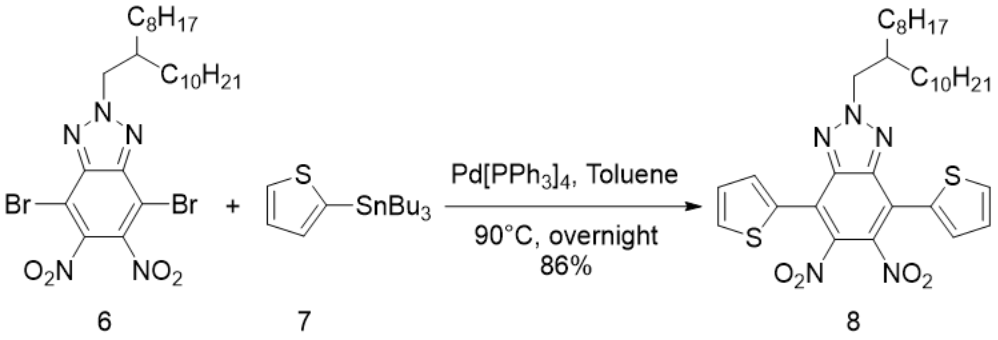

Figure 2.11. Synthetic route of 5,6-dinitro-2-(2-octyldodecyl)-4,7-di(thiophen-2-yl)-2H-benzo[d][1,2,3]triazole (8)

4,7-Dibromo-5,6-dinitro-2-(2-octyldodecyl)-2H-benzo[d][1,2,3]triazole (1.0 g, 1.54 mmol) and tributyl(thiophen-2-yl)stannane (2.31 g, 6.18 mmol) were added into a 100 mL of two necked round bottomed flask and vacuum/argon backfill was done. After the mixture kept under argon atmosphere for 1 h, tetrakis(triphenylphosphine)palladium(0) (0.18 g, 0.15 mmol) and toluene (40 mL) were added and temperature was raised to 90 °C. After the reaction was stirred for 18 h at 90 °C, toluene was removed under reduced pressure. Pure product was obtained as yellow solid by column chromatography on silica gel 2:1 hexane:dichloromethane (0.87 g, 86%). ^{1}H NMR (400 MHz, $CDCl_3$) δ: 7.66 (dd, 2H, J_1=5.1 Hz, J_2=1.0 Hz), 7.54 (dd, 2H, J_1=3.7 Hz, J_2=1.0 Hz), 7.21 (dd, 2H, J_1=5.1 Hz, J_2=3.8 Hz), 4.73 (d, 2H, J=6.7 Hz), 2.30 – 2.24 (m, 1H), 1.31 – 1.22 (m, 32H), 0.88 (t, 6H, J=6.5 Hz); ^{13}C NMR (100 MHz, $CDCl_3$) δ: 141.6, 139.7, 130.5, 130.3, 129.8, 127.9, 119. 5, 61.23, 39.20, 31.93, 31.28, 29.84, 29.65, 29.58, 29.3, 29.37, 26.14, 22.71, 14.15; HRMS (ESI, m/z): [M + H]+ calcd for C34H47N5O4S2, 653.3069; found, 653.3082.

2.3.9 Synthesis of 2-(2-octyldodecyl)-4,7-di(thiophen-2-yl)-2H-benzo[d][1,2,3]triazole-5,6-diamine (9)

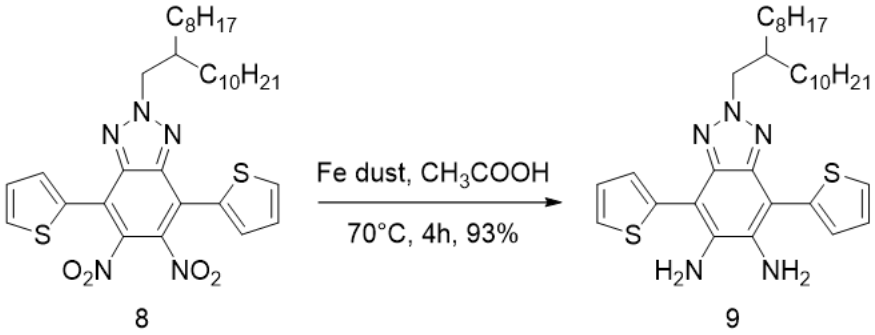

Figure 2.12. Synthetic route of 2-(2-octyldodecyl)-4,7-di(thiophen-2-yl)-2H-benzo[d][1,2,3]triazole-5,6-diamine (9)

5,6-Dinitro-2-(2-octyldodecyl)-4,7-di(thiophen-2-yl)-2H-benzo[d][1,2,3]triazole (0.79 g, 1.21 mmol) was dissolved in glacial acetic acid (24 mL) and iron dust (1.35 g, 24.2 mmol) was also added into the solution. Temperature of the reaction was raised to 70 °C and reaction mixture was stirred for 4 h. Reaction was quenched by pouring the mixture into distilled water and product was extracted by DCM. Organic layers were combined and dried over anhydrous Na_2SO_4. Product was obtained as yellow solid after the removal of solvent under reduced pressure[65] (0.67 g, 93 %). ^{1}H NMR (400 MHz, $CDCl_3$), δ: 7.49 (d, 2H, J=5.1 Hz), 7.45 (d, 2H, J=3.5 Hz), 7.23 (dd, 2H, J_1=5.1 Hz, J_2=3.6 Hz), 4.50 (d, 2H, J=7.0 Hz), 4.21 (s, 4H), 2.22 – 2.16 (m, 1H), 1.27 – 1.20 (m, 32H), 0.87 (t, 6H, J=7.0 Hz); ^{13}C NMR (100 MHz, $CDCl_3$) δ: 139.7, 136.1, 135.1, 127.8, 127.4, 126.3, 120.4, 59.49, 38.92, 31.92, 31.29, 29.97, 29.67, 29.61, 29.55, 29.38, 29.33, 26.16, 22.71, 14.15.

2.3.10 Synthesis of SBT (10)

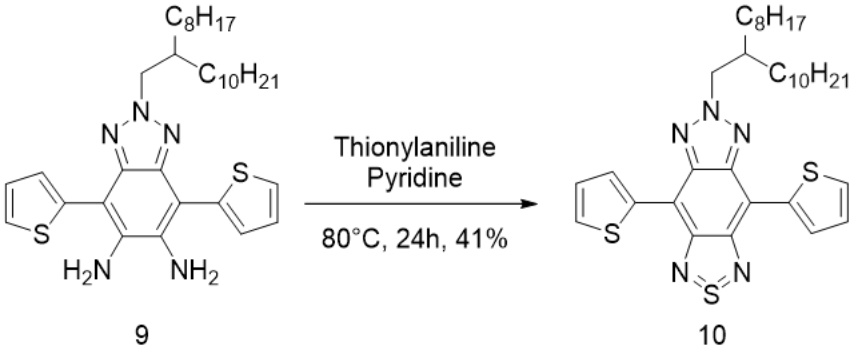

Figure 2.13. Synthetic route of SBT (10)

2-(2-Octyldodecyl)-4,7-di(thiophen-2-yl)-2H-benzo[d][1,2,3]triazole-5,6-diamine (0.45 g, 0.76 mmol) was taken to 50 mL of schlenk tube and kept under argon atmosphere for 1 h. N-Thionylaniline (0.21 g, 1.51 mmol) was also added and the mixture was dissolved in pyridine (12 mL). Reaction temperature was raised to 80 °C and the solution was refluxed for 24 h. Pyridine was removed under reduced pressure then residue was dissolved in dichloromethane and washed with dilute HCl and distilled water. Organic layers were combined and dried over anhydrous Na_2SO_4. After the solvent was removed under reduced pressure product was purified by column chromatography on silica gel using 1:2 dichloromethane:hexane as purple-blue solid[65] (0.19 g, 41 %). ^{1}H NMR (400 MHz, $CDCl_3$) δ: 8.87 – 8.83 (m, 2H), 7.64 -7.59 (m, 2H), 7.30 (dd, 2H, J_1=5.0 Hz, J_2=3.9 Hz), 4.88 (d, 2H, J=6.5 Hz), 2.45 – 2.38 (m, 1H), 1.47 – 1.36 (m, 8H), 1.29 – 1.20 (m, 24H), 0.89 – 0.82 (m, 6H); ^{13}C NMR (100 MHz, $CDCl_3$) δ: 147.8, 140.7, 135.1, 128.9, 127.2, 125.6, 109.9, 59.21, 37.25, 29.84, 29.52, 27.81, 27.56, 27.27, 24.27, 20.62, 12.06; HRMS (ESI, m/z): [M + H]+ calcd for C34H47N5S3, 621.2994; found, 621.2990.

2.3.11 Synthesis of SeBT (11)

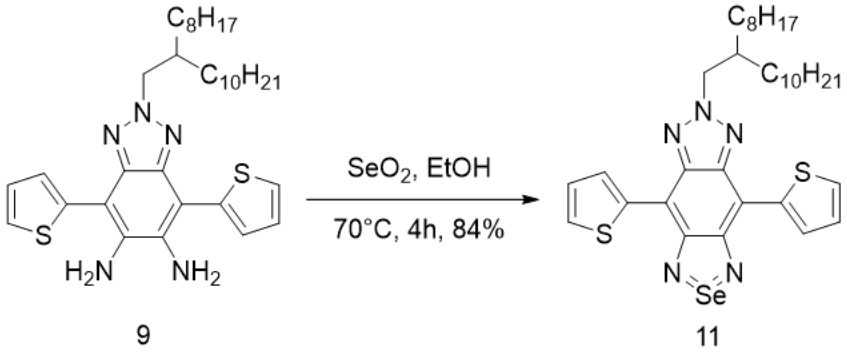

Figure 2.14. Synthetic route of SeBT (11)

2-(2-Octyldodecyl)-4,7-di(thiophen-2-yl)-2H-benzo[d][1,2,3]triazole-5,6-diamine (0.20 g, 0.34 mmol) was dissolved in ethanol (10 mL) under argon atmosphere. Selenium dioxide (0.05 g, 0.40 mmol) was also added and color change observed from yellow to blue. Reaction temperature was raised to 70 °C and solution was refluxed for 4 h. Ethanol was removed under reduced pressure. Product was purified by column chromatography on silica gel using 1:1 hexane: dichloromethane to obtain a green-blue solid[65] (0.19 g, 84 %). ^{1}H NMR (400 MHz, $CDCl_3$) δ: 8.80 (d, 2H, J=3.7 Hz), 7.60 (d, 2H, J=4.8 Hz), 7.26 (dd, 2H, J_1=8.5, J_2=4.4 Hz), 4.78 (d, 2H, J=6.5 Hz), 2.42 – 2.34 (m, 1H), 1.45 – 1.33 (m, 8H), 1.28 – 1.18 (m, 24H), 0.88 – 0.80 (m, 6H); ^{13}C NMR (100 MHz, $CDCl_3$) δ: 155.9, 143.2, 137.9, 131.2, 129.8, 127.4, 112.0, 61.24, 39.19, 31.95, 31.59, 29.92, 29.68, 29.38, 26.34, 22.72, 14.17; HRMS (ESI, m/z): [M + H]+ calcd for C34H47N5S2Se, 669.2438; found, 669.2442.

2.3.12 Synthesis of BrSBT (12)

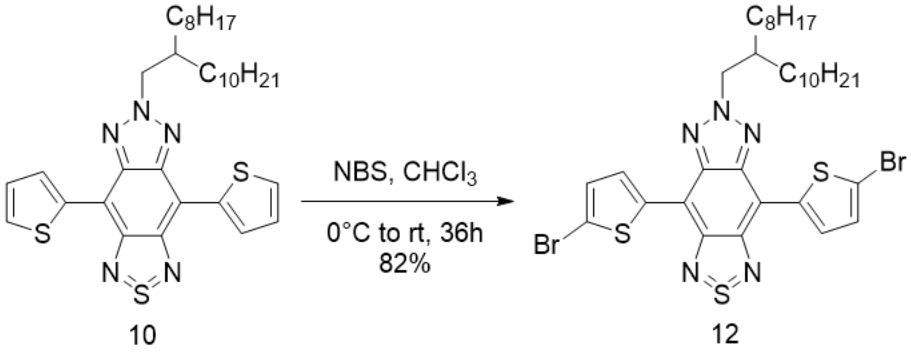

Figure 2.15. Synthetic route of BrSBT (12).

SBT (0.25 g, 0.40 mmol) was dissolved in chloroform (25 mL) and flask was taken to an ice-bath. N-Bromosuccinimide (0.16 g, 0.88 mmol) was added portion wise into the solution at 0 °C. Reaction mixture allowed to reach the room temperature and solution was stirred at dark for 36 h. Solution was poured into water to quench the reaction, product was extracted by dichloromethane and washed with $NaHCO_3$ solution and distilled water. Organic layers were combined, dried over anhydrous Na_2SO_4 and solvent was removed under reduced pressure. Pure product was obtained by column chromatography on silica gel using 1:3 dichloromethane: hexane[66] (0.26 g, 95%). ^{1}H NMR (400 MHz, $CDCl_3$) δ: 8.45 (d, 2H, J=4.1 Hz), 7.18 (d, 2H, J=4.1 Hz), 4.77 (d, 2H, J=6.4 Hz), 2.36 – 2.29 (m, 1H), 1.40 – 1.17 (m, 32H), 0.89 – 0.83 (m, 6H); ^{13}C NMR (100 MHz, $CDCl_3$) δ: 149.3, 142.1, 138.7, 131.1, 130.5, 117.8, 110.0, 61.20, 39.32, 31.93, 31.55, 29.91, 29.66, 29.36, 26.31, 22.70, 14.15.

2.3.13 Synthesis of BrSeBT (13)

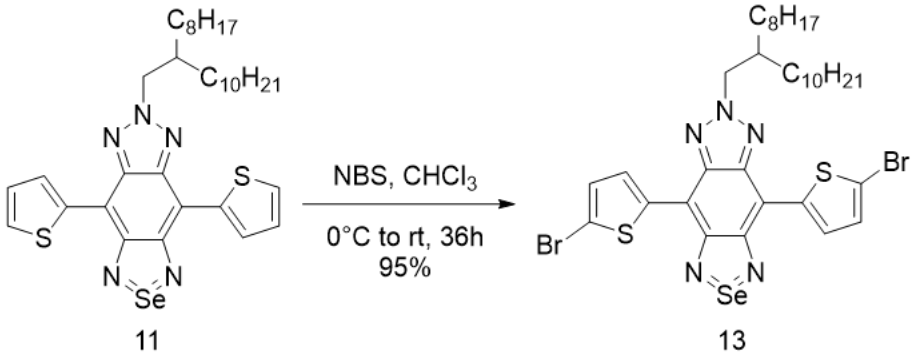

Figure 2.16. Synthetic route of BrSeBT (13)

SeBT (0.19 g, 0.28 mmol) was dissolved in chloroform (19 mL) and flask was taken to an ice-bath. N-Bromosuccinimide (0.11 g, 0.62 mmol) was added portion wise into the solution at 0 °C. Reaction mixture allowed to reach the room temperature and solution was stirred at dark for 36 h. Solution was poured into water to quench the reaction, product was extracted using dichloromethane and washed with $NaHCO_3$ solution and distilled water. Organic layers were combined, dried over anhydrous Na_2SO_4 and solvent was removed under reduced pressure. Pure product was obtained by column chromatography on silica gel using 1:2 dichloromethane: hexane[66] (0.23 g, 95%). ^{1}H NMR (400 MHz, $CDCl_3$) δ: 8.43 (d, 2H, J=4.1 Hz), 7.17 (d, 2H, J=4.2 Hz), 4.70 (d, 2H, J=6.5 Hz), 2.35 – 2.27 (m, 1H), 1.39 – 1.17 (m, 32H), 0.89 – 0.83 (m, 6H); ^{13}C NMR (100 MHz, $CDCl_3$) δ: 154.9, 142.3, 139.2, 131.1, 130.2, 118.4, 110.8, 61.1, 39.16, 31.96, 31.53, 29.97, 29.70, 29.41, 26.29, 22.74, 14.19.

2.4 Synthesis of Polymers

2.4.1 Synthesis of PSBT

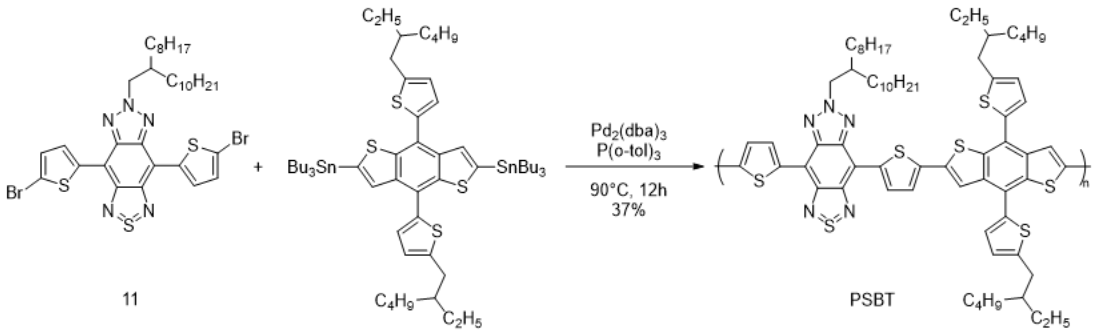

Figure 2.17. Synthetic route of PSBT

BrSBT (0.16 g, 0.21 mmol) and 4-(5-(2-ethylhexyl)thiophen-2-yl)-8-(5-(octan-3-yl)thiophen-2-yl)benzo[1,2-b:4,5b']dithiophene-2,6-diyl)bis(trimethylstannane (0.19 g, 0.21 mmol) were dissolved in anhydrous toluene (8 mL) in a 25 mL of schlenk tube. Tris(dibenzylideneacetone)dipalladium(0) (3.76 mg, 4.10 μmol) and tri(o-tolyl)phosphine (4.99 mg, 16.4 μmol) were also added into the solution and the solution was refluxed for 12 h at 90 °C under argon atmosphere. The reaction was monitored by TLC and tributyl(thiophen-2-yl)stannane (0.31 g, 0.82 mmol) was added as end-capper to remove bromine end groups and the reaction was stirred for 4 h. Then, chlorobenzene (0.27 g, 1.64 mmol) was added to remove the stannyl end groups and the reaction was stirred for another 4 h. After the reaction was completed, toluene was removed under reduced pressure and the resulting product was precipitated in cold methanol. Product was filtered and purified by Soxhlet extractor with methanol, acetone and hexane to remove oligomers and residual catalyst. Polymer was extracted using chloroform, the solvent was removed under reduced pressure and the polymer was precipitated from methanol. After filtration polymer was obtained as a brown solid. (Yield: 37 %) IR (KBr): ν = 2914 (-C-H), 1448 (-C=C), 1311 (-C=N), 789 cm−1 (=C-H); Anal. calcd. for $C_{70}H_{91}N_5S_7$: C, 68.53; H,

7.48; N, 5.71; S, 18.29; found: C, 66.89; H, 8.07; N, 5.64; S, 17.88. Mw: 3627 Da, Mn: 3363 Da, PDI: 1.08

2.4.2 Synthesis of PSeBT

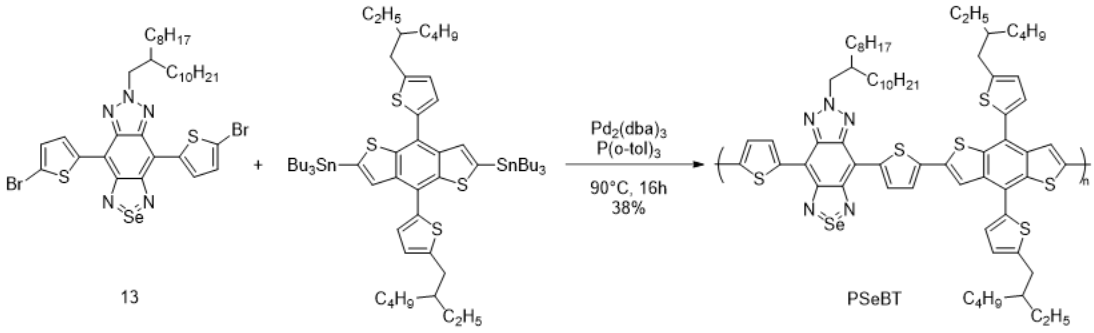

Figure 2.18. Synthetic route of PSeBT

BrSeBT (0.15 g, 0.18 mmol) and 4-(5-(2-ethylhexyl)thiophen-2-yl)-8-(5-(octan-3-yl)thiophen-2-yl)benzo[1,2-b:4,5-b']dithiophene-2,6-diyl)bis(trimethylstannane (0.16 g, 0.18 mmol) were dissolved in anhydrous toluene (6 mL) in a 25 mL of schlenk tube. Tris(dibenzylideneacetone)dipalladium(0) (3.32 mg, 3.63 μmol) and tri(o-tolyl)phosphine (4.42 mg, 14.5 μmol) were also added into the solution and the solution was refluxed for 16 h at 90 °C under argon atmosphere. The reaction was monitored by TLC and tributyl(thiophen-2-yl)stannane (0.27 g, 0.73 mmol) was added as end-capper to remove bromine end groups and the reaction was stirred for 4 h. Then, chlorobenzene (0.16 g, 1.45 mmol) was added to remove the stannyl end groups and the reaction was stirred for another 4 h. After the reaction was completed, toluene was removed under reduced pressure and the resulting product was precipitated in cold methanol. Product was filtered and purified by Soxhlet extractor with methanol, acetone and reduced pressure and the polymer was precipitated from methanol. After filtration polymer was obtained as a red solid. (Yield: 38 %) IR (KBr): ν = 2919 (-C-H), 1413 (-C=C), 1118 (-C=N), 789 cm−1 (=C-H); Anal. calcd. for $C_{70}H_{91}N_5S_6Se$: C, 66.00; H, 7.20; N, 5.50; S, 15.10; found: C, 62.51; H, 7.84; N, 5.62; S, 14.55. Mw: 4280 Da, Mn: 3940 Da, PDI: 1.09

2.5 Fabrication of the Electrochromic Device (ECD)

An electrochromic device (ECD) was fabricated in sandwich configuration by using ITO coated glass substrates as anode and cathode materials. Electrochromic polymer film, PSeBT, and poly(2,2,6,6- tetramethylpiperidinyloxy-4-yl methacrylate (PTMA) film were deposited by spray coating on ITO coated glass substrates and placed as facing each other with gel electrolyte between them. PTMA was synthesized according to the literature.[67] The charge on the electrodes were equilibrated using chronocoulometry technique to improve the optical stability of the ECD. The gel electrolyte was prepared as Bu_4NPF_6:ACN:poly(methyl methacrylate) (PMMA):propylene carbonate in the ratio of 3:70:7:20 by weight. In order to prepare the electrolyte, Bu_4NPF_6 was dissolved in ACN. Then PMMA was also added into the solution and mixture was heated and stirred vigorously. After all of the PMMA was completely dissolved propylene carbonate was also added, the mixture was continued to be stirred and heated until the highly conducting transparent gel was obtained.

2.6 Computational Methods

All calculations were carried out for tetramers in vacuum by using the hybrid B3LYP functional[68,69] and 6-311G* the triple zeta basis set in the Gaussian09 (Revision A.02) software.[70] Side chains were replaced by methyl groups to reduce the computational time required. Electrostatic potential surface (ESP), highest occupied molecular orbitals (HOMO) and lowest unoccupied molecular orbitals (LUMO), delocalization or resonance energies were calculated for the optimized geometries of tetramers. The singlet excited states of the oligomers were calculated by using time dependent DFT (TDDFT) at the same level of calculation quality. Although it does not include vdW dispersion corrections, B3LYP was successfully utilized for the modelling of conjugated polymers including donor-acceptor oligomers reported by Aviyente et. al.[71] and Seferos et. al.[72] with its reasonable computational cost and relatively good agreement with experimental results. Band gap was calculated by

using two different methods. Direct difference between the energy of HOMO and energy of LUMO for the optimized ground state were calculated in the first method and the vertical excitation energy of the lowest singlet excited state ($S_0 \rightarrow S_1$) were calculated by using TDDFT calculations in the second method.[71]

CHAPTER 3

RESULTS AND DISCUSSION

3.1 Electrochemical Characterizations of the Polymers

3.1.1 Cyclic Voltammetry Studies

Cyclic voltammetry (CV) studies were performed in order to investigate the redox behaviors of the polymers and determine their HOMO and LUMO energy levels. In order to conduct these studies, polymers (PSBT and PSeBT) were dissolved in chloroform and coated on ITO coated glass substrates as thin films via spray coating. Three electrode cell system was used to perform cyclic voltammetry with ITO coated glass as working electrode and silver and platinum wires as the reference and counter electrodes, respectively. Cyclic voltammograms of the polymer films were recorded in a solution of 0.1 M Bu_4NPF_6/ACN electrolyte/solvent couple at a scan rate of 100 mV/s.

The single scan cyclic voltammogram of polymer film of PSBT is given in the potential range between -1.80 eV and 1.30 eV in the Figure 3.1. The cyclic voltammetry study indicated the ambipolar character of PSBT which is an important characteristic for possible applications. Through the potential scans between the stated potentials above, PSBT exhibited two p-type reversible redox couples (doping/dedoping) at 0.60 V/0.45 V and 1.05 V/0.97 V and two n-type reversible redox couples (doping/dedoping) at -1.05 V/-0.72 V and -1.40 V/-1.18 V. All of the redox couples are reversible which is a very important property looking from the application point of view. This shows that the polymer could be reversed to its neutral state after the doping processes.

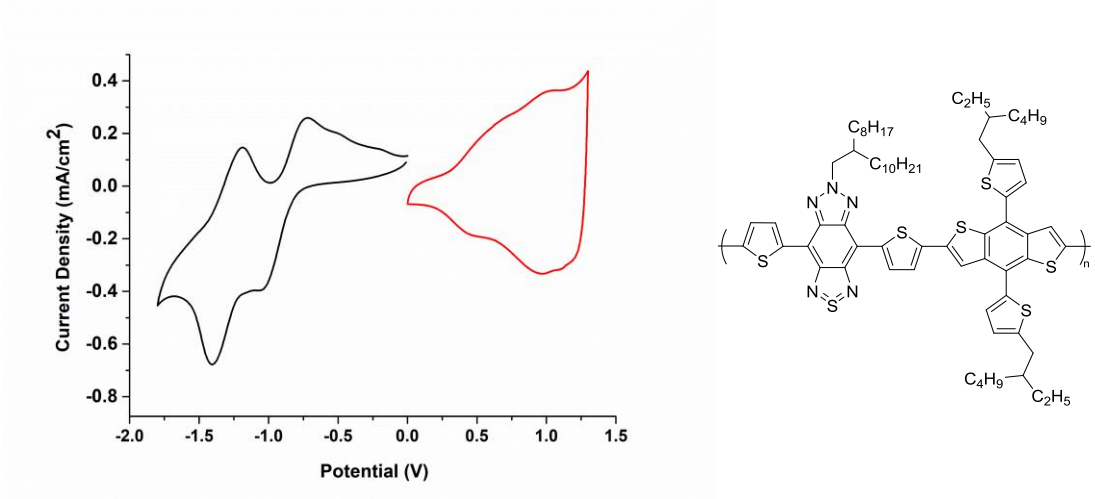

Figure 3.1. Single scan cyclic voltammogram of PSBT in 0.1 M Bu_4NPF_6/ACN solution at 100 mV/s scan rate

In the Figure 3.2., the single scan cyclic voltammogram of PSeBT polymer is shown in the potential range between -1.50 eV and 1.10 eV. Similar with its sulfur analogue, PSeBT demonstrated both p- and n- dopable character. PSeBT also possessed two p-type reversible redox couples (doping/dedoping) at 0.40 V/0.35 V and 0.90 V/0.75 V and two n-type reversible redox couples (doping/dedoping) at -0.90 V/-0.55 V and -1.35 V/-1.06 V through the potential scans between the stated potentials above. As in the case with PSBT, all of the redox couples of PSeBT is reversible indicating that the polymer could be reversed to its neutral stated after the doping process. Cyclic voltammograms of the polymers PSBT and PSeBT are very similar due to their parallel structural design with only one small difference which is the central chalcogen (sulfur/selenium) atom on the chalcogenazole linkage.

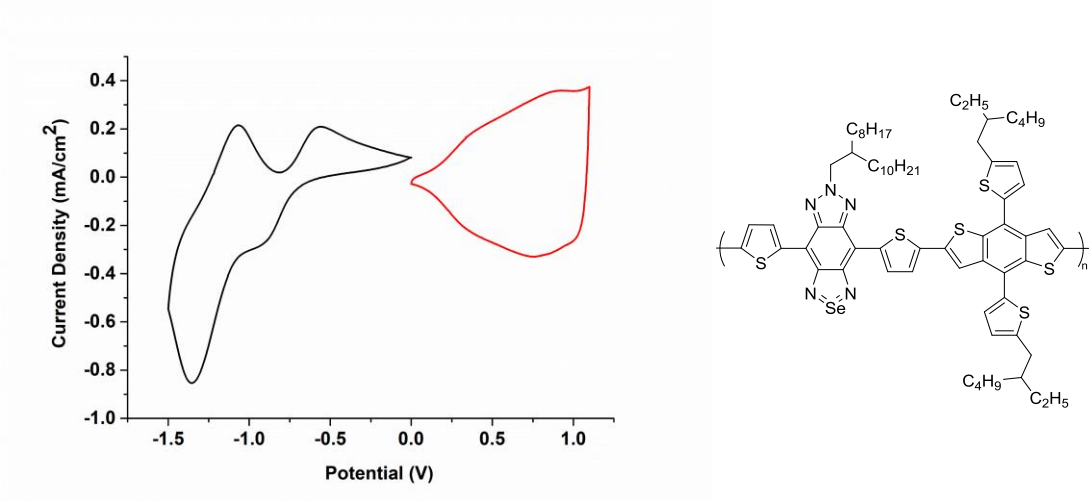

Figure 3.2. Single scan cyclic voltammogram of PSeBT in 0.1 M Bu_4NPF_6/ACN solution at 100 mV/s scan rate

HOMO and LUMO energy levels of the polymers were calculated from the first oxidation and reduction onset potentials, respectively. Onsets of first oxidation and reduction potentials were determined from the intersection of baseline and tangent drawn from top of the peak. HOMO and LUMO energy levels were calculated considering the value of NHE as -4.75 eV with respect to the vacuum level using the following equations:

$$E_{HOMO} = -\left(E_{onset,ox} + 4.75\right)\ (eV)$$

$$E_{LUMO} = -\left(E_{onset,red} + 4.75\right)\ (eV)$$

Electronic band gaps of the polymers were calculated from the difference of HOMO and LUMO energy levels by using the following equation:

$$E_g^{el} = E_{HOMO} - E_{LUMO}\ (eV)$$

HOMO energy levels of the polymers were calculated as -5.00 eV for PSBT and -4.86 eV for PSeBT and; LUMO energy levels were calculated as -3.92 eV for PSBT and -4.04 eV for PSeBT. Electronic band gaps of the polymers were calculated as 1.08 eV and 0.82 eV for PSBT and PSeBT, respectively. The electrochemical properties of the polymers can be seen in the Table 3.1.

Table 3.1. Electrochemical properties of the polymers.

Polymers	$E_{p\text{-}doping}$ (V)	$E_{p\text{-}dedoping}$ (V)	$E_{n\text{-}doping}$ (V)	$E_{n\text{-}dedoping}$ (V)	*HOMO* (eV)	*LUMO* (eV)	E_g^{el}
PSBT	0.60/ 1.05	0.45/ 0.97	-1.05/ -1.40	-0.72/ -1.18	-5.00	-3.92	1.08
PSeBT	0.40/ 0.90	0.35/ 0.75	-0.90/ -1.35	-0.55/ -1.06	-4.86	-4.04	0.82

As it was mentioned before, the hypervalent sulfur and selenium in the chalcogenazole linkage was claimed as a band gap narrowing effect for conjugated polymers due to their ability of adopting a quinoidal structure on the π-electron system through D-A interactions. However, owing to more detailed studies chalcogenazole linkages are described better as three-center-four-electron bond which the central chalcogen (sulfur/selenium) atom expected to bear a +1 charge. Therefore, electron deficiency was produced on these systems which caused a decrease in the LUMO energy levels and the band gaps of corresponding polymers.[62] According to detailed investigations, PSeBT possessed a lower band gap than PSBT. Larger polarizability of selenium atom could be pointed as the reason for that leading to a larger contribution to LUMO level.[73]

3.2 Spectroelectrochemical Characterizations of the Polymers

Spectroelectrochemical studies were performed to investigate the electronic and optical properties of the polymers. In order to analyze the response of polymers to the p-type doping process, the UV-vis-NIR absorption spectra of polymer films were monitored in 0.1 M Bu_4NPF_6/ACN solution. For this study, thin films of the polymers were prepared by dissolving them in chloroform and spray coating onto ITO coated glass substrate.

In the Figure 3.3, change in the absorption of polymer film PSBT is given as a function of wavelength by increasing the applied potential incrementally between 0.00 V and 1.30 V. As seen from the figure, the UV-vis-NIR absorption spectrum of the neutral polymer film exhibits three absorption peaks at wide absorption band ranging from 300 nm to 1200 nm. During the stepwise oxidation, these three absorption peaks were decreased while new transitions arose at higher wavelengths proving the formation of new charge carriers namely polarons and bipolarons on the polymer backbone. When the UV-vis-NIR spectrum of the neutral state of the polymer investigated thoroughly, it could be seen that the two of the absorption peaks lie at 340 nm and 500 nm attributed to π-π* transition within the polymer backbone. In addition to them, the maximum absorption wavelength was recorded at 900 nm, corresponding to the intramolecular charge transfer (ICT).[63,64]

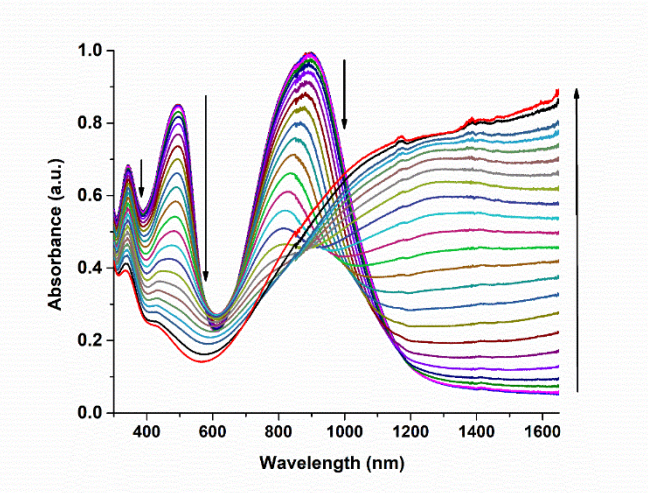

Figure 3.3. Electronic absorption spectra of PSBT film in 0.1 M Bu_4NPF_6/ACN solution between the potentials of 0.00 V and 1.30 V

In the Figure 3.4, change in the absorption of polymer film PSeBT is given as a function of wavelength by increasing the applied potential incrementally between 0.00 V and 1.10 V. Similar with PSBT, the UV-vis-NIR absorption spectrum of the neutral film of PSeBT polymer exhibited three absorption peaks at wide absorption band ranging from 300 nm to 1400 nm. All of the three absorption peaks were

decreased while new transitions arose at higher wavelengths proving the formation of new charge carriers on the polymer backbone during the oxidation process. When the UV-vis-NIR spectra of the neutral state of the polymer film is investigated thoroughly, the two of the absorption peaks lie at 360 nm and 515 nm are attributed to π-π* transition within the polymer backbone. The third peak gives the maximum absorption wavelength which is recorded at 1010 nm corresponding to the intramolecular charge transfer (ICT).

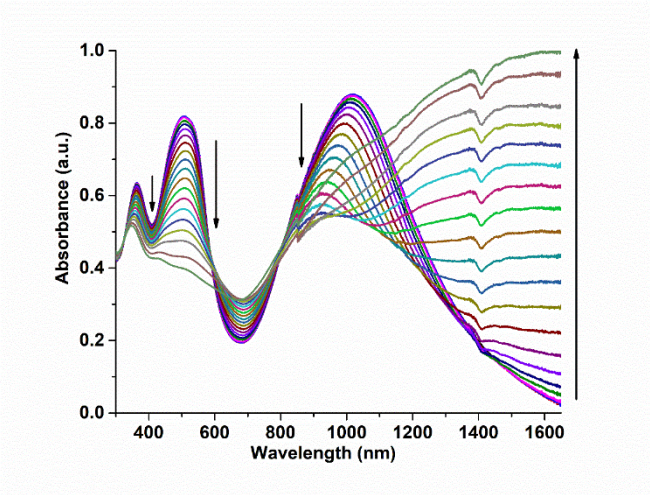

Figure 3.4. Electronic absorption spectra of PSeBT film in 0.1 M Bu_4NPF_6/ACN solution between the potentials of 0.00 V and 1.10 V

The strong donor-acceptor interactions in the polymer backbone cause to electron polarization and electron transfer on the π-bridge which is connecting the electron donor and electron acceptor on the polymer backbone. It was already proven that the formal positive charge on the chalcogen (sulfur/selenium) atom on chalcogenazole linkage could be transferred to π-bridge due to the resonance contribution.[62] These strong interactions in the polymer backbone and the charge transfer through the π-bridge could be pointed as the reason of ICT.[63,64]

The optical band gaps of the polymers were calculated using the following equation:

$$E_g^{op} = \frac{hc}{\lambda_{onset}} = \frac{1241}{\lambda_{onset}} (eV)$$

where

h is Planck's constant ($h = 6.626 \times 10^{-34} J.s$)

c is the speed of light ($c = 2.998 \times 10^{8} m.s^{-1}$)

Optical band gaps of the polymers were calculated as 1.07 eV for PSBT and 0.82 eV for PSeBT from the onsets of absorption maxima which were determined as 1162 nm and 1505 nm for PSBT and PSeBT, respectively. It is clear that, PSeBT demonstrates more red-shifted absorption maxima and reduced optical band gap than PSBT as it was expected due to the larger polarizability of selenium. The spectroelectrochemical properties of the polymers can be seen in the Table 3.2.

Table 3.2. Spectroelectrochemical properties of the polymers.

Polymers	λ_{max} *(nm)*	λ_{onset} *(nm)*	E_g^{opt} *(eV)*
PSBT	900	1162	1.07
PSeBT	1010	1505	0.82

The absorption spectra of the polymers were displayed as thin film and in solution. As it was mentioned above, in thin film form the maximum absorption wavelengths were recorded at 900 nm and 1010 nm for PSBT and PSeBT. In solution form, however the maximum absorption wavelengths were observed at 880 nm and 985 nm for PSBT and PSeBT. In the solid states of the polymers, the enhanced π-π stacking resulted in red shifts of 20 nm for PSBT and 25 nm for PSeBT where two polymers demonstrated very similar results.

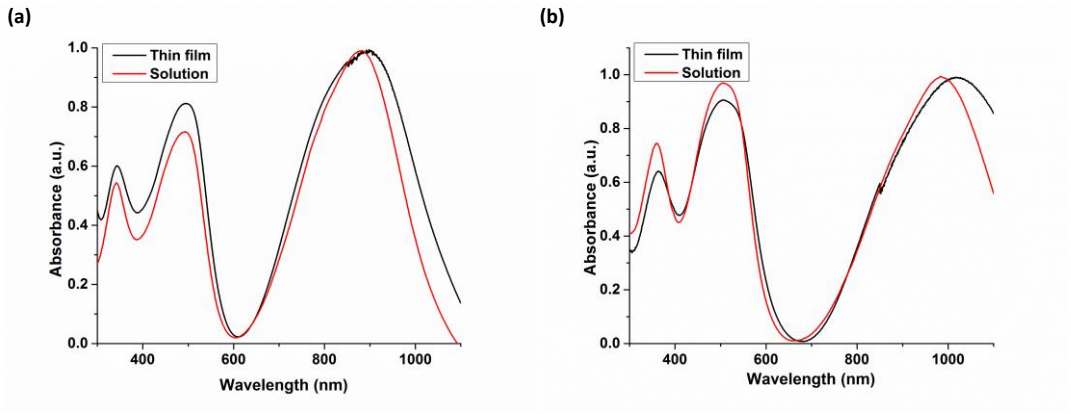

Figure 3.5. Electronic absorption spectra of (a) PSBT and (b) PSeBT as thin film and in solution.

3.2.1 Colorimetric Studies

Both of the polymers revealed different colors in their neutral and doped states displaying electrochromic behavior. Color changes of the polymers were resulted due to the formation of polarons and bipolarons by stepwise oxidation.

Color changes of PSBT polymer film is demonstrated in the Figure 3.5. The polymer exhibits brown color in its neutral state and multicolored oxidation and reduction states. The color of the polymer switches color to darker brown upon p-doping, then grey upon further p-doping. Also, it switches color to blue then green upon n-doping.

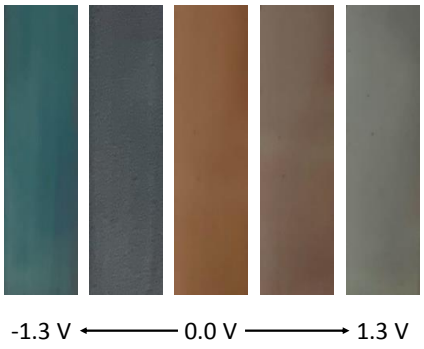

Figure 3.6. Colors of PSBT at different potentials

Color changes of PSeBT polymer film is shown in the Figure 3.6. The polymer possesses red color in its neutral state and multicolored oxidation and reduction states. It switches color to brown upon oxidation then grey upon further oxidation. Likewise, it changes its color to purple upon reduction, then blue and grey upon further reductions.

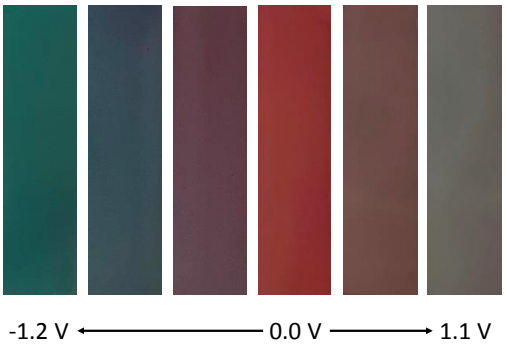

Figure 3.7. Colors of PSeBT at different potentials

It was seen that, PSeBT has better switching colors than its sulfur analogue displayed in all RGB and it could be a promising candidate for electrochromic device (ECD) applications. For the scientific expressions of the color of polymer films, colorimetry measurements were done and CIE (Commission Internationale de l'Eclairage) coordinates were determined with the parameters of L, a, b. Details of colorimetry measurements of the polymers are in the Table 3.3.

Table 3.3. Colorimetry measurements of the polymers.

Type of Travel	*Applied potential*	*L*	*a*	*b*
PSBT	0.00 V	45.020	14.500	24.180
	1.00 V	41.350	7.672	12.610
	1.30 V	49.250	-1.530	3.383
	-1.00 V	35.890	-3.749	-3.413
	-1.30 V	40.340	-14.400	-5.999
PSeBT	0.00 V	36.500	39.460	21.390
	0.80 V	34.700	14.650	10.380
	1.10 V	39.900	0.070	4.875
	-0.80 V	30.320	17.730	0.117
	-0.90 V	31.270	-8.374	-10.010
	-1.20 V	28.870	-20.010	-4.538

3.2.2 Kinetic Studies

Kinetic studies were performed in order to determine optical contrasts and switching times of the corresponding polymers. Optical contrast is reported as percent transmittance change which is recorded by changing the applied potentials continuously between fully neutral and oxidized states within a time interval of 5 s at specified wavelengths which were previously determined from UV-vis-NIR spectra. The switching time is the time needed for the color-changing process at a 95% contrast value. Kinetic studies were conducted with both of the polymer films coated on ITO electrodes in a solution of 0.1 M of Bu_4NPF_6/ACN.

Percent optical contrast values of PSBT polymer film are recorded at specified wavelengths which are 500 nm in visible region and 900 nm and 1500 nm in NIR region as it can be seen in the Figure 3.5. During the potential switching in 5 seconds time interval, optical transmittances of polymer film were monitored using UV-vis-

NIR spectrometer. Percent transmittance changes were calculated as 25% at 500 nm, 16% at 900 nm and 65% at 1500 nm for PSBT polymer film. Also, the switching times of the film were calculated as 2.1 s at 500 nm, 1.9 s at 900 nm and 1.6 s at 1500 nm.

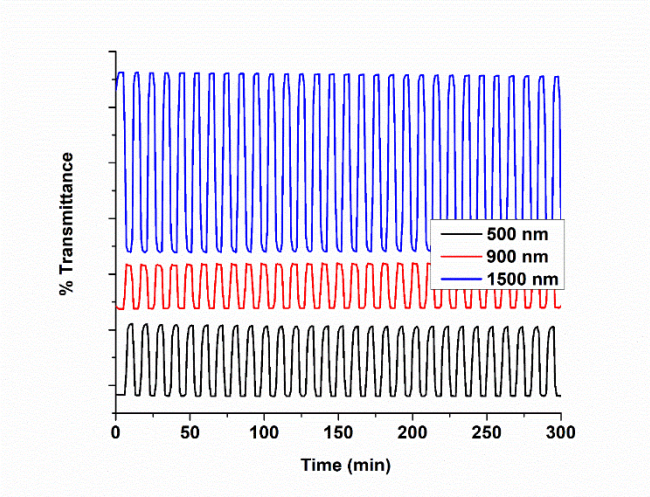

Figure 3.8. Percent transmittance changes of PSBT film in 0.1 M Bu_4NPF_6/ACN solution at maximum absorption wavelengths

As in the case with PSBT, percent optical contrast values of PSeBT polymer film are recorded at specified wavelengths which are 515 nm in visible region and 1010 nm and 1550 nm in NIR region as it can be seen in the Figure 3.6. Similarly, optical transmittances of the polymer film were monitored using UV-vis-NIR spectrometer during the potential switching in 5 seconds time intervals. Percent transmittance changes were calculated as 35% at 515 nm, 7% at 1010 nm and 60 % at 1550 nm for PSeBT polymer film. Switching times of the film were calculated as 1.8 s at 515 nm, 1.8 s at 1010 nm and 1.9 s at 1550 nm.

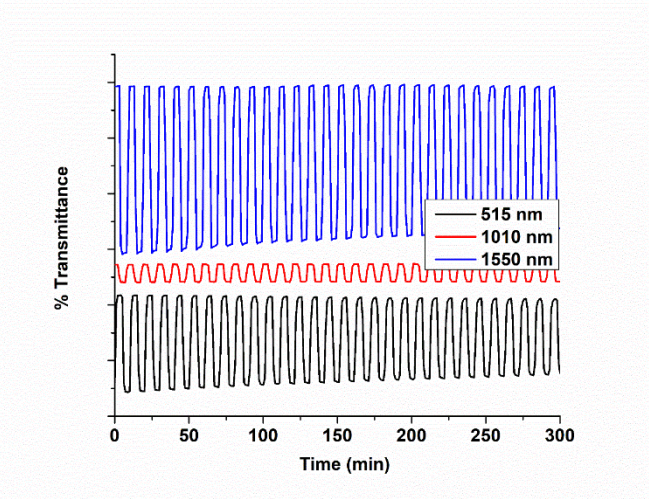

Figure 3.9. Percent transmittance changes of PSeBT film in 0.1 M Bu_4NPF_6/ACN solution at maximum absorption wavelengths

Although PSBT has lower optical contrast than PSeBT at the visible region (515 nm for PSeBT, 500 nm for PSeBT) it has slightly better optical contrast at the NIR region (1010 nm and 1550 nm for PSeBT, 900 nm and 1500 nm for PSBT). Switching times of PSBT are higher than PSeBT at the visible region (515 nm for PSeBT, 500 nm for PSeBT) when it is less at the NIR region (1010 nm and 1550 nm for PSeBT, 900 nm and 1500 nm for PSBT). Although one of the polymers is not strongly superior to the other one, optical contrast and switching time of PSeBT in the visible region is slightly better than its sulfur analogue which is significant for an electrochromic device. However, both of the polymers did not demonstrate very good optical contrasts and switching times when compared with the results in literature. Kinetic properties of corresponding polymers are reported in Table 3.4.

Table 3.4. Optical contrasts and switching times of polymers.

		Optical Contrast	
Polymers	*λ (nm)*	*(ΔT %)*	*Switching Time (s)*
PSBT	500	25	2.1
	900	16	1.9
	1500	65	1.6
PSeBT	515	35	1.8
	1010	7	1.8
	1550	60	1.9

3.3 Electrochromic Device Applications and Characterizations

3.3.1 Spectroelectrochemical Studies

The ECD was prepared in sandwich configuration by glass/ITO/PSeBT// Bu_4NPF_6 gel electrolyte//PTMA/ITO/glass device construction. Spectroelectrochemical behavior of the PSeBT/PTMA device was investigated under an applied potential between -1.50 V and 2.00 V as it can be seen in the Figure 3.7. At a low applied voltage of -1.50 V PSeBT was reduced and PTMA was oxidized. It can be seen from the figure that, there is an absorption peak at 510 nm due to the π-π* transition within the polymer backbone at this state. As the voltage supplied to the device was switched to 2.00 V, this peak disappeared and the color change was observed for the device.

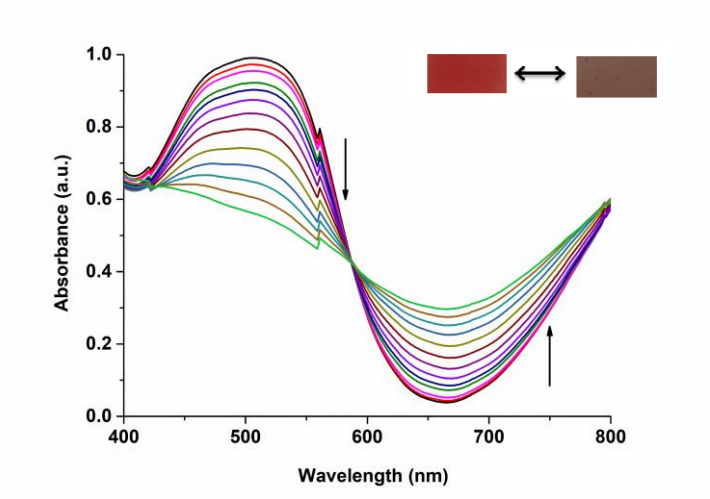

Figure 3.10. Electronic absorption spectra of PSeBT/PTMA device

3.3.2 Kinetic Studies

Kinetic studies were performed in order to determine the optical contrast and the switching time of the PSeBT/PTMA device. The percent transmittance change of the device was monitored by changing the applied potentials continuously between –1.50 V and +2.00 V within a time interval of 5 s at 510 nm since it was the maximum absorption wavelength determined from UV-vis-NIR spectra. As it can be seen from the Figure 3.8, the percent transmittance change is determined as 12 % for the device and its switching time was calculated as 2.6 s.

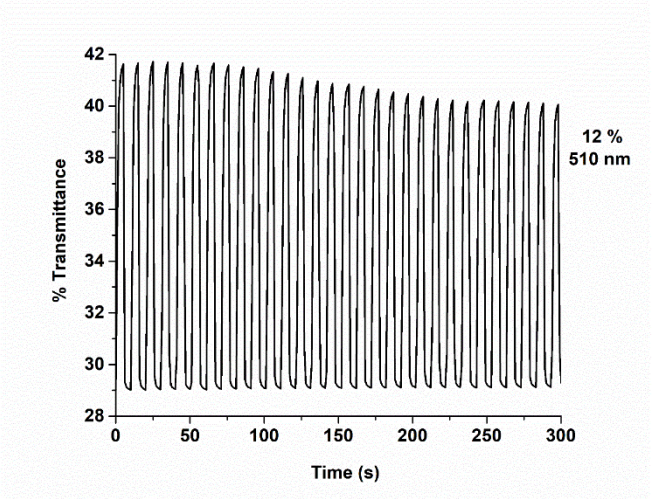

Figure 3.11. Percent transmittance change of PSeBT/PTMA device at maximum absoption wavelength

3.3.3 Open Circuit Memory

The open circuit memory of PSeBT/PTMA device was also investigated since it is an important parameter for an ECD which is defined as the ability of the device to remember its color and optical density under zero current. As seen in the Figure 3.9, the optical spectrum for the ECD was monitored as a function of time at 510 nm while a potential (-1.5 V and + 2.0 V) was applied with pulses for 1 s then holding the device at open circuit conditions for 200 s. When the device was polarized at -1.5 V, there was no transmittance change proving a true permanent memory effect. However, when the device was polarized at +2.0, the initial optical contrast was changed slightly after every 200 s under open circuit conditions.

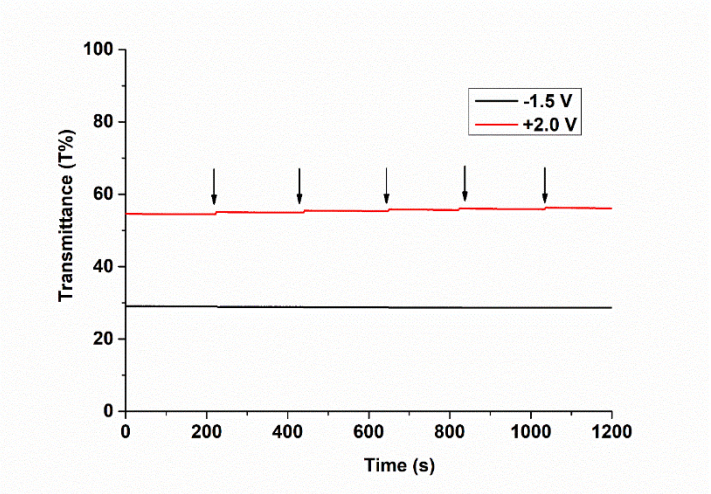

Figure 3.12. Open circuit memory of PSeBT/PTMA device at -1.50 V and 2.00 V

3.4 Computational Results

Optimized geometries of both PSBT and PSeBT tetramers have highly planar geometries as given in Figure 3.13 for edge view of the PSeBT. Dihedral angles between the bridging thiophene and acceptor were less than 1° for both copolymers. Dihedral angles between bridging thiophene and benzodithiophene donor is less than 10° for both copolymers where this angle is slightly lower for PSeBT compared to PSBT indicating stronger planarity for PSeBT (Fig. S1). Effect of this planarity can be observed by the delocalization or resonance energy per monomer calculated by the difference between the original energy and Lewis energy, determined as 388 eV for PSBT and 611 eV for PSeBT pointing out higher electron delocalization for PSeBT conjugated backbone. Side chains have 60° with the backbone chains for both copolymers. ESPs indicate strong donor-acceptor behaviour along backbone for both copolymers as demonstrated for PSeBT (Fig. 3.14). HOMOs are distributed along the the backbone and LUMOs are highly concentrated on acceptor for both copolymers as given for PSeBT (Fig. 3.13 c-d). This result is also valid for HOMO-1 and LUMO+1 frontier orbitals as demonstrated in Figure 3.14 e-f.

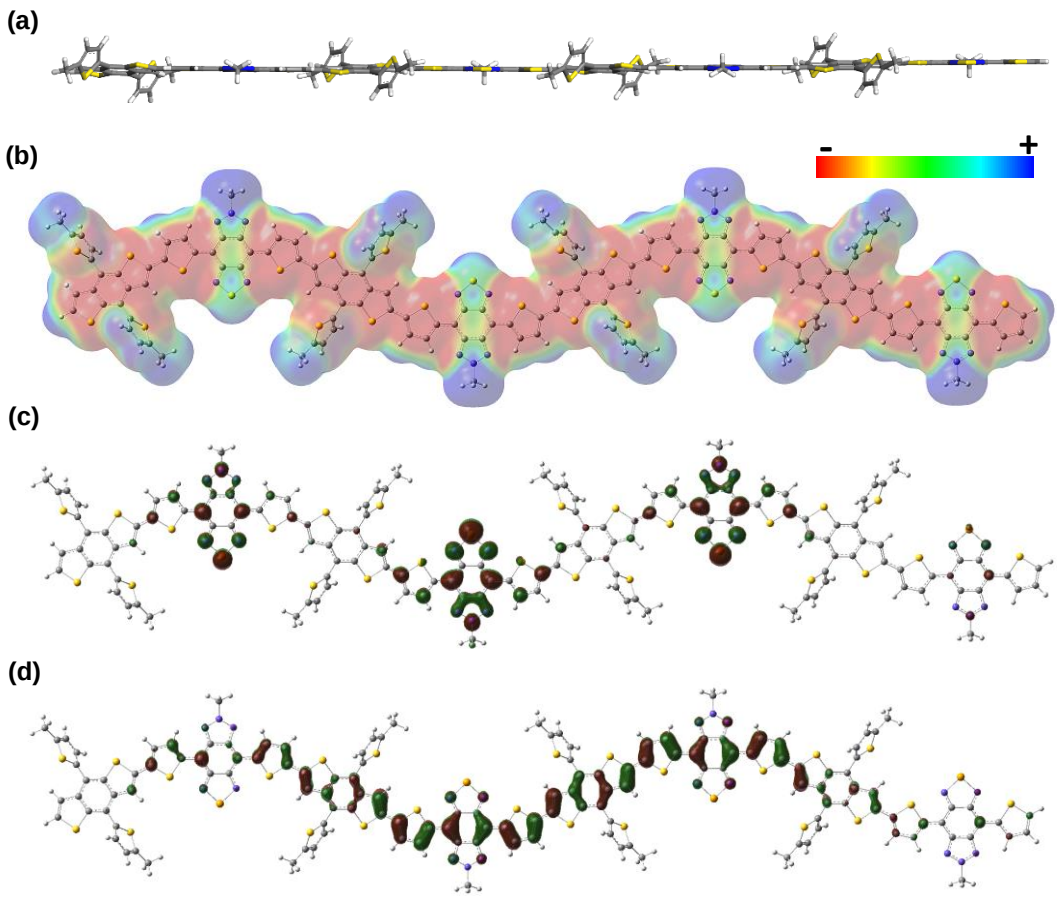

Figure 3.13. (a) The edge view for the optimized geometry of PSeBT tetramer. (b) Electrostatic potential surface for PSeBT tetramer. Graphical representation for the computed (c) LUMO and (d) HOMO for PSeBT tetramer.

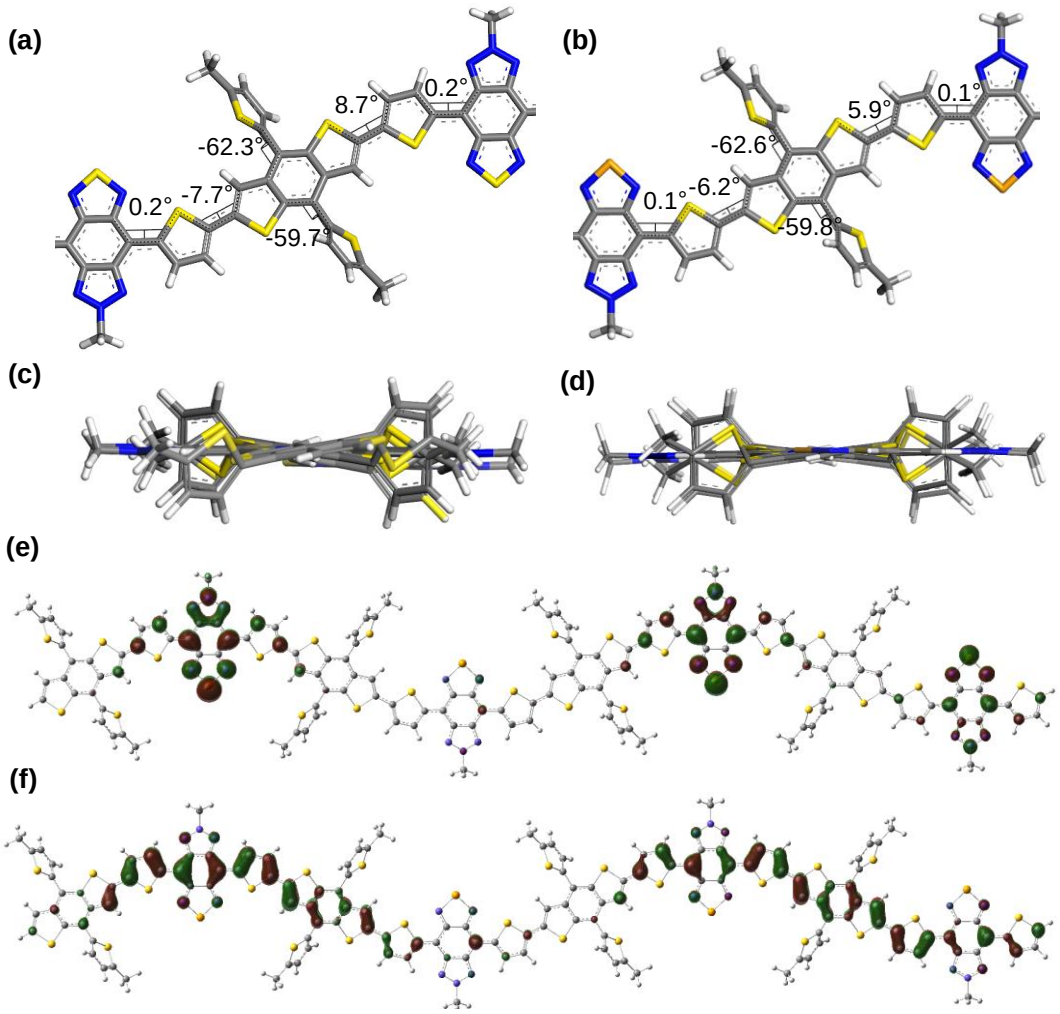

Figure 3.14. Dihedral angles between bridging thiophene and [1,2,5]chalcogenazolo[3,4-f]-benzo[1,2,3]triazole acceptors, between bridging thiophene and benzodithiophene donor, between backbone and side chains for (a) PSBT and (b) PSeBT copolymers. End view along the chain for (c) PSBT and (d) PSeBT copolymers. Graphical representation for the computed (e) LUMO+1 and (f) HOMO-1 for PSeBT tetramers.

CHAPTER 4

CONCLUSION

Novel conjugated D-A type alternating copolymers were designed to investigate the effect of acceptor strength throughout the polymer backbone. Two [1,2,5]chalcogenazolo[3,4-f]-benzo[1,2,3]triazole derivatives were synthesized and used as the acceptor moiety with the central chalcogen atom as sulfur and selenium on chalcogenazole ring. The chalcogen atom on [1,2,5]chalcogenazolo[3,4-f]-benzo[1,2,3]triazole units are differentiated to compare their effects on the optoelectronic properties of the polymers. Electrochemical, spectroelectrochemical and optical characterization of the corresponding polymers were carried out successfully. Electrochemical characterizations revealed the ambipolar character of both PSBT and PSeBT with narrow electronic band gaps around 1 eV. Spectroelectrochemical characterizations also demonstrated that optical band gaps of the polymers are similar to their electronic band gaps with red-shifted absorption due to intramolecular charge transfer (ICT) on the polymer backbones. PSeBT indicated lower band gap than PSBT as expected since selenium has a larger contribution to LUMO level due to larger polarizability. Both of the polymers also showed electrochromic behavior with multicolored oxidation and reduction states. Regarding the better switching colors displayed by PSeBT than its sulfur analogue, an electrochromic device (ECD) was prepared by using it as the electrochromic material. Although PSBT did not possess good properties as much as PSeBT it is also promising for ECD applications. Therefore, another ECD could also be constructed by using PSBT polymer as a future study. The results of the constructed ECD is promising for possible applications with necessary further optimizations. Besides the ECD applications, trials in organic photovoltaic (OPV) applications were carried on using the polymers, but generated results were not promising for future optimizations.

REFERENCES

1. Harun, M. H., Saion, E., Kassim, A., Yahya, N. & Mahmud, E., *UCSI Acad. J. J. Adv. Sci. Arts.,* 2007, **2**, 63–68.
2. Labes, M. M., Love, P., Nichols, L. F., *Chem. Rev., 1*979, **79**, 1–15.
3. Shirakawa, H., Louis, E. J., MacDiarmid, A. G., Chiang, C. K., Heeger, A. J., *J. Chem. Soc., Chem. Commun.,* 1977, 578–580.
4. Heeger, A. J., *Rev. Mod. Phys.*, 2001, **73**, 681–700.
5. Facchetti, A., *Chem. Mater.,* 2011, **23**, 733–758.
6. Azeri, Ö., Aktas, E., Istanbulluoglu, C., Hacioglu, S. O., Cevher, S. C., Toppare, L. Cirpan, A., *Polymer,* 2017, **133**, 60–67.
7. Tisovský, P., Gáplovský, A., Gmucová, K., Novota, M., Pavúk, M., Weis, M., *Org. Electron.,* 2019, **68**, 121–128.
8. Buber, E., Kesik, M., Soylemez, S., Toppare, L., *J. Electroanal. Chem.,* 2017, **799**, 370–376.
9. Xu, Z., Zhang, Y., Wang, B., Liu, Z., Zhao, J., Xie, Y. Y., *Electrochim. Acta,* 2019, **302**, 373–384.
10. Kaur, G., Adhikari, R., Cass, P., Bown, M., Gunatillake, P., *RSC Adv.,* 2015, **5**, 37553–37567.
11. Tomczykowa, M., Plonska-Brzezinska, M. E., *Polymers,* 2019, **11**, 350.
12. Skotheim, T. A., Elsenbaumer, R. L., Reynolds, J. R. *Handbook of Conducting Polymers*. (Marcel Dekker, 1998).
13. MacDiarmid, A. G., Mammone, R. J., Kaner, R. B., Porter, S. J., *Phil. Trans. R. Soc. Lond. A.,* 1985, **314**, 3–15.
14. Le, T. H., Kim, Y., Yoon, H., *Polymers,* 2017, **9**, 150.
15. Singh, A. K., Prakash, R., *2nd Natl. Work. Adv. Optoelectron. Mater. Devices, AOMD,* 2008, 65–74.
16. Gao, M., Zhu, L., Peh, C. K., Ho, G. W., *Energy Environ. Sci., 2019,* **12**, 841–864.
17. Reddinger, J. L., Reynolds, J. R., *Adv. Polym. Sci.,* 1999, **145**, 59–122.

18. Su, Y. W., Lin, Y. C., Wei, K. H., *J. Mater. Chem. A,* 2017, **5**, 24051–24075.
19. Cavallaro, S., Colligiani, A., Cum, G., *J. Therm. Analysis.,* 1992, **38**, 2649–2655.
20. Bao, Z., Chan, W., Yu, L., *Chem. Mater.,* 1993, **5**, 2–3.
21. Fei, Z., Kim, J. S., Smith, J., Domingo, E. B., Anthopoulos, T. D., Stingelin, N., Watkins, S. E., Kim, J., Heeney, M., *J. Mater. Chem.,* 2011, **21**, 16257.
22. Dogan Demir, K., Kiskan, B., Yagci, Y. *Macromolecules,* 2011, **44**, 1801–1807.
23. Kumar, R., Singh, S., Yadav, B. C., *Int. Adv. Res. J. Sci. Eng. Technol.,* 2015, **2**, 110-124.
24. Zotti, G., Schiavon, G., Berlin, A., Pagani, G., *Chem. Mater.,* 1993, **5**, 430–436.
25. Eftekhari, A., Jafarkhani, P., *Polym. J.,* 2006, **38**, 651–658.
26. Myers, R. E., *J. Electron. Mater.,* 1986, **15**, 61–69.
27. Huang, W. S., Humphrey, B. D., MacDiarmid, A. G., *J. Chem. Soc. Faraday Trans. 1,* 1986, **82**, 2385–2400.
28. Scott, W. J., Crisp, G. T., Stille, J. K., *Org. Synth.,* 1993, **8**, 97.
29. Stille, J. K., *Angew. Chemie Int. Ed. English,* 1986, **25**, 508–524.
30. Stille, J. K., Echavarren, A. M., Williams, R. M., Hendrix J. A., *Org. Synth.,* 1993, **71**, 97.
31. Miyaura, N., Suzuki, A., *Chem. Rev.,* 1995, **95**, 2457–2483.
32. Suzuki, A., *Pure Appl. Chem.* 1991, **63**, 419–422.
33. Sonogashira, K., *J. Organomet. Chem.,* 2002, **653**, 46–49.
34. Stambuli, J. P., Bühl, M., Hartwig, J. F., *J. Am. Chem. Soc.* 2002, **124**, 9346–9347.
35. Kohnen, A. L., Danheiser, R. L., Denmark, S. E., Liu, X., *Org. Synth.* 2007, **84**, 77-87.
36. Wang, H. J., Chen, C. P., Jeng, R. J., *Materials.* 2014, **7**, 2411–2439.
37. Havinga, E. E., ten Hoeve, W., Wynberg, H., *Polym. Bull.,* 1992, **29**, 119–126.

38. Müllen, K., Pisula, W., *J. Am. Chem. Soc.* 2015, **137**, 9503–9505.
39. Reichardt, C., *Chem. Soc. Rev.,* 1992, 147–153.
40. Deb, S. K., *Appl. Opt.,* 1969, **8**, 192–195.
41. Argun, A. A., Aubert, P. H., Thompson, B. C., Schwendeman, I., Gaupp, C. L., Hwang, J., Pinto, N. J., Tanner, D. B. MacDiarmid, A. G., Reynolds, J. R., *Chem. Mater.* 2004, **16**, 4401–4412.
42. Berzelius, J. J. *Afh. Fys. Kemi Miner.* 1815, 293.
43. Wöhler, F. *Ann. Phys.* 1834, 350.
44. Gottesfeld, S., McIntyre, J. D. E., Beni, G., Shay, J. L., *Appl. Phys. Lett.,* 1978, **33**, 208.
45. Michaelis, L., Hill, E. S., *J. Gen. Physiol.,* 1933, **16**, 859–873.
46. Bird, C. L., Kuhn, A. T., *Chem. Soc. Rev.,* 1981, **10**, 49–82.
47. Bartoll, J., *9th Int. Conf. NDT Art,* 2008, 25–30.
48. Robin, M. B., *Inorg. Chem.* 1962, **1**, 337–342.
49. Hyodo, K., *Electrochim. Acta,* 1994, **39**, 265–272.
50. Arslan Udum, Y., Gündoğdu Hizliates, C., Ergün, Y., Toppare, L., *Thin Solid Films* 2015, **595**, 61–67.
51. Shin, H., Seo, S., Park, C. Na, J., Han, M., Kim, E., *Energy Environ. Sci.,* 2016, **9**, 117.
52. Mortimer, R. J., Dyer, A. L., Reynolds, J. R., *Displays,* 2006, **27**, 2–18.
53. Ardakan, A. M., Sok, E., Niemasz, J., *Energy Procedia,* 2017, **122**, 343–348.
54. Zhang, G., Ma, S.,Wang, W., Zhao, Y., Ruan, J., Tang, L., Lu, H., Qiu, L., Ding, Y., *Front. Chem.,* 2019, **7**, 359.
55. Li, Z., Liu, S., Liu, D., *Open J. Polym. Chem.,* 2012, **2**, 152–158.
56. Oklem, G., Song, X., Toppare, L., Baran, D., Gunbas, G., *J. Mater. Chem. C,* 2018, **6**, 2957–2961.
57. Meng, H., Tucker, D., Chaffins,S., Chen, Y., Helgeson, R., Dunn, B., Wudl, F., *Adv. Mater.,* 2003, **15**, 146–149.
58. Wang, P. I., Shie, W. R., Jiang, J. C., Li, L. J., Liaw, D. J., *Polym. Chem.,* 2016, **7**, 1505.

59. Karikomi, M., Kitamura, C., Tanaka, S., Yamashita, Y., *J. Am. Chem. Soc.,* 1995, **117**, 6791–6792.
60. Ono, K., Tanaka, S., Yamashita, Y., *Angew. Chem. Int. Ed. Engl.,* 1994, **33**, 1977–1979.
61. Tam, T. L., Li, H., Lam, Y. M., Mhaisalkar, S. G., Grimsdale, A. C., *Org. Lett.* 2011, **13**, 4612–4615.
62. Patel, D. G., Feng, F., Ohnishi, Y. Y., Abboud, K. A., Hirata, S., Schanze, K. S., Reynolds, J. R., *J. Am. Chem. Soc.* 2012, **134**, 2599–2612.
63. Zhou, E., Hashimoto, K., Tajima, K., *Polymer,* 2013, **54**, 6501–6509.
64. Wang, T. L., Huang, S. C., Yang, C. H., Chuang, Y. Y., Chen, C. H., *Express Polym. Lett.,* 2015, **9**, 881–893.
65. Tregnago, G., Steckler, T. T., Fenwick, O., Andersson, M. R., Cacialli, F., *J. Mater. Chem. C,* 2015, **3**, 2792.
66. Ashraf, R. S., Meager, I., Nikolka, M., Kirkus, M., Planells, M., Schroeder, B. C., Holliday, S., Hurhangee, M ., Nielsen, C. B. Sirringhaus, H., McCulloch, I., *J. Am. Chem. Soc.* 2015, **137**, 1314−1321.
67. Chan, H., Wang, Y., Boudouris, B. W., *Thin. Solid. Films.* 2015, **577**, 56-61.
68. Lee, C., Yang, W., Parr, R. G., *Phys. Rev. B: Condens. Matter Mater. Phys.* 1988, **37**, 785–789.
69. Becke, D., *J. Chem. Phys.* 1993, **98**, 5648–5652.
70. Frisch, M. J., Trucks, G. W., Schlegel, H. B., Scuseria, G. E., Robb, M. A., Cheeseman J. R., et al., *Gaussian 09, Revision A.02*, Gaussian, Inc., Wallingford CT, 2009.
71. Turan, H. T., Kucur, O., Kahraman, B., Salman, S., Aviyente, V., *Phys. Chem. Chem. Phys.* 2018, **20**, 3581—3591.
72. McCormick, T. M., Bridges, C. R., Carrera, E. I., DiCarmine, P. M., Gibson, G. L., Hollinger, J., Kozycz, L. M., Seferos, D. S., *Macromolecules.* 2013, **46**, 3879–3886.
73. Tam, T. L. D., Ye, W., Tan, H. H. R., Zhou, F., Su, H., Mhaisalkar, S. G., Grimsdale, A. C., *J. Org. Chem.* 2012, **77**, 10035−10041.

APPENDICES

A. NMR Spectra

Each molecule analyzed by Bruker Spectrospin Avance DPX-400 Spectrometer with $CDCl_3$ or DMSO as the solvent and TMS as the internal reference.

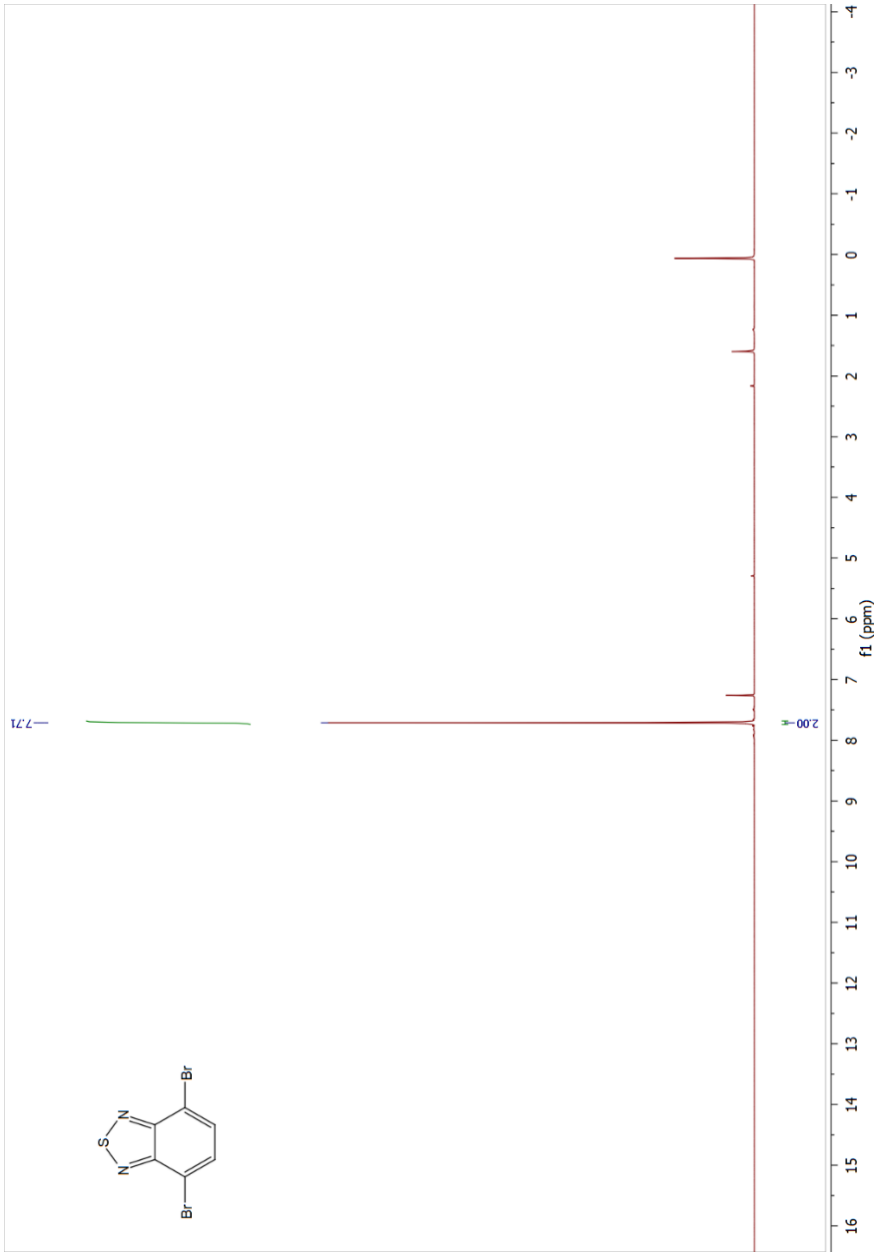

Figure A.1. ^{1}H NMR spectrum of 4,7-dibromobenzothiadiazole (1)

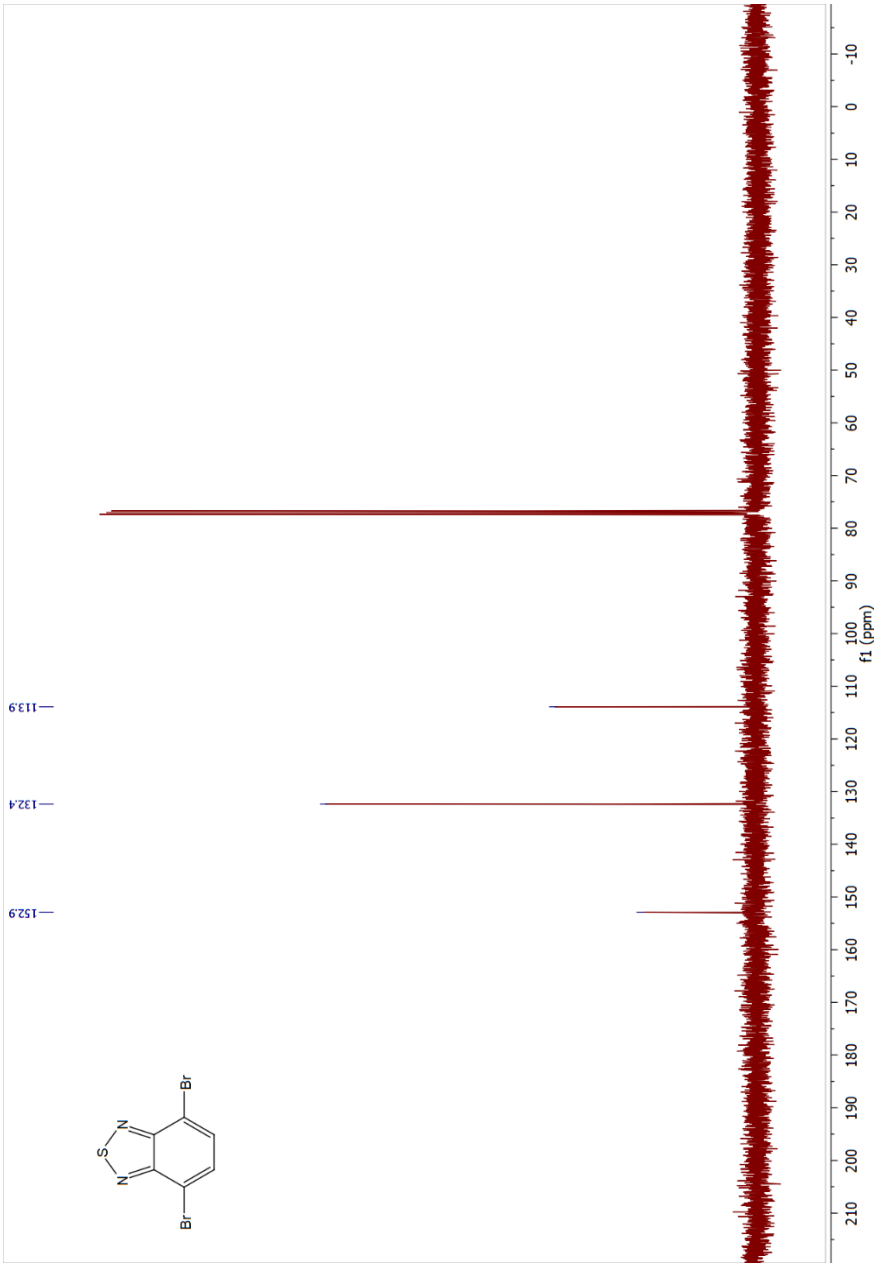

Figure A.2. ^{13}C NMR spectrum of 4,7-dibromobenzothiadiazole (1)

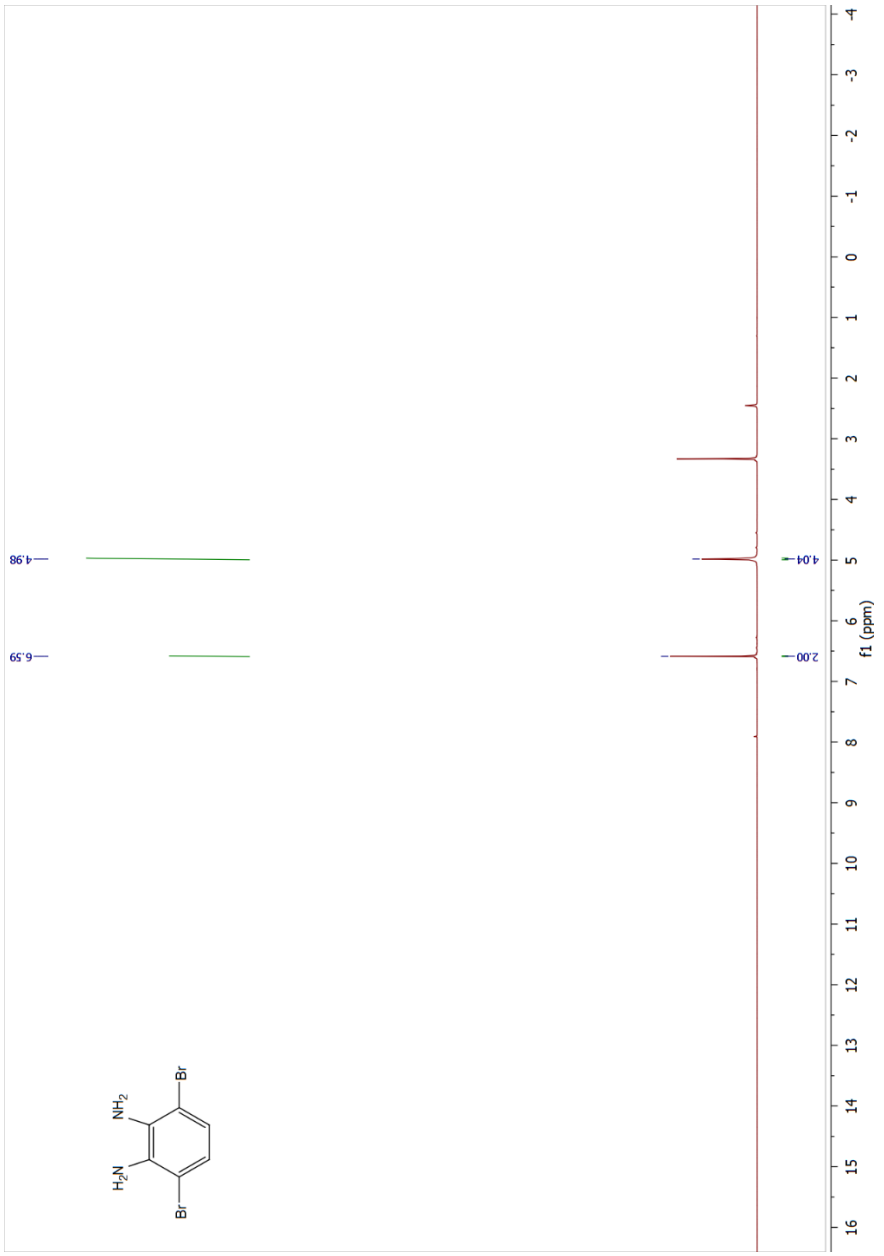

Figure A.3. ^{1}H NMR spectrum of 3,6-dibromobenzene-1,2-diamine (2)

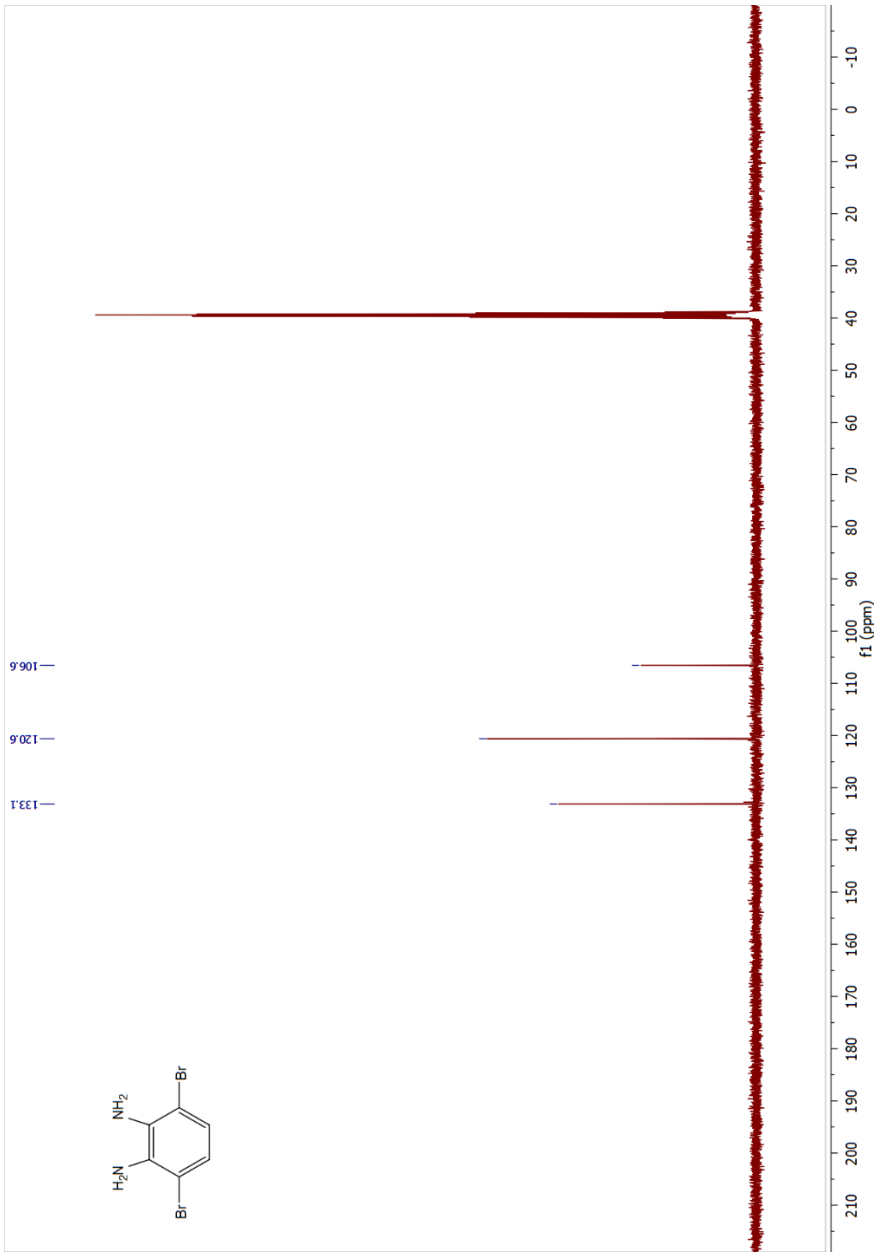

Figure A.4. ^{13}C NMR spectrum of 3,6-dibromobenzene-1,2-diamine (2)

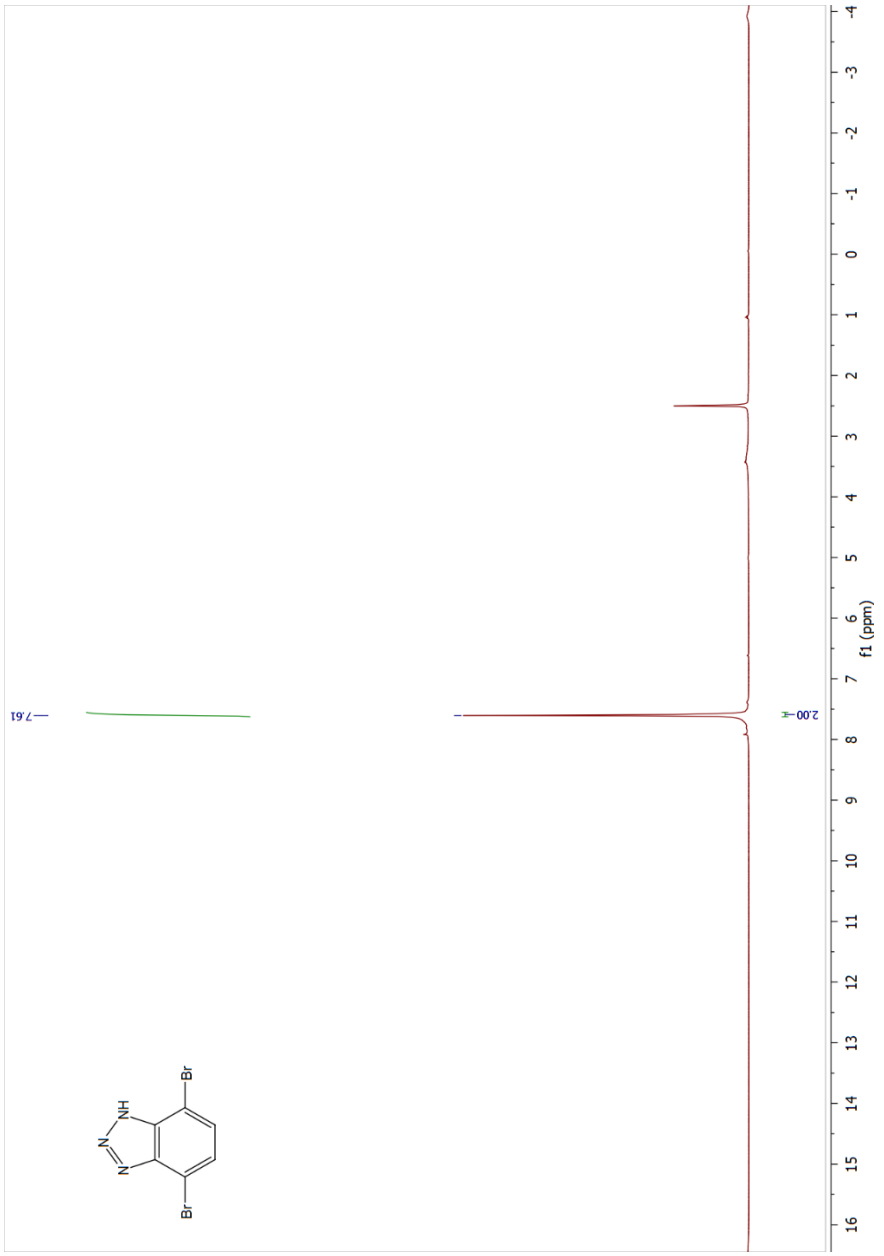

Figure A.5. ^{1}H NMR spectrum of 4,7-dibromo-1H-benzo[d][1,2,3]triazole (3)

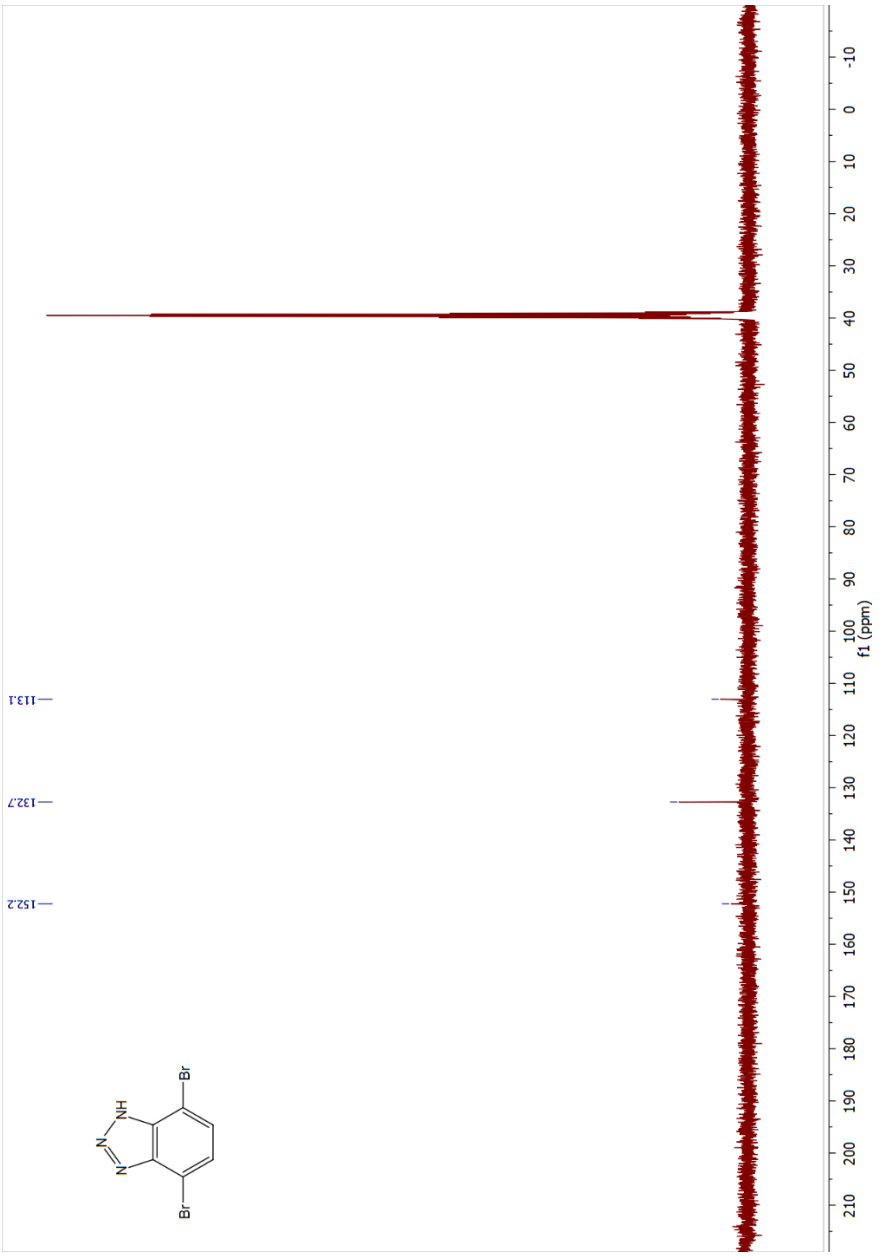

Figure A.6. ^{13}C NMR spectrum of 4,7-dibromo-1H-benzo[d][1,2,3]triazole (3)

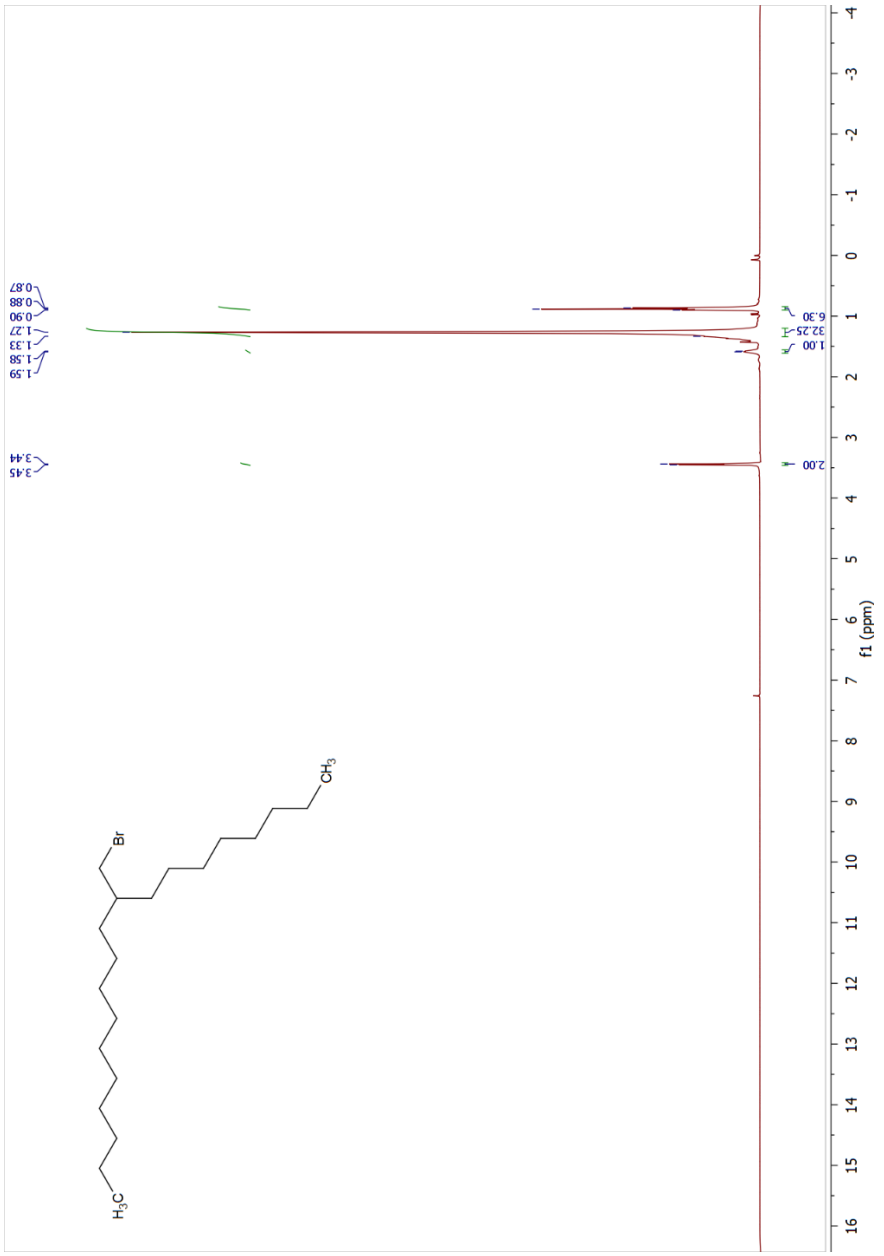

Figure A.7. ^{1}H NMR spectrum of 9-(bromomethyl)nonadecane (4)

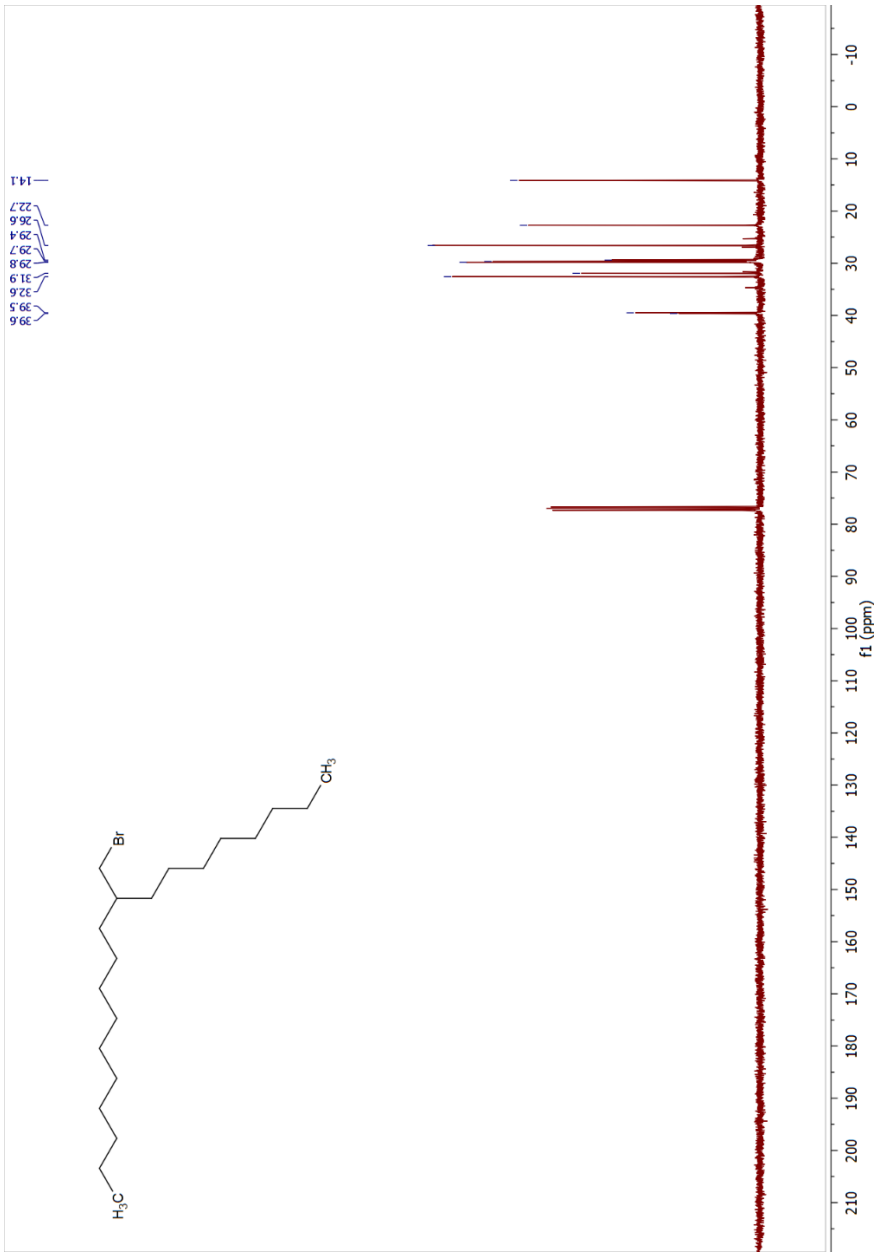

Figure A.8. ^{13}C NMR spectrum of 9-(bromomethyl)nonadecane (4)

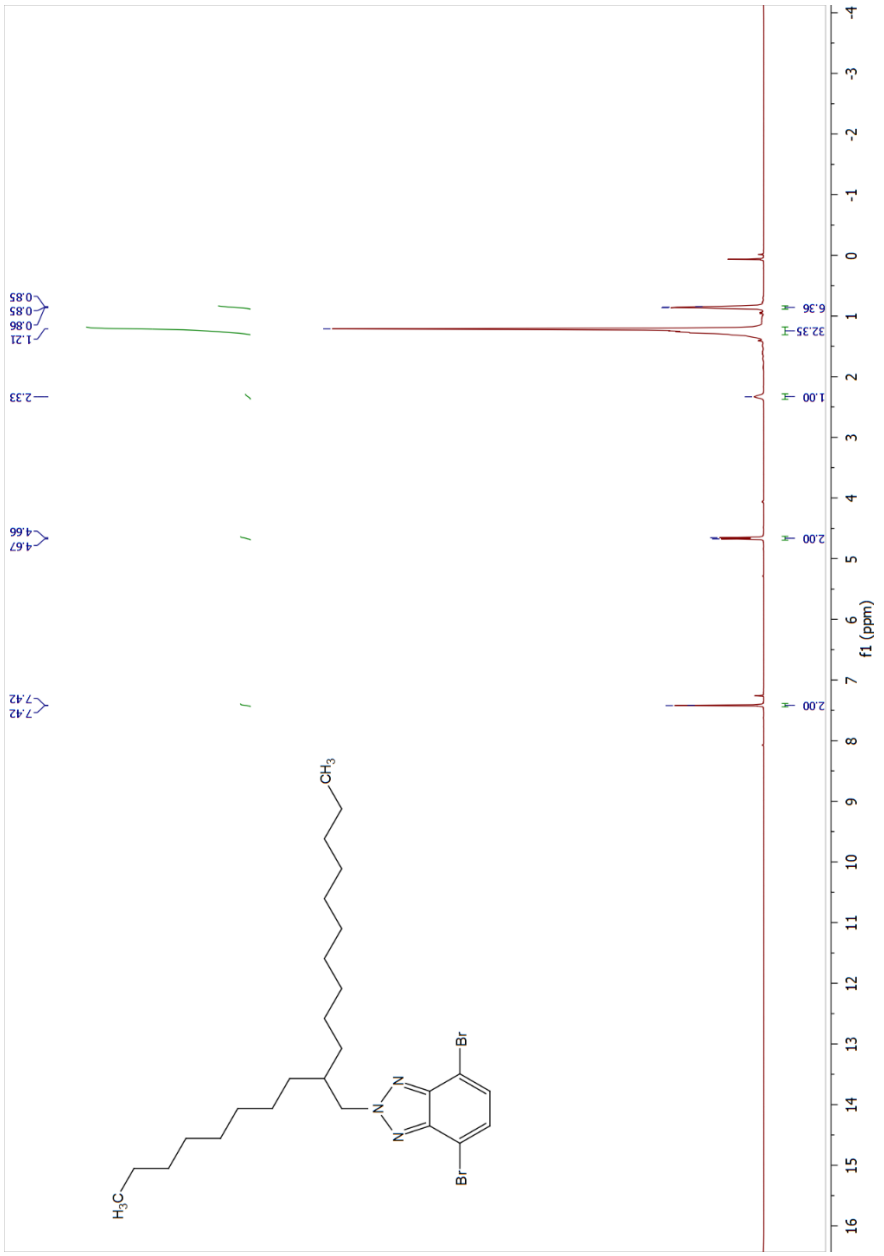

Figure A.9. ^{1}H NMR spectrum of 4,7-dibromo-2-(2-octyldodecyl)-2H-benzo[d][1,2,3]triazole (5)

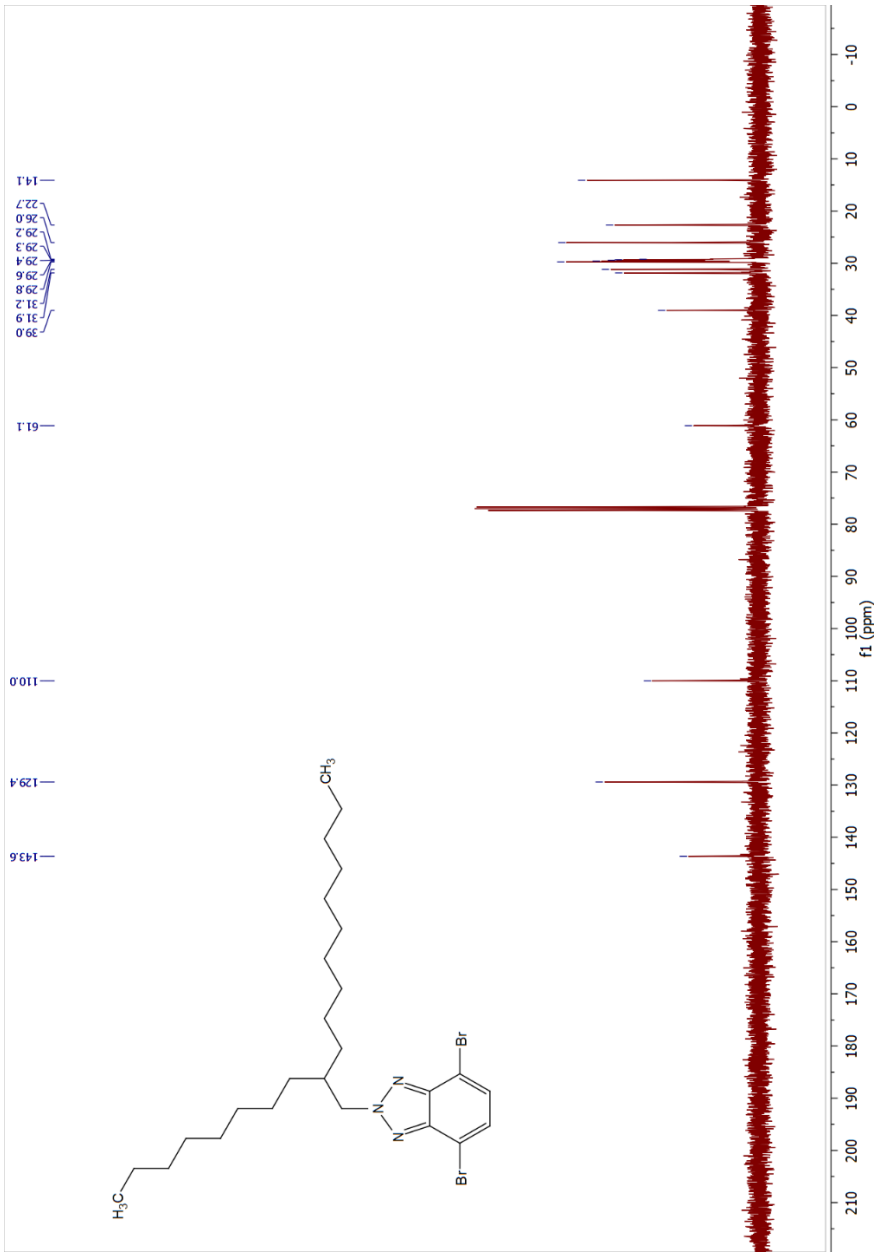

Figure A.10. ^{13}C NMR spectrum of 4,7-dibromo-2-(2-octyldodecyl)-2H-benzo[d][1,2,3]triazole (5)

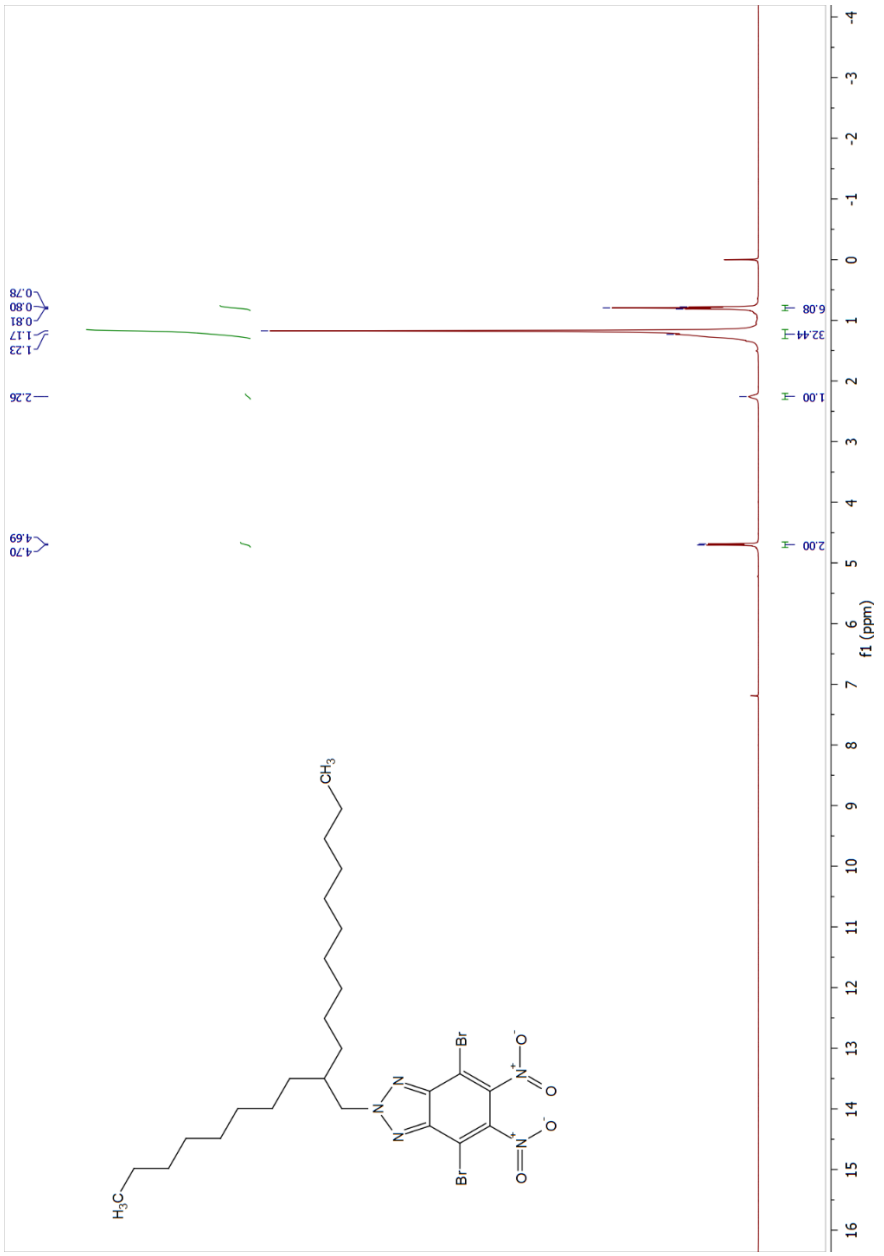

Figure A.11. ^{1}H NMR spectrum of 4,7-dibromo-5,6-dinitro-2-(2-octyldodecyl)-2H-benzo[d][1,2,3]triazole (6)

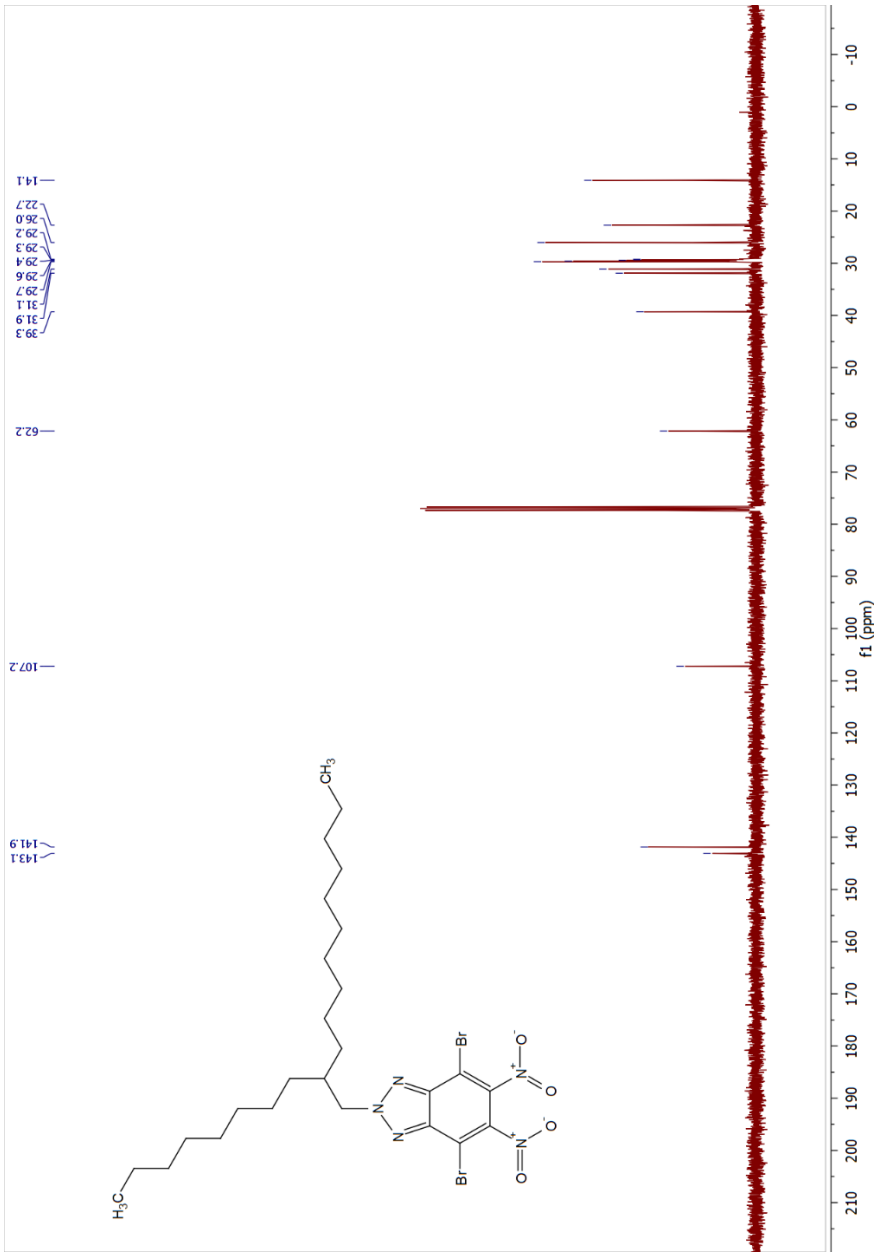

Figure A.12. ^{13}C NMR spectrum of 4,7-dibromo-5,6-dinitro-2-(2-octyldodecyl)-2H-benzo[d][1,2,3]triazole (6)

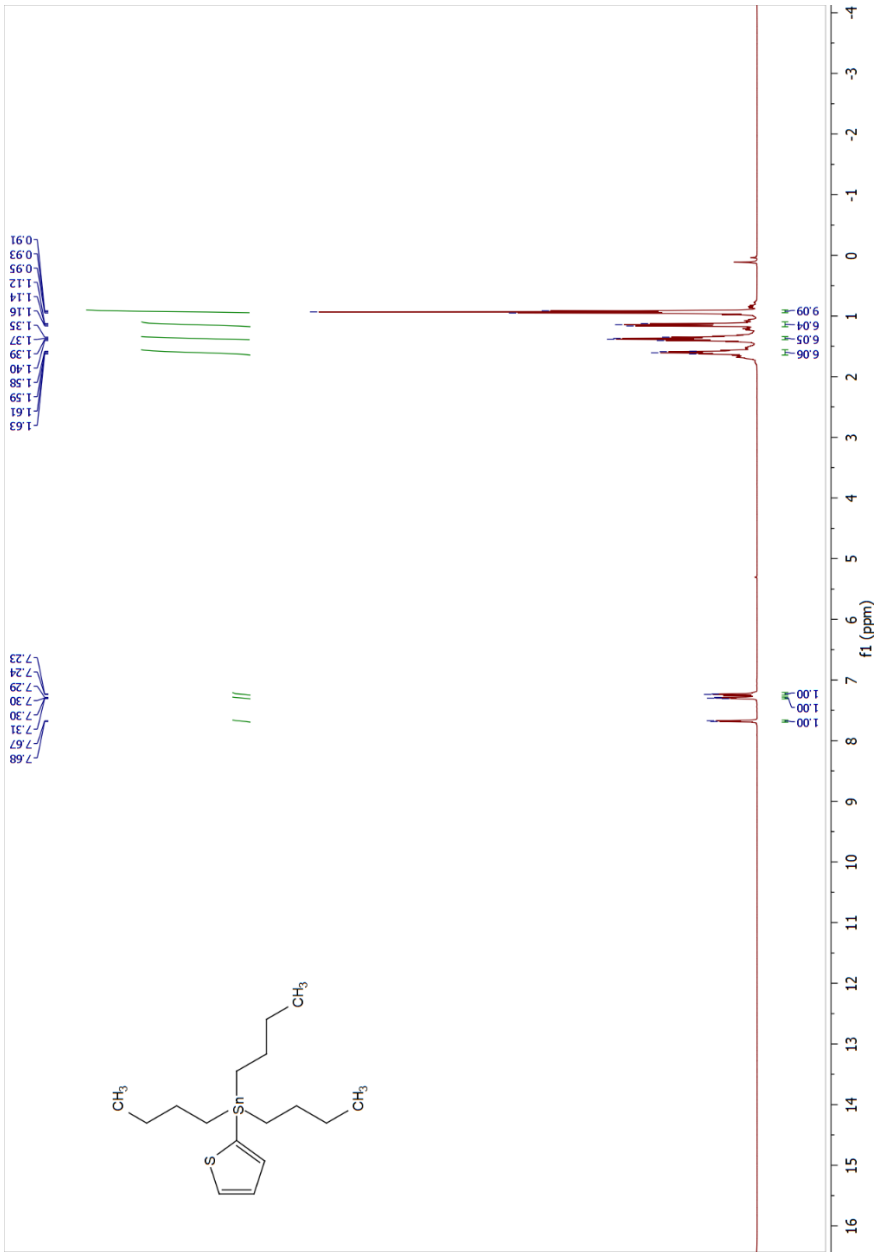

Figure A.13. ^{1}H NMR spectrum of tributyl(thiophen-2-yl)stannane (7)

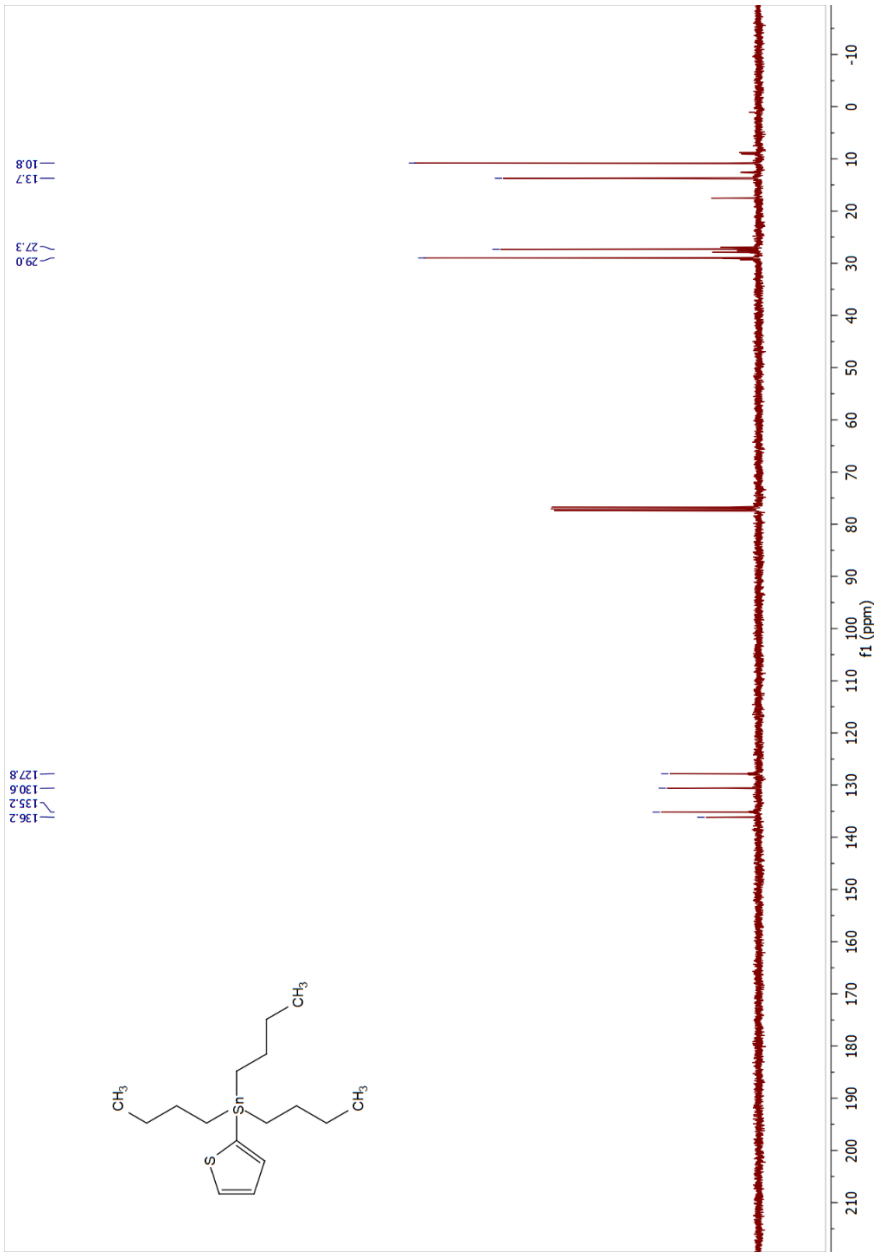

Figure A.14. ^{13}C NMR spectrum of tributyl(thiophen-2-yl)stannane (7)

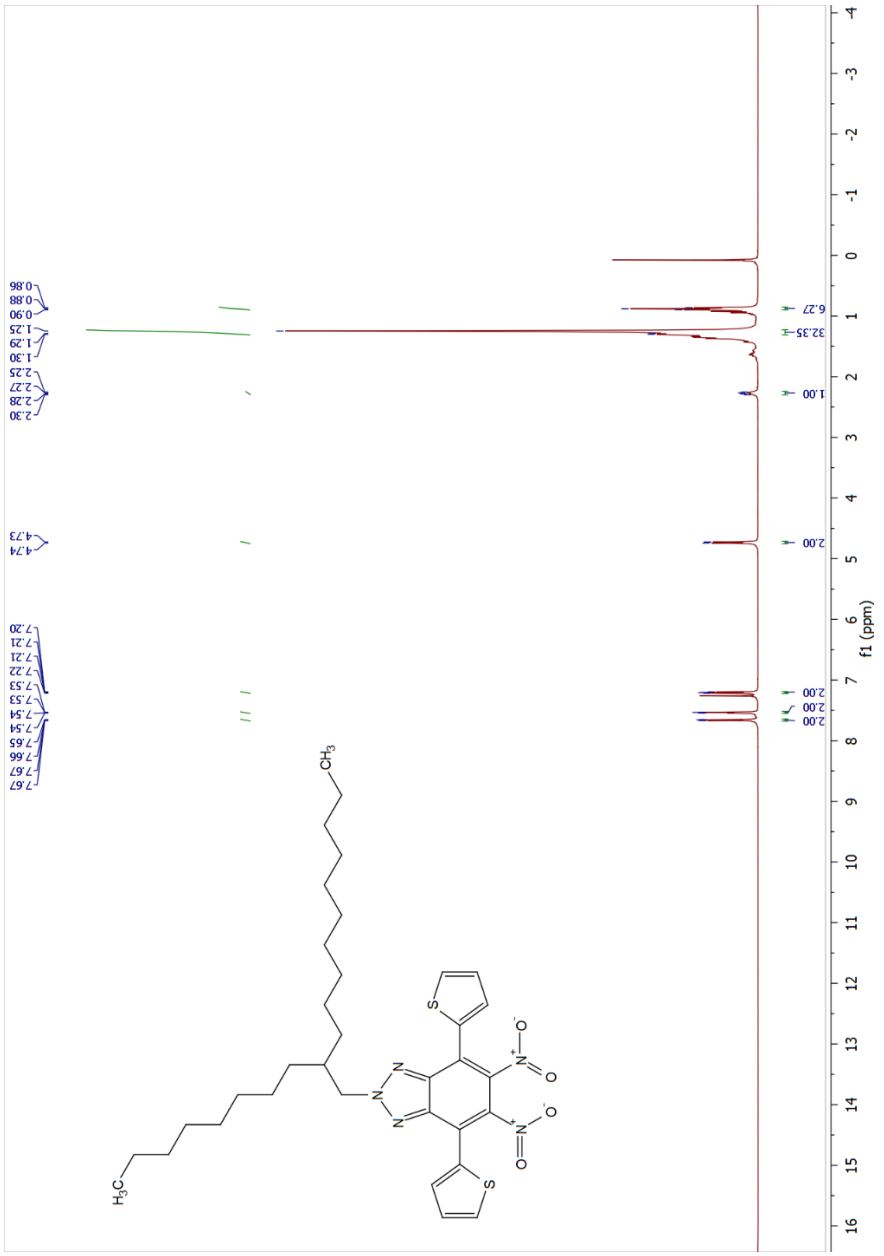

Figure A.15. ^{1}H NMR spectrum of 5,6-dinitro-2-(2-octyldodecyl)-4,7-di(thiophen-2-yl)-2H-benzo[d][1,2,3]triazole (8)

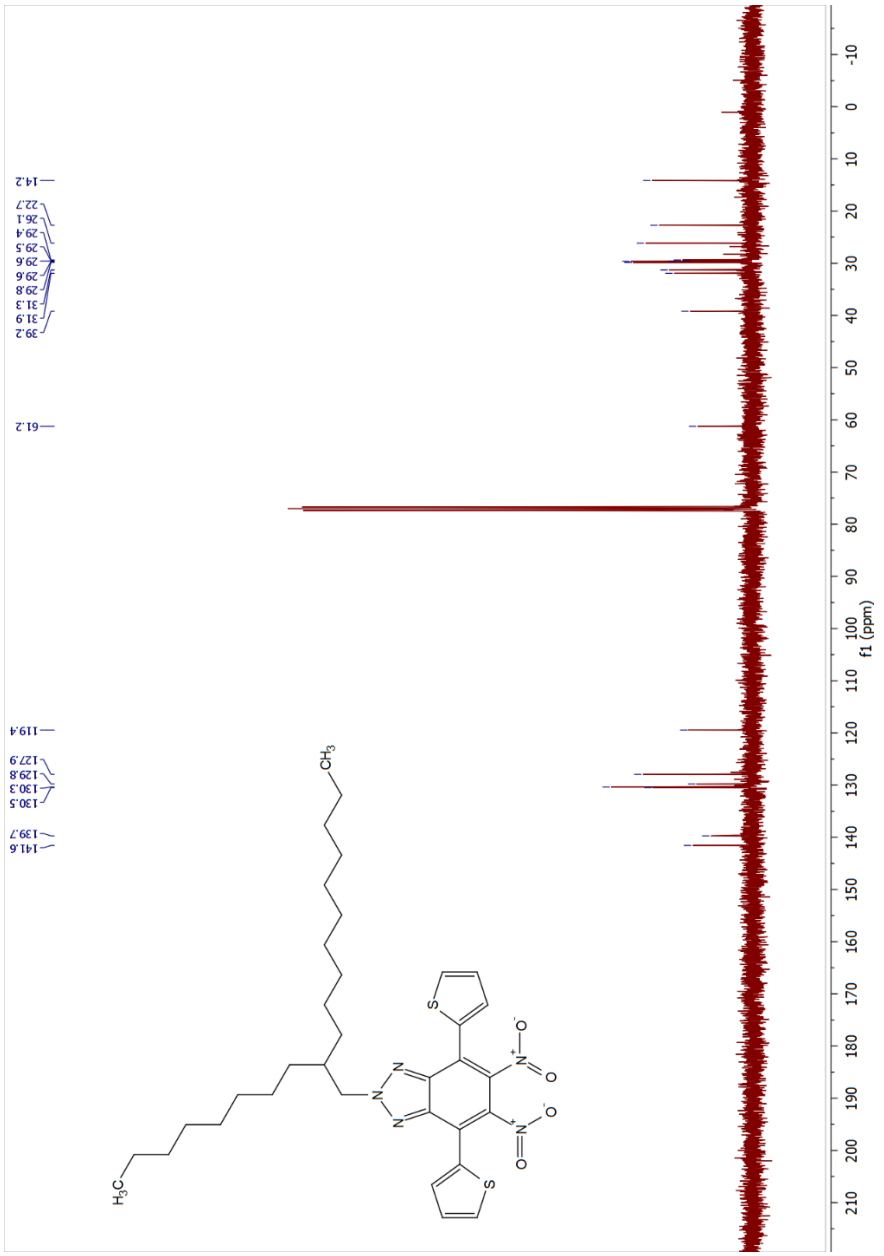

Figure A.16. ^{13}C NMR spectrum of 5,6-dinitro-2-(2-octyldodecyl)-4,7-di(thiophen-2-yl)-2H-benzo[d][1,2,3]triazole (8)

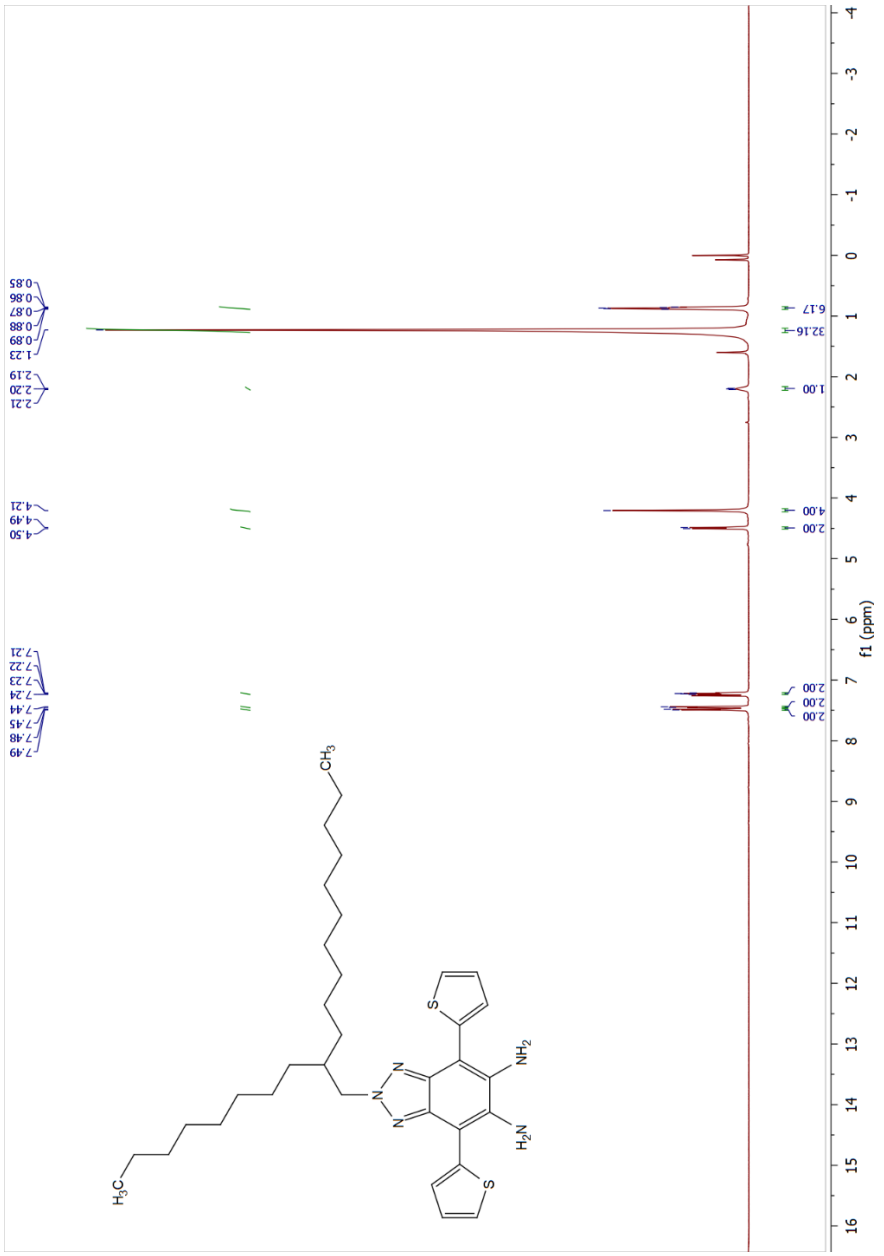

Figure A.17. ^{1}H NMR spectrum of 2-(2-octyldodecyl)-4,7-di(thiophen-2-yl)-2H-benzo[d][1,2,3]triazole-5,6-diamine (9)

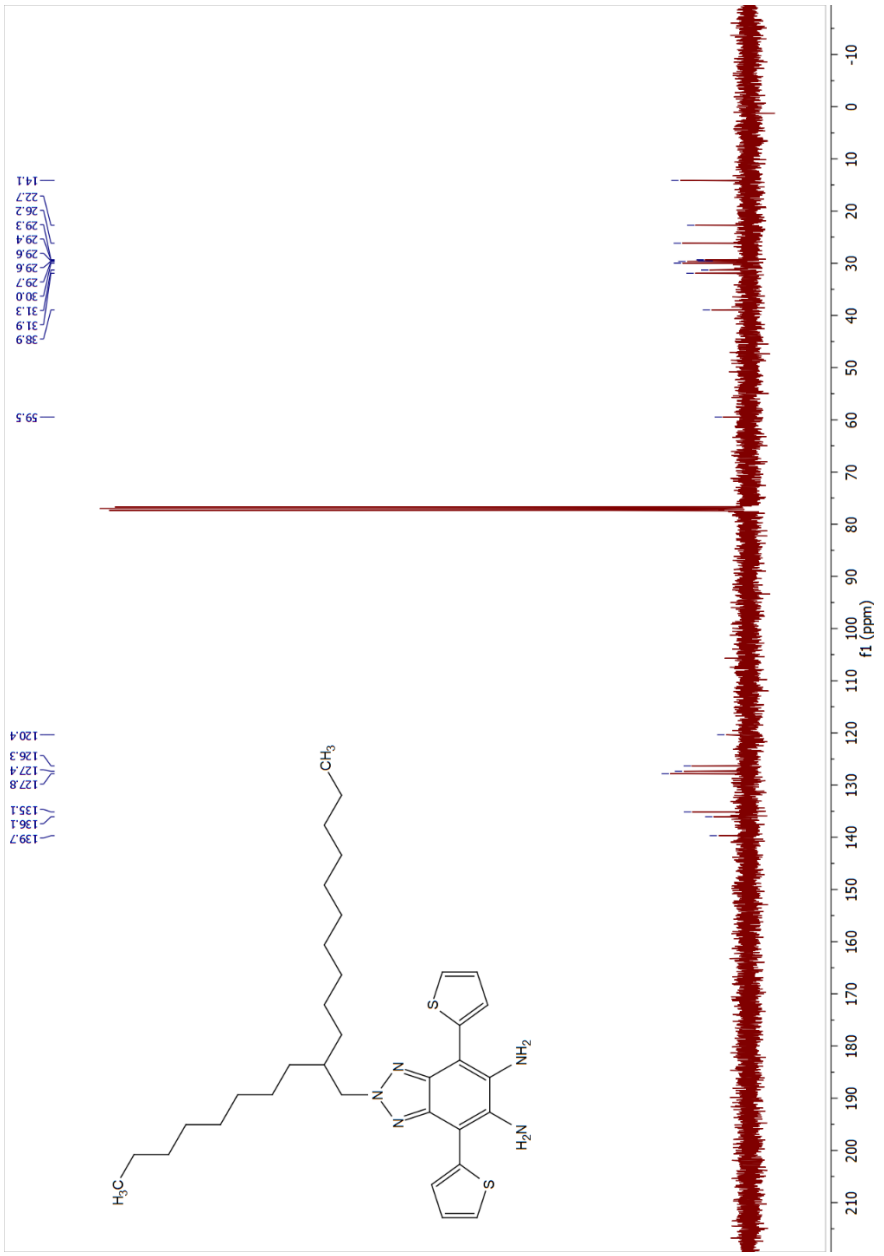

Figure A18. ^{13}C NMR spectrum of 2-(2-octyldodecyl)-4,7-di(thiophen-2-yl)-2H-benzo[d][1,2,3]triazole-5,6-diamine (9)

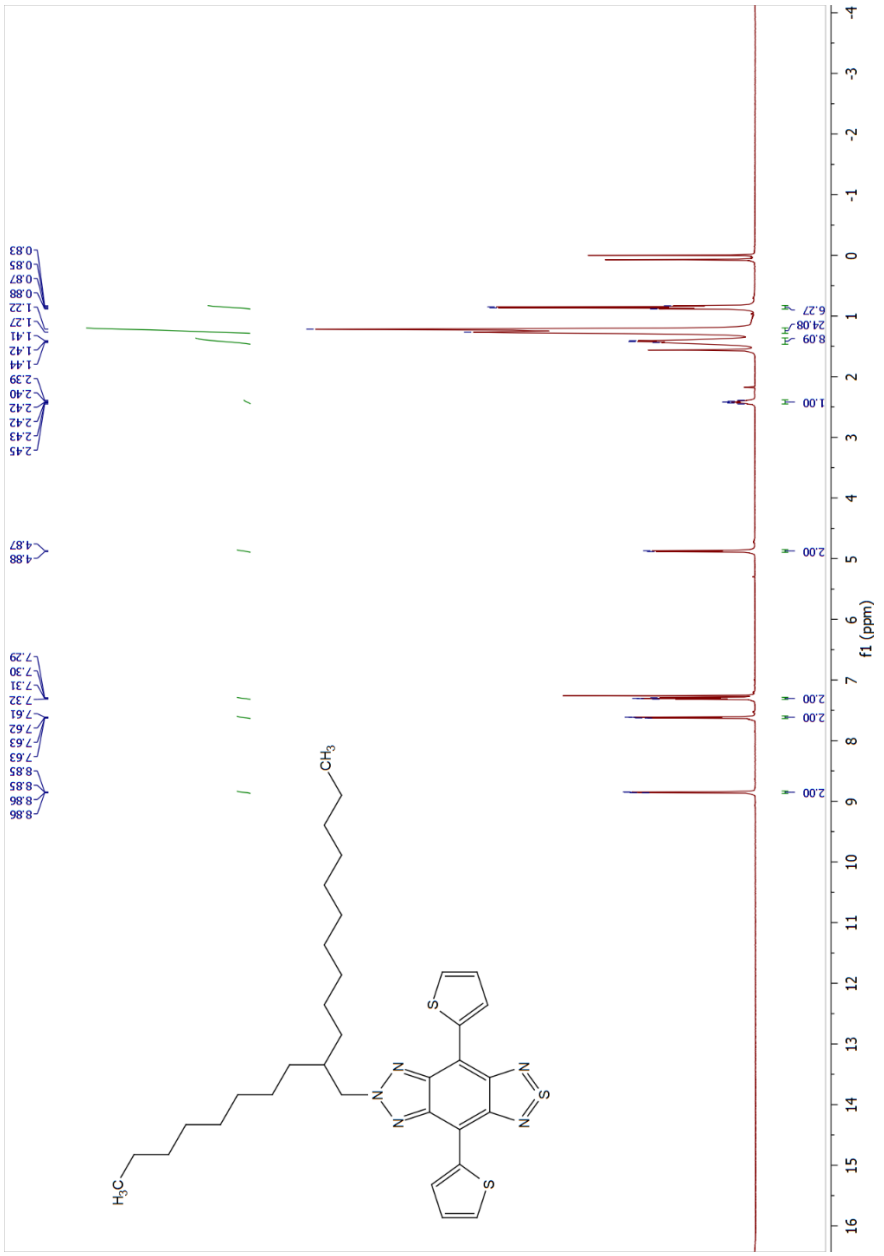

Figure A.19. ^{1}H NMR spectrum of SBT (10)

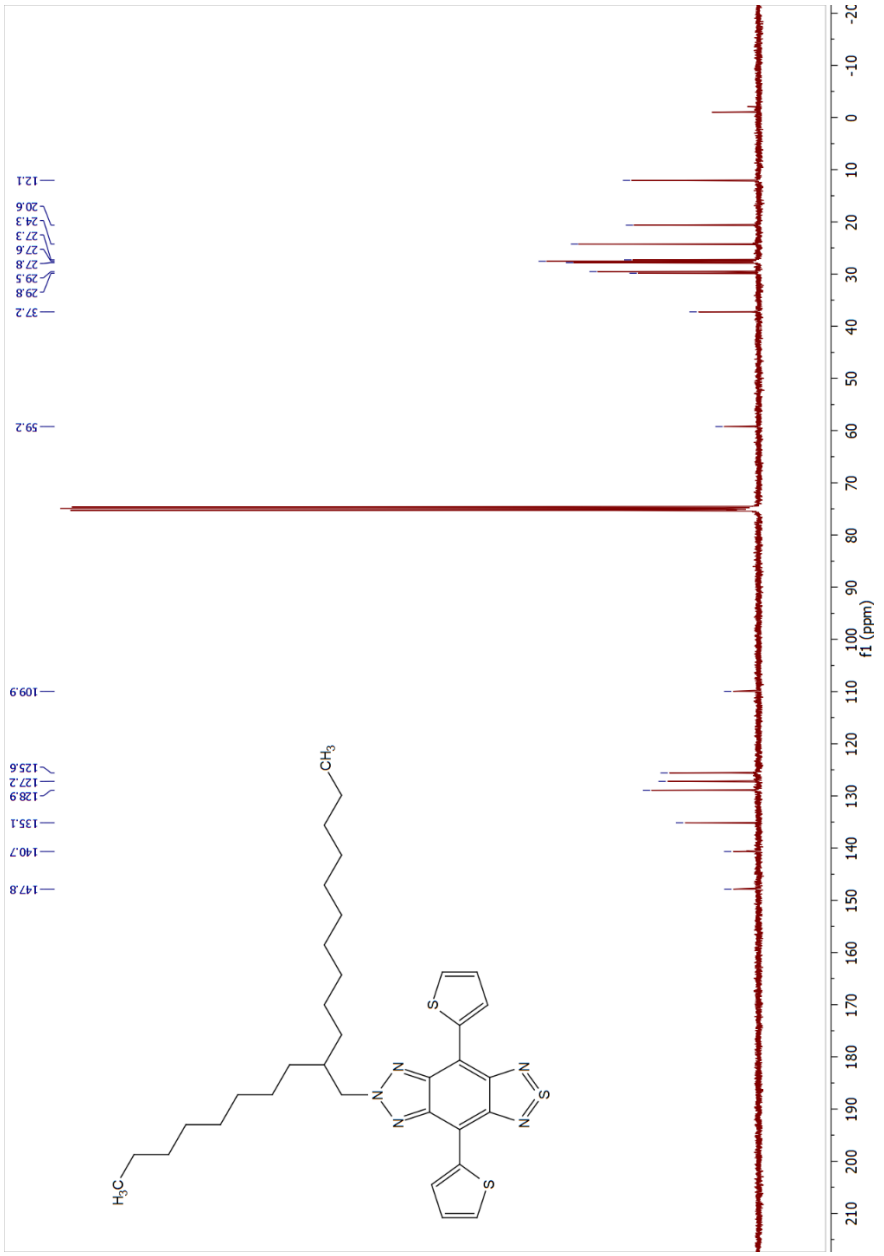

Figure A.20. ^{13}C NMR spectrum of SBT (10)

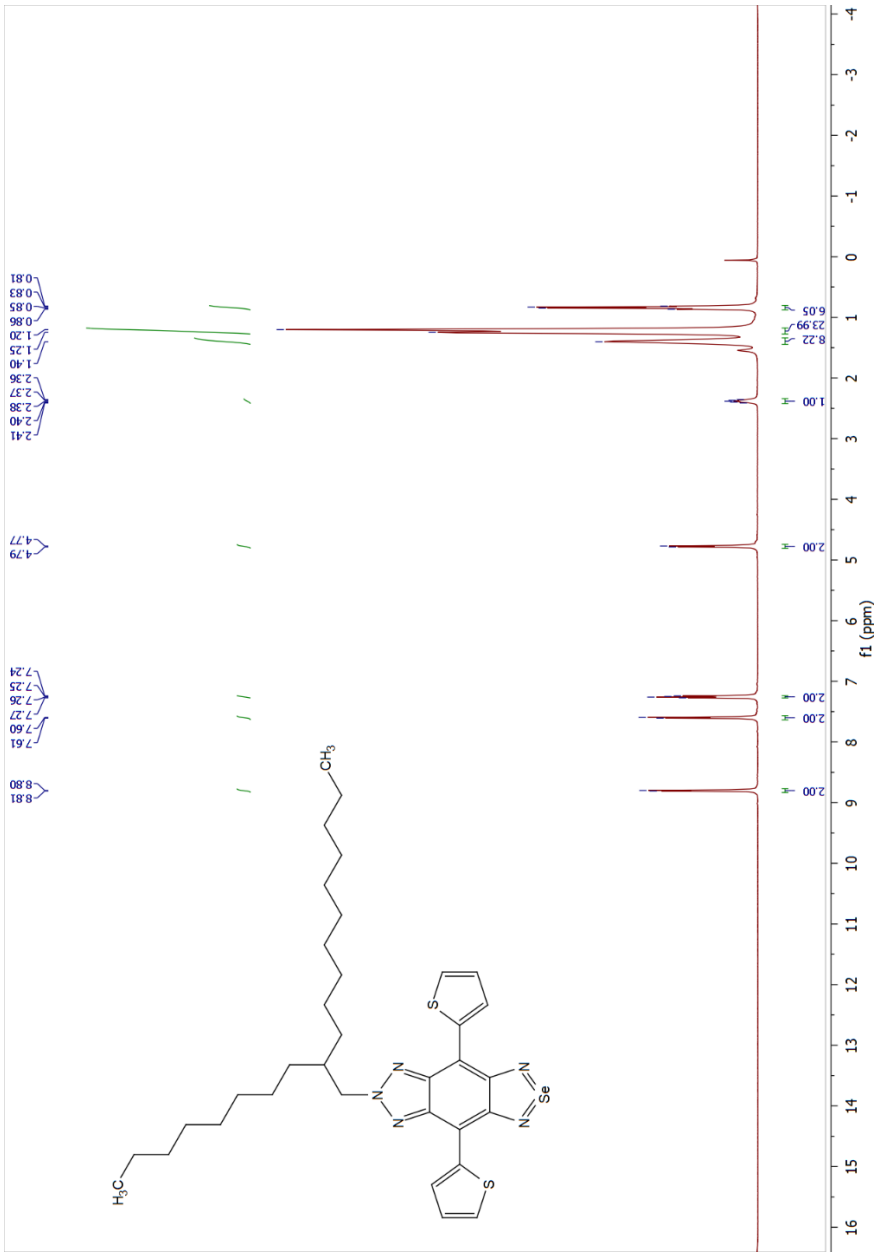

Figure A.21. ^{1}H NMR spectrum of SeBT (11)

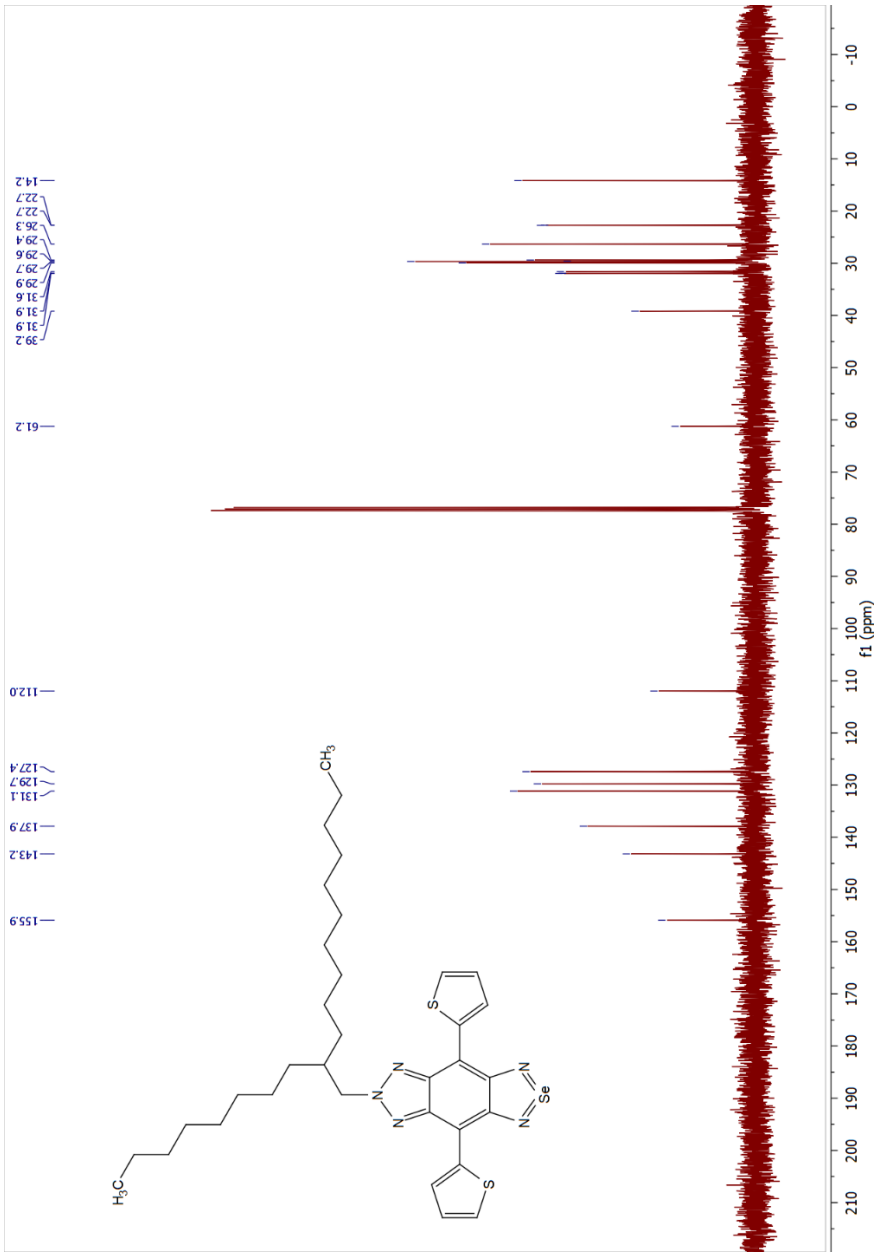

Figure A.22. ^{13}C NMR spectrum of SeBT (11)

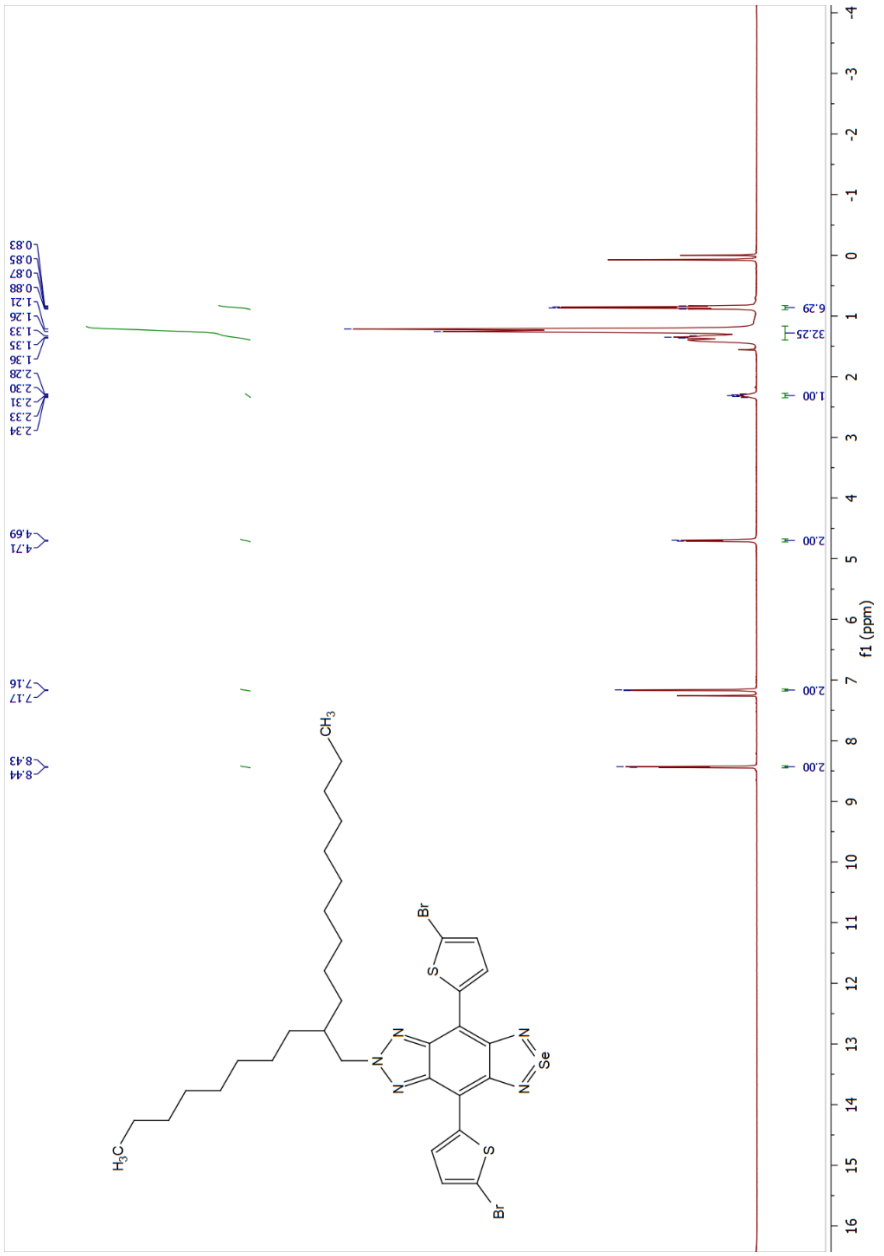

Figure A.23. ^{1}H NMR spectrum of BrSBT (12)

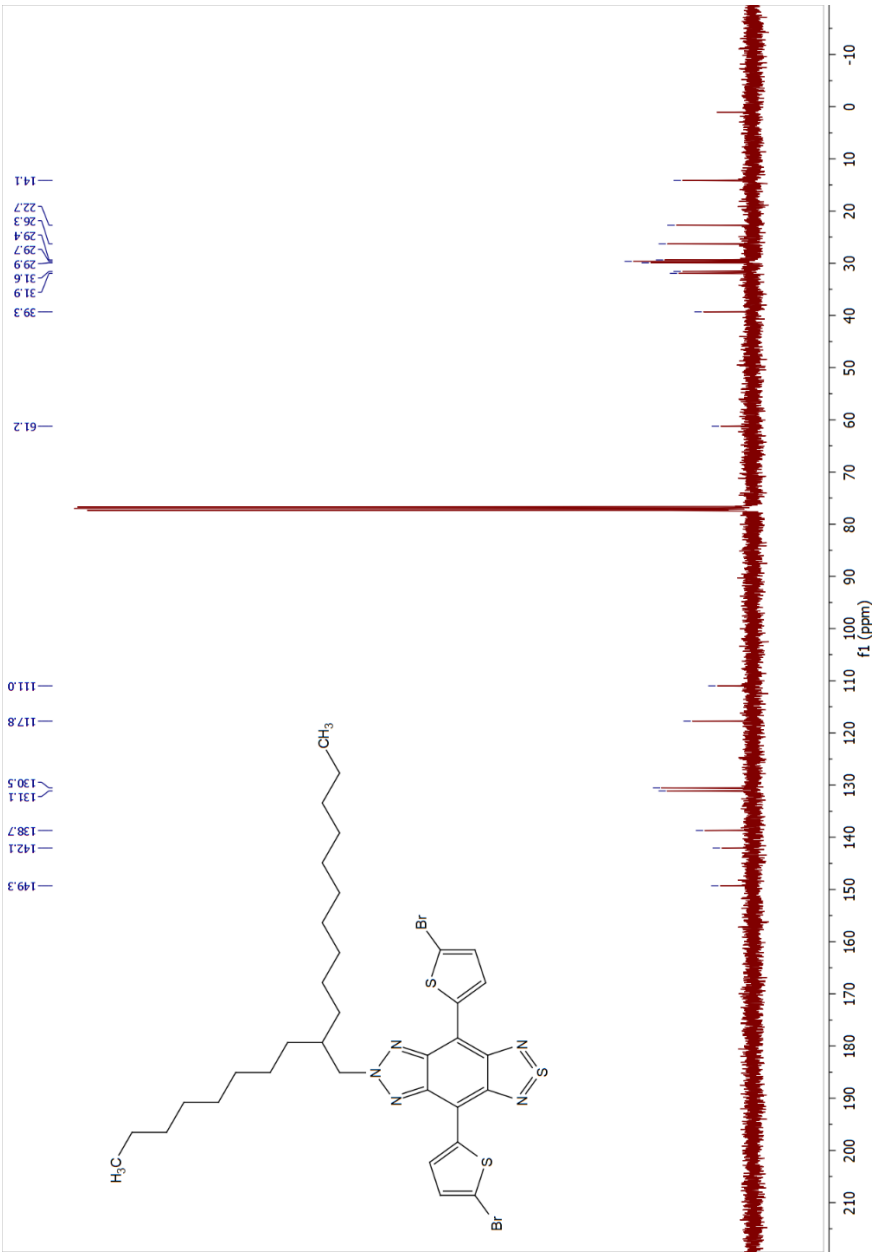

Figure A.24. ^{13}C NMR spectrum of BrSBT (12)

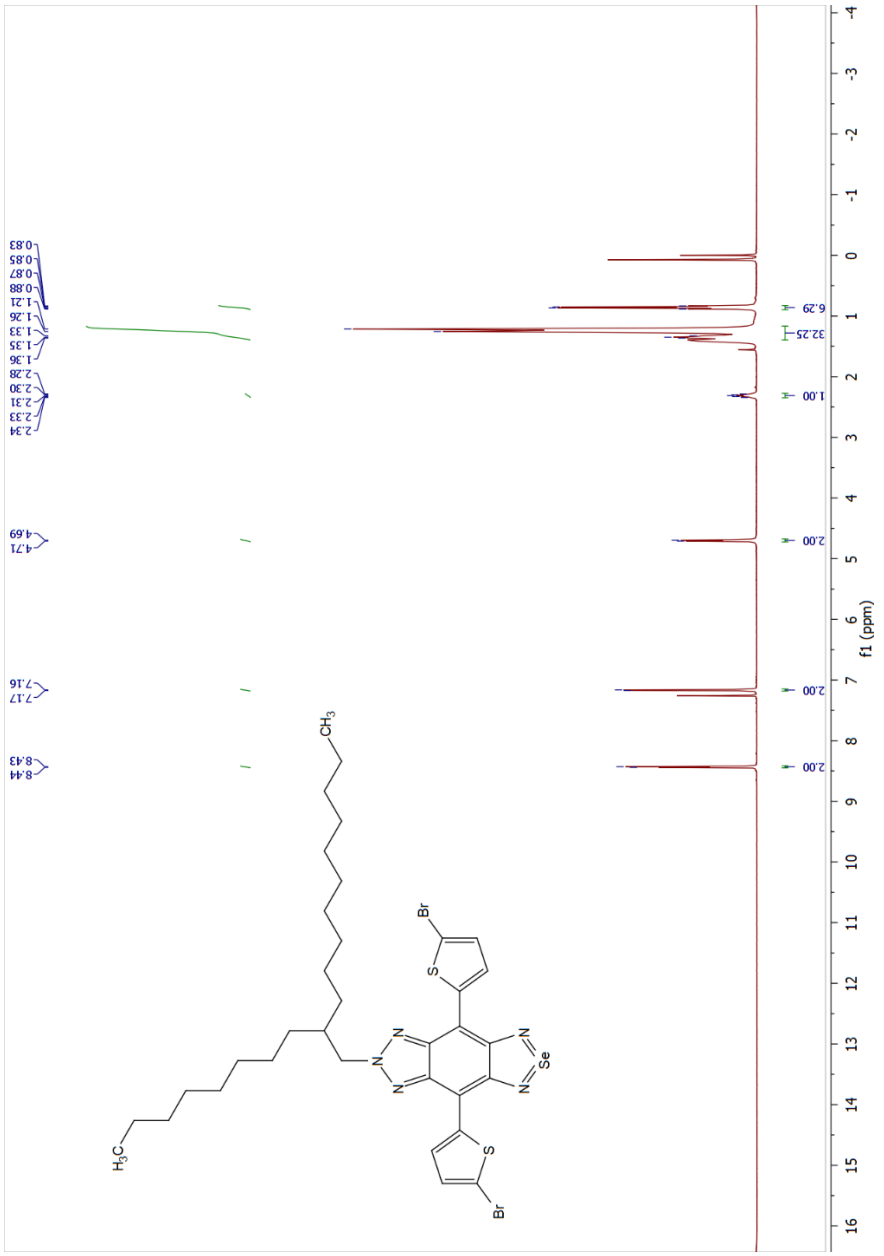

Figure A.25. ^{1}H NMR spectrum of BrSeBT (13)

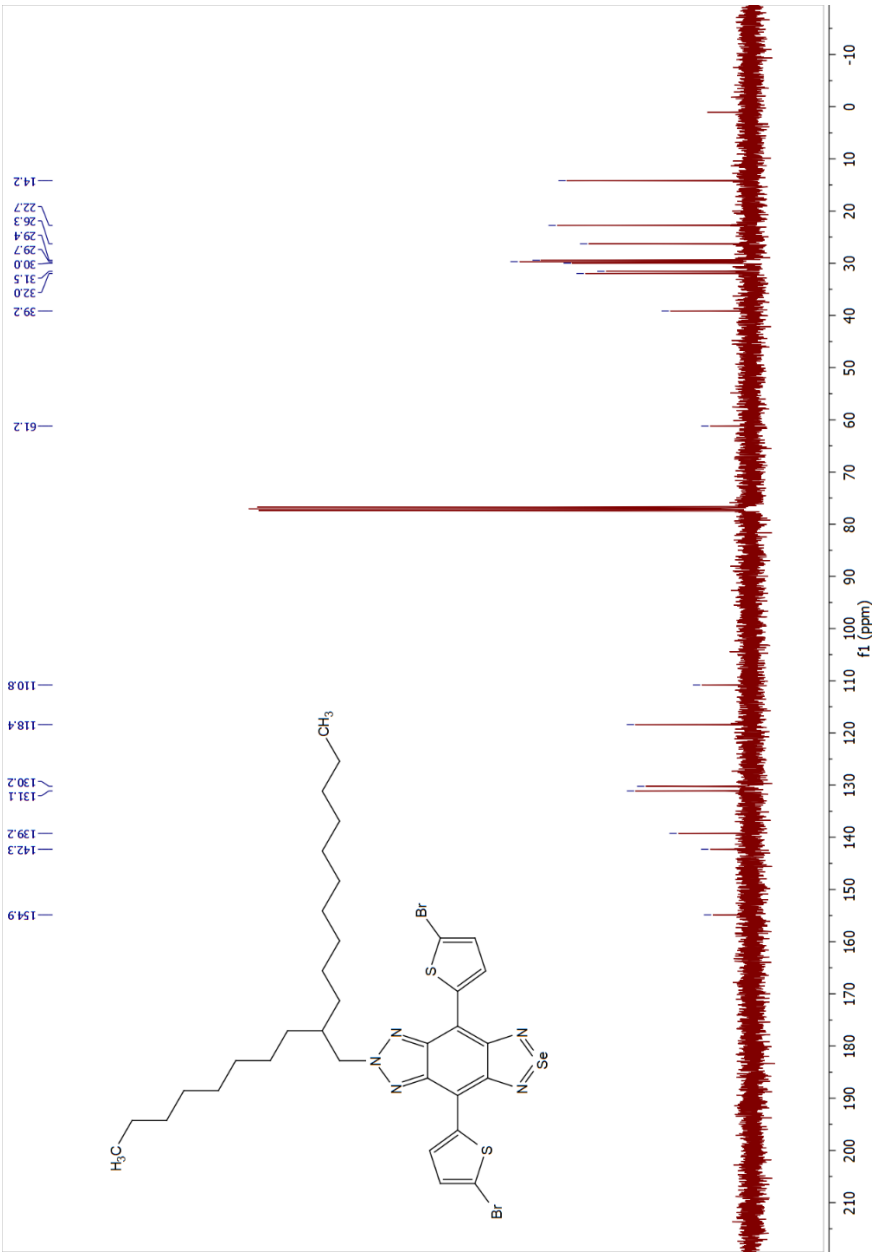

Figure A.26. ^{13}C NMR spectrum of BrSeBT (13)

B. HRMS Spectra

Each molecule is analyzed by WATERS Synapt G1 High Resolution Mass Spectrometer.

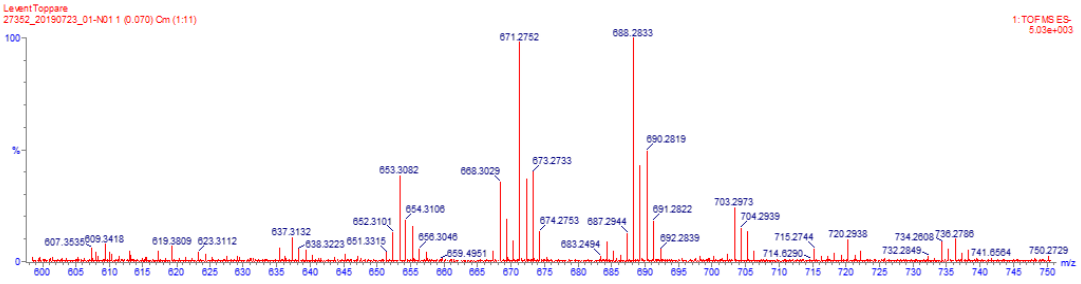

Figure B.1. HRMS spectrum of 5,6-dinitro-2-(2-octyldodecyl)-4,7-di(thiophen-2-yl)-2H-benzo[d][1,2,3]triazole (8)

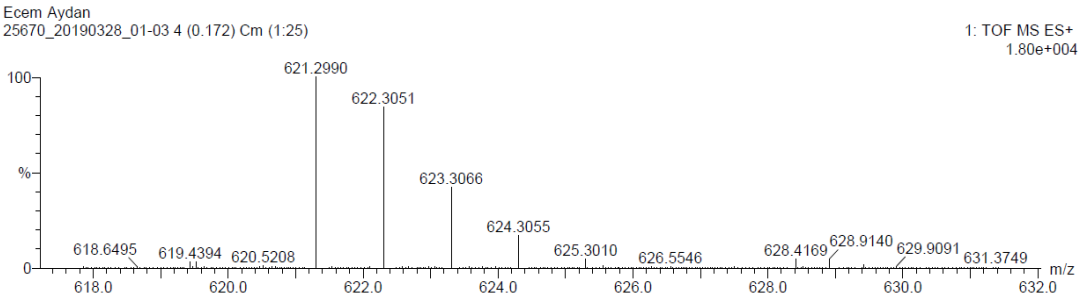

Figure B.2. HRMS spectrum of SBT (10)

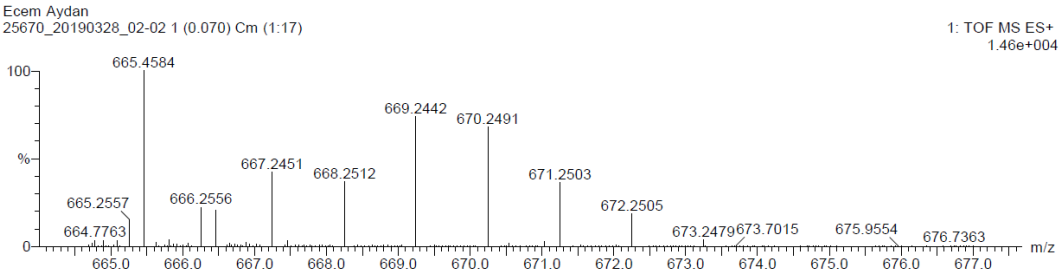

Figure B.3. HRMS spectrum of SeBT (11)

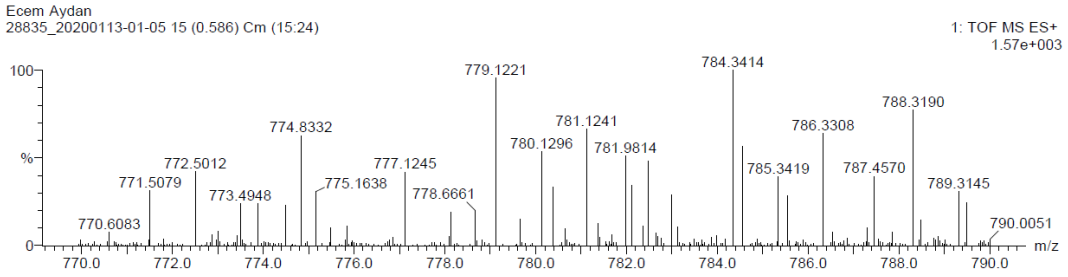

Figure B.4. HRMS spectrum of BrSBT (12)

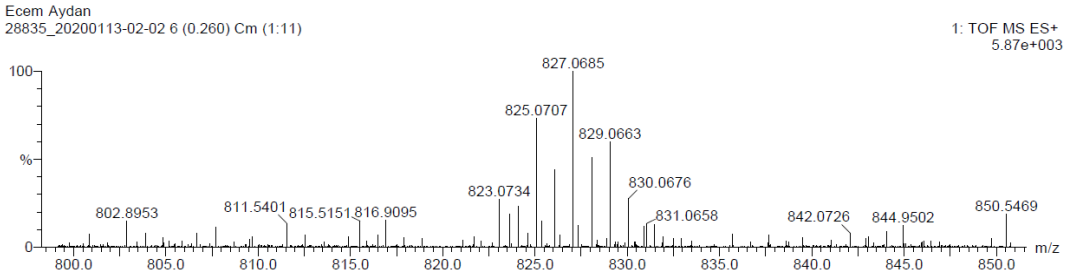

Figure B.5. HRMS spectrum of BrSeBT (13)

C. FTIR Spectra

Each molecule is analyzed by Bruker IFS 66/S Hyperion 1000 device.

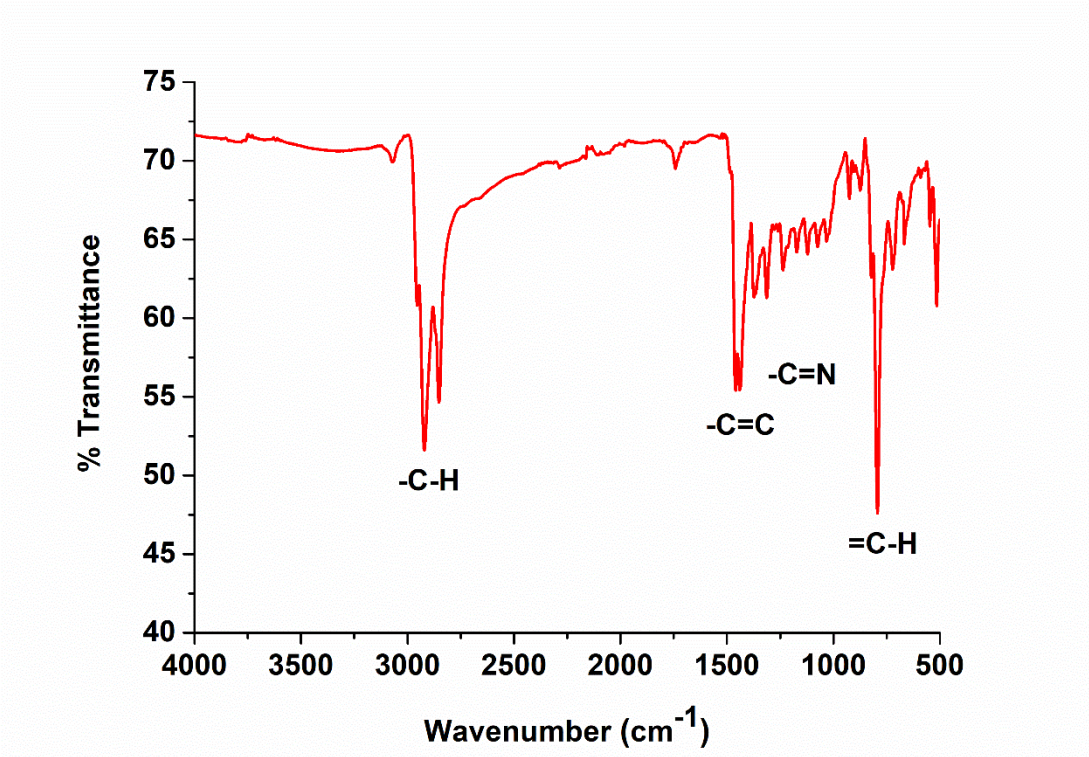

Figure C.1. FTIR spectrum of PSBT

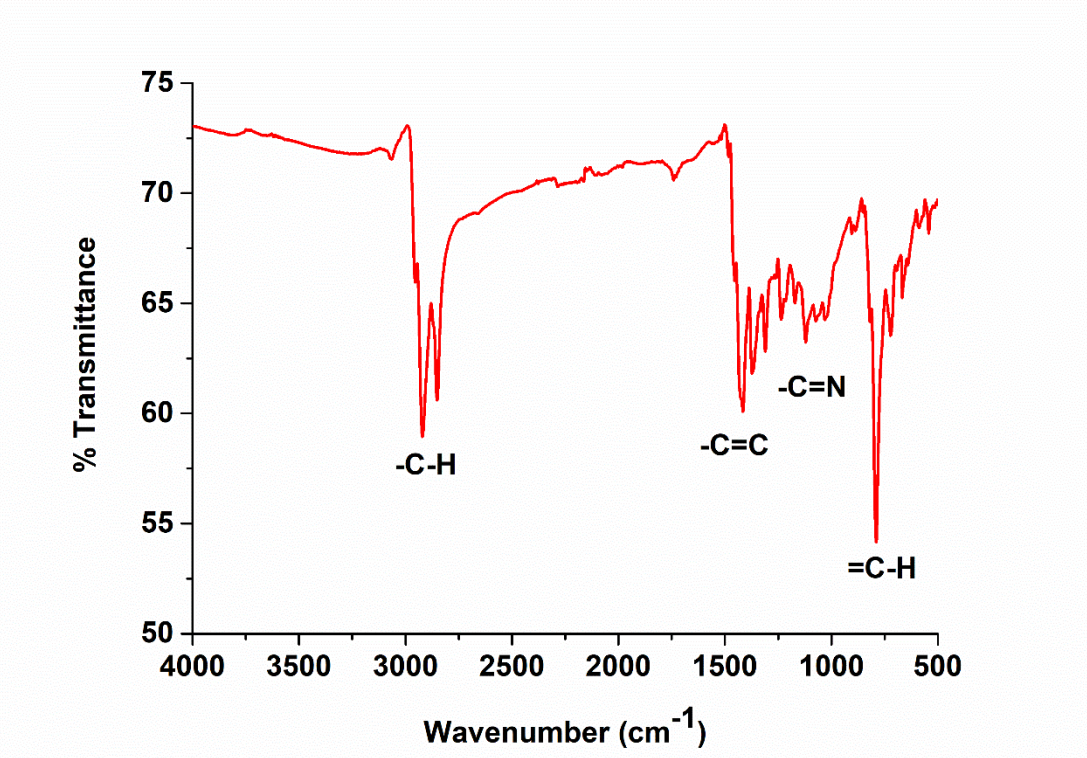

Figure C.2. FTIR spectrum of PSeBT